NTNU
Norwegian University of
Science and Technology

Evaluation of Rankine cycles with mixed component working fluids

Monika Nikolaisen

Mechanical Engineering
Submission date: June 2017
Supervisor: Petter Nekså, EPT
Co-supervisor: Brede Andre Larsen Hagen, SINTEF Energi
Trond Andresen, SINTEF Energi

Norwegian University of Science and Technology
Department of Energy and Process Engineering

NTNU

Norwegian University
of Science and Technology

Department of Energy
and Process Engineering

EPT-M-2017-56

MASTER THESIS

for

Student Monika Nikolaisen

Spring 2017

Evaluation of Rankine cycles with mixed component working fluids

Vurdering av blandinger som arbeidsmedier i Rankine prosesser

Background and objective

In lack of competitive options, vast amounts of industrial surplus heat are dumped to the ambient all over the globe. If a local or internal need for heat exist, direct use of the heat will most often be a cost efficient option, but in general the need is very low compared to available amounts of heat.

The COPRO project, led by SINTEF Energy Research, primarily targets recovery of industrial waste heat in the temperature range of 125-250 °C for conversion to electricity. This is a temperature range where profitable energy recovery currently is challenging, but with large amounts of heat available. The long term goal within this scientific project is to find mixtures of fluids that have ideal thermophysical properties for use in Rankine cycles for the intended applications, and exploit these properties optimally with specifically designed components, cycle configurations, at optimal operating conditions.

Exploration of potential fluids and mixtures at varying conditions and for different cases are highly valuable, but identifying a basis for fair comparison without resorting to exhaustive detailed component design is challenging.

The aim of this Master thesis work is to further develop a modeling framework to be used for investigation and a "fair comparison" of different Rankine cycles utilising relevant mixtures of fluids. A "fair basis" could for example be to compare systems with identical total heat exchanger area, and thereby allow individually different cycle configurations and operating conditions.

The following tasks are to be considered:

1. Literature survey related to heat transfer and pressure drop of fluid mixtures relevant for use as working fluids in Rankine cycles
2. Quantify impact on heat exchanger design when using fluid mixtures compared to pure fluids
3. Further develop existing model framework for Rankine cycles, e.g. to include internal heat exchanger/recuperator, utilization of improved heat transfer correlations and model accuracy
4. Define relevant cases and constraint conditions for existing and future applications of Rankine cycles
5. Investigate the selected cases using the new model framework and compare the results to results from earlier models

-- " --

Within 14 days of receiving the written text on the master thesis, the candidate shall submit a research plan for his project to the department.

When the thesis is evaluated, emphasis is put on processing of the results, and that they are presented in tabular and/or graphic form in a clear manner, and that they are analyzed carefully.

The thesis should be formulated as a research report with summary both in English and Norwegian, conclusion, literature references, table of contents etc. During the preparation of the text, the candidate should make an effort to produce a well-structured and easily readable report. In order to ease the evaluation of the thesis, it is important that the cross-references are correct. In the making of the report, strong emphasis should be placed on both a thorough discussion of the results and an orderly presentation.

The candidate is requested to initiate and keep close contact with his/her academic supervisor(s) throughout the working period. The candidate must follow the rules and regulations of NTNU as well as passive directions given by the Department of Energy and Process Engineering.

Risk assessment of the candidate's work shall be carried out according to the department's procedures. The risk assessment must be documented and included as part of the final report. Events related to the candidate's work adversely affecting the health, safety or security, must be documented and included as part of the final report. If the documentation on risk assessment represents a large number of pages, the full version is to be submitted electronically to the supervisor and an excerpt is included in the report.

Pursuant to "Regulations concerning the supplementary provisions to the technology study program/Master of Science" at NTNU §20, the Department reserves the permission to utilize all the results and data for teaching and research purposes as well as in future publications.

The final report is to be submitted digitally in DAIM. An executive summary of the thesis including title, student's name, supervisor's name, year, department name, and NTNU's logo and name, shall be submitted to the department as a separate pdf file. Based on an agreement with the supervisor, the final report and other material and documents may be given to the supervisor in digital format.

☐ Work to be done in lab (Water power lab, Fluids engineering lab, Thermal engineering lab)
☐ Field work

Department of Energy and Process Engineering, 15. January 2017

Adjunct Prof. Petter Nekså
Academic Supervisor

Research Advisors/Co-supervisors:
Brede A. L. Hagen, SINTEF Energy Research
Trond Andresen, SINTEF Energy Research

PREFACE

The following is a master thesis written at the Department of Energy and Process Engineering at NTNU. The work has been conducted in collaboration with SINTEF Energy Research for the COPRO project, which targets recovery of industrial surplus heat.

The purpose of the work is to evaluate Rankine cycles with mixed component working fluids. A model developed in the project thesis is further developed, and applied for different cases representative of Rankine cycle applications. The project thesis was completed in the fall of 2016 and can be found at the Department of Energy and Process Engineering at NTNU.

Acknowledgement is given to my supervisors, Petter Nekså, Trond Andresen and Brede Hagen, for guidance in the model development and application.

SUMMARY

The thesis evaluates the performance of Rankine cycles with mixed component hydrocarbon working fluids, or hydrocarbon mixtures. The objective is to compare mixtures with pure fluids on the basis of the same total heat exchanger (HX) area. This is achieved through further development and application of a three-step cycle optimization model developed in the project work, which calculates the maximum work output for a pre-defined value of total HX area. The model simultaneously calculates the optimum distribution of HX area between the condenser and the heat recovery heat exchanger (HRHE).

A literature review is performed that studies heat transfer and pressure drop of working fluid mixtures through horizontal smooth tubes to evaluate and implement improved correlations. The literature review demonstrates that several methods are available for predicting heat transfer coefficients (HTCs), and that a method by Bell and Ghaly (1973) is most common for condensation, and a method by Thome (1996) is most common for evaporation.

The cycle optimization model is further developed though implementation of new heat transfer correlations better suited for hydrocarbons. A more comprehensive estimation of overall HTC is made, and the option of internal heat exchanger (IHX) is included. A more detailed working fluid comparison is made through the study of optimum heat exchanger designs, including the distribution of condenser and HRHE area for different values of pre-defined total HX area. The specific working fluid affects HX design in terms of pinch points and distributions between condenser and HRHE area. Moreover, HX pressure loss is determined by working fluid overall HTCs and operating pressure, and the number of tubes and tube diameter is most affected by pressure levels.

Four cases are defined that represent present and future applications of Rankine cycle. Case 1 and 2 consider a heat source at 100℃, with no lower limit on heat source outlet temperature. In case 1, the heat sink outlet temperature fixed and in case 2 it is allowed to vary. In case 1 and 2, butane, ethane and ethane (0.6/0.4) are studied. Case 3 and 4 consider a heat source cooled from 200℃ to 80℃. Case 4 differs from case 3 in that the optimization tool is given the choice to include an IHX, and does so if this contributes to an increased work output. In case 3 and 4, butane and butane-propane (0.6/0.4) are studied. For all cases, work output is maximized for different values of pre-defined total HX area.

Contrary to the case studied in the project work, the results for case 1 and 2 demonstrate that the hydrocarbon mixture has the potential to achieve significantly higher work output than the pure fluids for the same total HX area (up to 34 %). Variable heat sink outlet temperature allow small improvements in work output from case 1, and the improvement is greater for the pure fluids.

In case 3, the pure fluid achieves on average 3.7 % higher work output than the mixture. However, a working fluid screening demonstrated that other mixtures may have more potential in this case. With the inclusion of IHX, work outputs increases between 1.5 % and 11.6 % for the same total HX area, with increased potential for improvement at relatively high values of total HX area. In fact, the IHX was not included in the optimum solutions for lower-range values of area. Improvement with IHX was highest for the mixture, which enabled it to achieve the same levels of work output as the pure fluid. Despite the low potential of the mixture in this case, it may be more applicable for high values of total HX area than the pure fluid due to its relatively hgih pinch point temperatures.

A significant increase in work output can be achieved with increasing heat source temperature. For the heat source at 100°C, work outputs reaches around 25 kW for high values of total HX area. For a case studied in the project work with a heat sources at 150°C, work outputs reaches 50 kW, and for the heat source at 200°C in the current work, work output reaches 100 kW.

SAMMENDRAG

Denne oppgaven tar for seg bruk av hydrokarbonblandinger som arbeidsmedier i Rankinesykler. Målet er å sammenligne blandinger med rene medier basert på det samme totale varmevekslerarealet. Dette oppnås gjennom forbedring og bruk av en tre-stegs sykel-optimaliseringsmodell som ble utviklet i prosjektoppgaven. Modellen regner ut maksimalt kraftutbytte for et forhåndsbestemt totalt varmevekslerareal. Den regner samtidig ut optimal fordeling av varmevekslerareal i kondenser og varmegjenvinnings-varmeveksleren (VGV).

Et litteraturstudie knyttet til varmeovergang og trykktap for arbeidsmedieblandinger gjennom horisontale, glatte rør ble utført for å evaluere og implemetere bedre korrelasjoner. Litteraturstudiet viste at det finnes flere tilgjengelig metoder for å regne ut lokale varmeovergangstall, og at metoden til Bell og Ghaly (1973) er mest vanlig for kondensering, og metoden til Thome (1996) er mest vanlig for koking.

Optimaliseringsmodellen ble utviklet gjennom implementering av nye varmeovergangskorrelasjoner som er bedre egnet for hydrokarboner. Et mer omfattende estimat av varmeovergangstall ble gjort, og muligheten for internvarmeveksler ble inkludert. En mer detaljert sammenligning av arbeidsmedier ble gjort gjennom studie av optimale varmevekslerdesign, inkludert fordeling av kondenser og VGV-areal. Arbeidsmediet påvirket pinch-punktene til varmevekslerene, samnt fordeling av kondenser og VGV areal. Trykktap bestemmes av varmeovergangstallet og trykknivået til fluidet, og varmevekslerens rørdiamteter og antall rør påvirkes mest av av trykknivået.

Fire case blir definert som representerer aktuelle og fremtidige applikasjoner av Rankinesykler. Case 1 og 2 tar for seg en varmekilde ved 100℃, med ingen nedre grense på utløpstemperatur. I case 1 er utløpstemperaturen til varmesluket konstant, mens den i case 2 kan variere. I disse casene blir butan, etan og etan-propan (0.6/0.4) studert. Case 3 og 4 tar for seg en varmekilde på 200℃ som kjøles til 80℃. Case 4 skiller seg fra case 3 ved at optimaliseringsverktøyet får velge om den vil inkludere internvarmeveksler, noe den velger å gjøre dersom det fører til økt kraftutbytte. I case 3 og 4 blir butan og butan-propan (0.6/0.4) studert. I alle casene blir kraftutbyttet maksimert for forksjellige verdier av totalt varmevekslerareal.

I motsetning til caset som ble studert i prosjektoppgaven, viser resultatene for case 1 og 2 at hydrokarbonblandingen har potensiale til å oppnå betydelig høyere kraftutbytte enn de rene mediene for samme varmevekslerareal (opp til 34 %). Variabel utløpstemperatur på varmesluket fører til små forbedringer i kraftutbytte i forhold til case 1, og forbedringen er større for de rene mediene.

I case 3 oppnår det rene mediet en gjennomsnittlig forbedring i kraftutbytte på 3.7 % i forhold til blandingen. Derimot viste en "pinch-punkt"-screening at andre blandinger enn den som ble vurdert har større potensiale i forhold til det rene mediet. Med inkludering av internvarmeveksler øker kraftutbytte mellom 1.5 % og 11.6 %, med størst potensiale ved relativt store verdier av totalt varmevekslerareal. Faktisk ble ikke internvarmeveksler inkludert i de optimale løsningene for lave verdier av total varmevekslerareal. Videre ble forbedringen med internvarmeveksler større for blandingen, som gjorde at den fikk tilsvarende kraftutbytte som det rene mediet. På tross av det lave potensialet til blandingen i dette caset, kan den allikevel være et mer praktisk valg for store totalareal, ettersom den har større "pinch-punkt"-temperaturer.

En betydelig forbedring i kraftutbytte kan oppnås ved økt varmekildetempertur. For en varmekilde på 100°C når kraftutbyttet rundt 25 kW for høye verdier av totalt varmevekslerareal. For et case studert i prosjektoppgaven med en varmekildetemperatur på 150°C, når kraftutbyttet rundt 50 kW. For varmekilden på 200°C når kraftutbyttet 100 kW.

TABLE OF CONTENTS

NOMENCLATURE

Symbols

A	Surface area, m^2
A_1	Equation for pressure loss calculation
A_2	Equation for pressure loss calculation
a	Constant
Bo	Boiling number
b	Constant
C	Constant
c	Constant
c_p	Specific heat capacity, J/kg·K
d	Tube diameter, m
E	Enhancement factor
F	Enhancement factor
F_2	Enhancement factor
F_c	Mass transfer factor
Fr	Two-phase Froude number
f	Darcy friction factor
G	Mass flux, kg/m^2s
g	Gravitational acceleration, 9.81 m/s^2
h	Heat transfer coefficient, W/m^2K
i	Enthalpy, J/kg
i_{fg}	Latent heat, J/kg
k	Thermal conductivity, W/m·K
L	Tube length, m
M	Molar mass, g/mol
$\dot{m}$	Mass flow rate, kg/s
N	Number of tubes
Nu	Nusselt number
Pr	Prandtl number
p	Pressure, Pa
p_c	Critical pressure, Pa
p_r	Reduced pressure
Δp	Pressure loss, Pa
$\frac{dp}{dz}$	Pressure loss gradient, Pa/m
$\dot{Q}$	Heat transfer rate, W
q	Heat flux, W/m^2
R	Tube outside to inside area ratio
Re	Reynolds number
S	Suppression factor
S^*	Suppression factor
S_2	Suppression factor
T	Temperature, K
T_0	Ambient temperature, K
$\frac{\Delta T}{\Delta i}$	Temperature glide, K·kg/kJ
U	Overall heat transfer coefficient, W/m^2K
V	Average velocity, m/s
We	Two-phase Weber number
$\dot{W}$	Work output, W
X	Martinelli parameter
X_c	Correlation factor
x	Vapor fraction
Z	Abbreviated equation

Greek symbols

η_{is}	Isentropic efficiency
η_{mech}	Mechanical efficiency
μ	Dynamic viscosity, kg/ms
ν	Kinematic viscosity, m^2/s
ρ	Density, kg/m^3
ρ_{tp}	Homogeneous density, kg/m^3
σ	Surface tension, J/m^2
ϕ_{lo}^2	Two-phase multiplier

Subscripts

av	Average
bub	Bubble point
cb	Convective boiling
$cond$	Condenser
$crit$	Critical point
dew	Dew point
fit	Best fit
HP	High pressure
$HRHE$	Heat recovery heat exchanger
i	Tube inside
in	Inlet
is	Isentropic
IHX	Internal heat exchanger
l	Liquid
lo	Liquid only
LP	Low pressure
n	Enthalpy interval
Nb	Nucleate boiling
Nb^*	Nucleate boiling
net	Netto
o	Tube outside
out	Outlet
$pool$	Pool boiling
sat	Saturated state
$sink$	Water heat sink
$source$	Air heat source
tot	Total
v	Vapor
vo	Vapor only, $G_{vo} = xG$
wf	Working fluid
1	High pressure side of IHX
2	Low pressure side of IHX

Abbreviations

$AMTD$	Arithmetic mean temp. difference, ℃
$HRHE$	Heat recovery heat exchanger
HTC	Heat transfer coefficient
HX	Heat exchanger
IHX	Internal heat exchanger
$LMTD$	Logarithmic mean temp. difference, ℃
Max	Maximum
Min	Minimum

LIST OF FIGURES

LIST OF TABLES

1 INTRODUCTION

1.1 Motivation

An increasing interest to lessen greenhouse gas emissions has prompted a number of industry initiatives to improve energy efficiency of industrial processes. SINTEF Energy, along with several industry partners, is currently involved in a project that aims at improving the performance of Rankine cycle technology for electricity production from low temperature surplus heat. Improvement and implementation of such technology will enable reduced specific electricity consumption for industry partners.

Satisfactory cost efficiency of Rankine cycles is currently challenging in the low temperature region (100℃ to 250℃), which reduces the attractiveness of cycle implementation. The motivation for the current work is to investigate the possibility for improvement in cycle work output with the use of working fluid mixtures instead of pure fluids. At the same time, it is desirable to compare different working fluids based on similar component sizes, or costs. Comparison on the basis of equal total HX surface area can provide a more fair basis for comparison than conventional “pinch-point analysis”, as total HX area can to some degree be indicative of HX costs. Hydrocarbons are considered as working fluids due to their low global warming potential, and because the projects aims at developing green technology.

The project work suggested that it is possible to achieve higher work output with mixtures compared to pure fluids for the same total heat exchanger. However, percentage improvements were low, and significant area was required for the mixtures to outperform the pure fluids. The motivation for the master thesis therefore is to investigate conditions under which mixtures may significantly outperform pure fluids, and to improve the cycle and optimization model developed in the project work.

1.2 Objectives and scope

Task 1: A literature survey on heat transfer and pressure loss of working fluid mixtures is performed in Chapter 3 in order to research and implement correlations suited for hydrocarbons. The literature survey is limited to smooth, fully developed flow through tubes. The studied correlations are summarized and evaluated for implementation in Section 5.1.2. The implemented condensation correlation is studied and compared to the correlation used in the project work in the discussion, Section 9.6. Less focus is given to the evaporation correlations both due to time limitations and the fact that 4 out of 5 fluids studied are transcritical (and do not evaporate in the HRHE).

Task 2: The effect of mixture vs. pure fluid on HX design is studied by comparing optimum pressure loss, pinch points, number of tubes and tube diameters in the HXs. The results for this is given in Section 8.1.1 and 8.2.1, and discussed in Section 0 and 9.3.3. Furthermore, HX design is evaluated by comparing distributions between condenser and HRHE (and IHX) area. The results for this is given in Section 8.1 and 8.2, and discussed in Section 0 and 0.

Task 3: The model used in the project work is further developed through implementation of new heat transfer correlations from task 1, and through other smaller adjustments that may improve model accuracy. The optimization model and its adjustments is explained in Chapter 6. Cycle parameters, HX theory and geometry from Chapter 4 and 5 is implemented in the model. Moreover, the optimization model is developed to include the option of an internal heat exchanger, as explained in the optimization model chapter in Section 0 , with HX geometry from Section 5.3.1.

Task 4: In Chapter 4, four cases are defined that are relevant for present and future applications of Rankine cycles. The cases include different constraints on heat source and heat sink temperatures, and one of the cases includes the use of an internal heat exchanger.

Task 5: The selected cases are investigated with the updated model, and results for the different cases are given in Chapter 8. Relevant pure fluids and mixtures are selected through a pinch point screening in Chapter 7. The cases are discussed and compared under a whole, including the project work case, in the discussion, Section 9.4.

2 BACKGROUND THEORY

2.1 The Rankine cycle

The Rankine cycle is a thermodynamic process for heat to power conversion. The process operates between two thermal reservoirs, commonly referred to as the heat source and the heat sink. The cycle consists of four main components as sketched in Figure 2-1, including a pump, expander, heat recovery heat exchanger (HRHE) and condenser. Power production is achieved by circulating a working fluid through the components, illustrated with green arrows in the figure. The cycle can be plotted in a temperature-enthalpy diagram, as in Figure 2-2.

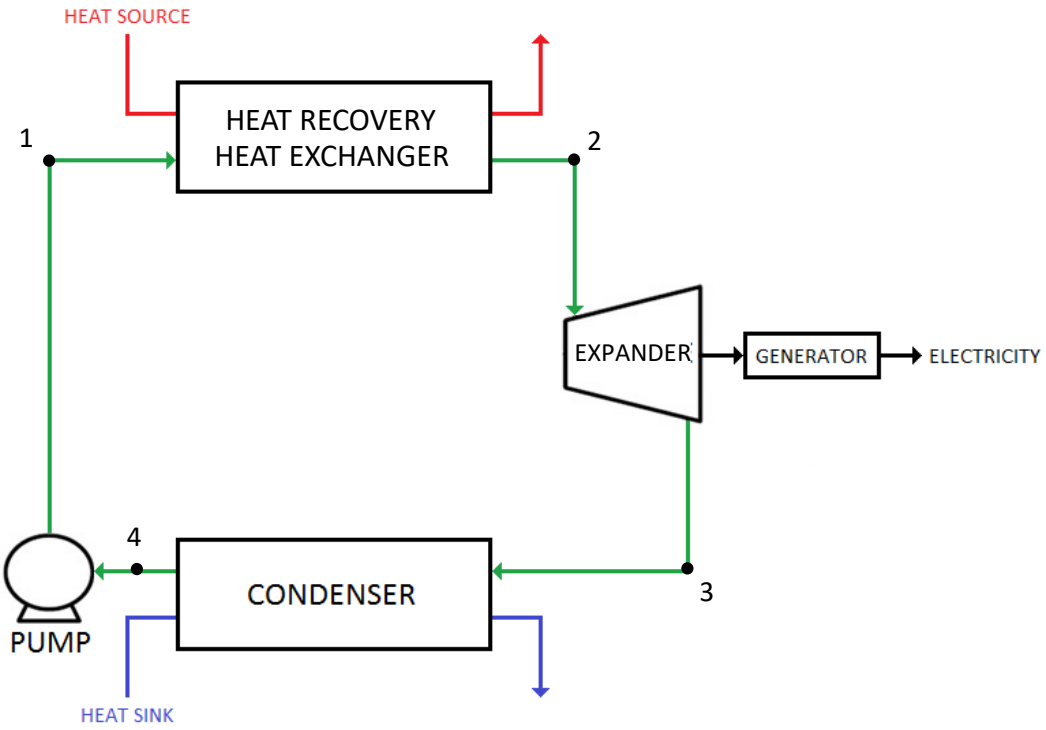

Figure 2-1 Principle sketch of the Rankine Cycle.

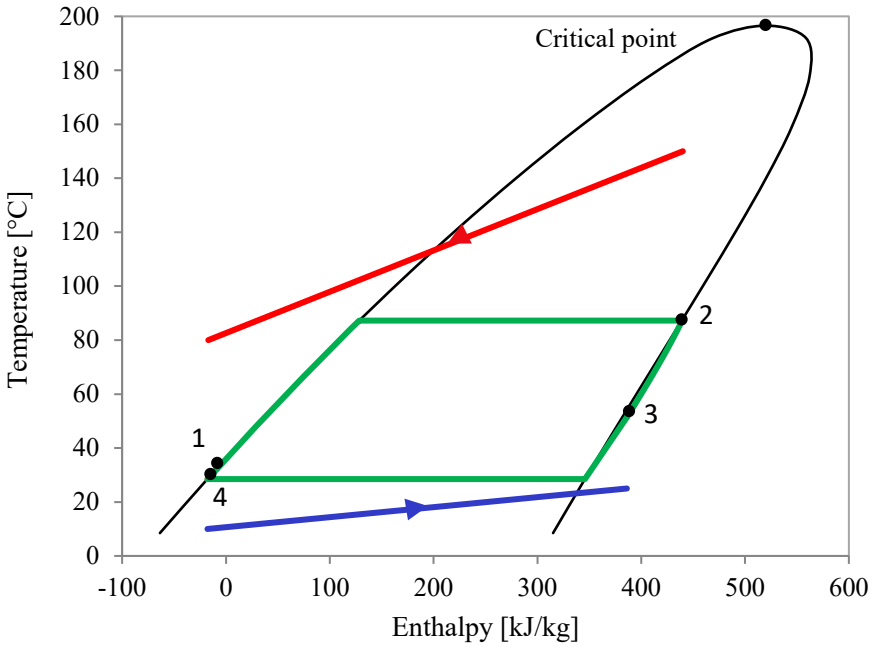

Figure 2-2 Temperature-enthalpy diagram of a Rankine cycle.

The state points and component processes are recognized in Figure 2-2, where 1-2 is the heat receiving process in the HRHE, 2-3 is the expansion process, 3-4 is the heat rejection process in the condenser and 4-1 is the pumping process. Also shown is the heat source in red and the heat sink in blue with arrows to indicate the direction of enthalpy change. The black curve is the phase envelope of the working fluid, and the black mark at the top of the phase envelope is the critical point of the working fluid. The cycle may also be transcritical, for which the heating process takes place above the critical pressure.

2.1.1 Internal heat exchanger (IHX)

A principle sketch of a Rankine cycle with IHX is shown in Figure 2-3. The “low pressure side” (LP) of the IHX refers to points 3-4 and the “high pressure side” (HP) refers to points 6-1.

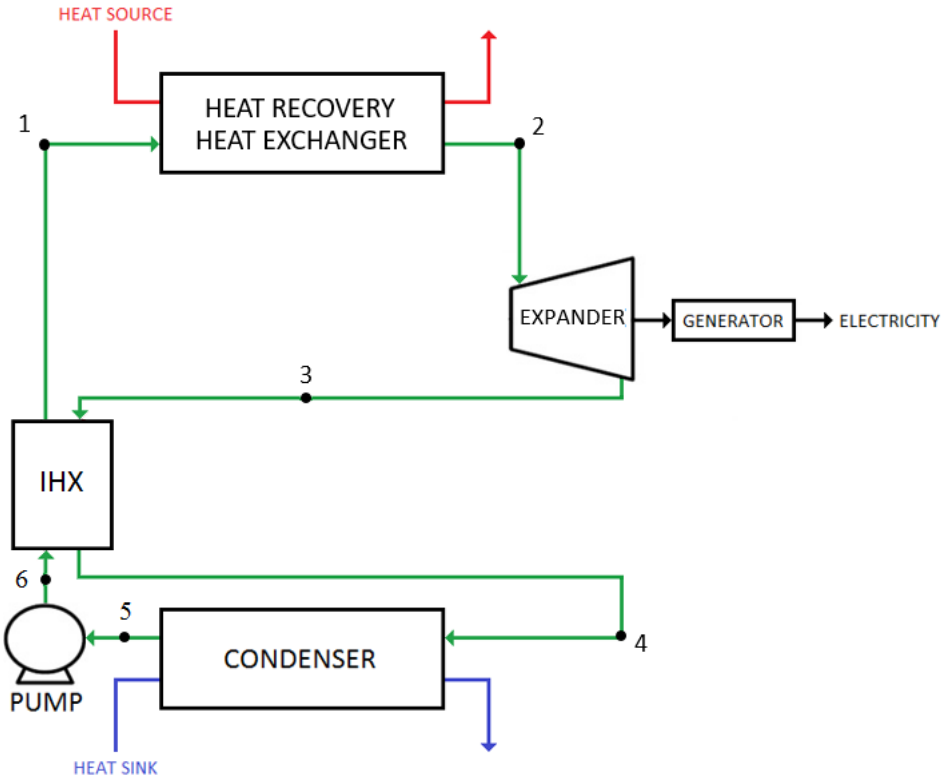

Figure 2-3 Principle sketch of an internal heat exchanger in a Rankine cycle.

2.2 Use of working fluid mixtures

A number of research papers, in addition to the project, work has shown that it is possible to increase the cycle work output by using working fluid mixtures. This is possible due to the ability of mixtures to condense and evaporate at gliding temperatures. This allows for lower temperature differences in the heat exchangers and reduced heat exchanger exergy losses. Exergy refers to the maximum potential for power production from a system. There is a well-established connection between high HX temperature differences and high exergy loss, meaning that high temperature differences reduce the potential for power production.

Examples of temperature-enthalpy diagrams of a transcritical pure fluid and a transcritical mixture are given in Figure 2-4 and Figure 2-5. The pumping process is difficult to observe, as the temperature increase is relatively low.

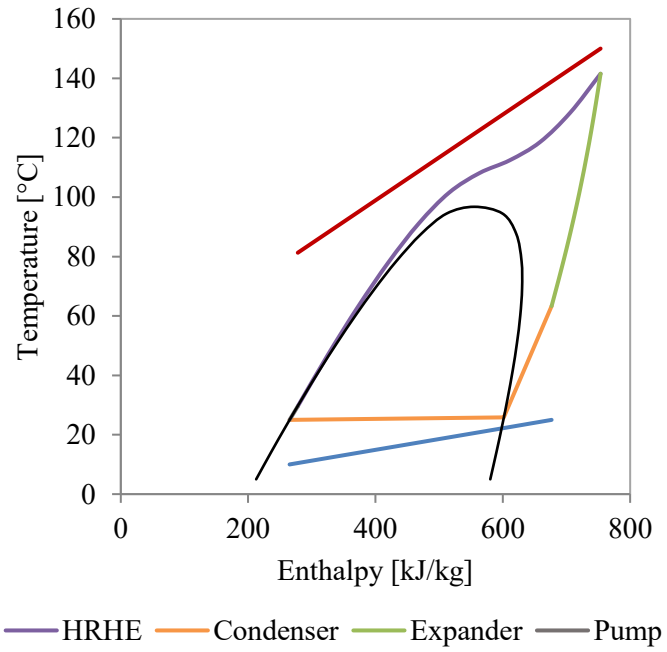

Figure 2-4 Temperature-enthalpy diagram for a transcritical pure working fluid.

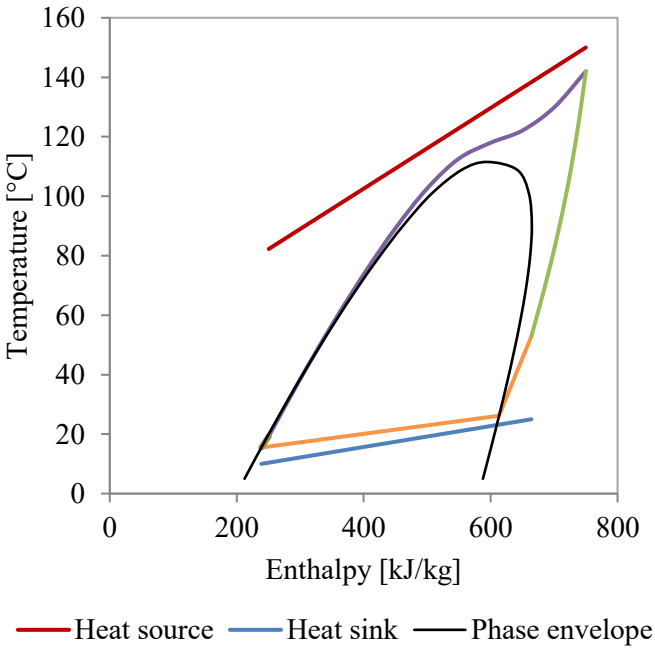

Figure 2-5 Temperature-enthalpy diagram for a transcritical working fluid mixture.

2.3 Condensation and evaporation of mixtures

A working mixture between two components condenses and evaporates at gliding temperature due to the difference in boiling points between the two components. The difference in bubble and dew point temperature of the mixture is commonly referred to as its temperature glide. Concentration differences also arise during heat transfer, leading to a mass transfer resistance and a resulting reduction in HTC compared to what one would expect from interpolation between the pure fluid components.

It is challenging to predict HTCs during phase change of both pure fluids and mixtures. Methods for calculating HTCs of mixtures are less researched than methods for pure fluids, and are subject to the difficulty of calculating mass transfer resistance. Several methods have been proposed, with different assumptions and degrees of complexity. A typical distinction is made between equilibrium and non-equilibrium models, where the former assumes equilibrium between liquid and vapor phase. Moreover, models are typically distinguished between empirical (developed based on experimental data), and "physical" (developed by solving conservation equations such as the mass and energy balances). The latter are often more numerically challenging and time consuming to both implement and solve.

3 LITERATURE REVIEW ON MIXTURES

The following is a literature survey on models for predicting heat transfer coefficients and pressure loss of working fluid mixtures during condensation and evaporation through horizontal smooth tubes.

3.1 Condensation

There are three common ways of calculating the HTC of working fluid mixtures during condensation: The equilibrium method by Bell and Ghaly (1973), the non-equilibrium film method by Colburn and Drew (1937) and empirical methods that adjust pure fluid correlations (Macdonald 2015).

The Bell and Ghaly (1973) model is an annular equilibrium method that corrects a pure fluid correlation for mass transfer resistance in the vapor phase. The mass transfer resistance, resulting from preferential condensation of the less volatile component, is estimated with the sensible heat transfer resistance in the vapor phase, enabling the HTC to be expressed as the following:

$$h = \left(\frac{1}{h_{pure}} + \frac{x c_{p,v}}{h_v} \cdot \frac{T_{bub} - T_{dew}}{i_{bub} - i_{dew}} \right)^{-1} \tag{3-1}$$

h_{pure} is the pure fluid HTC, h_v is the vapor phase HTC, and the term $\frac{x c_{p,v}}{h_v} \cdot \frac{T_{bub} - T_{dew}}{i_{bub} - i_{dew}}$ accounts for mass transfer resistance. The HTC reduces with increasing temperature glide, $T_{bub} - T_{dew}$, such that fluids with higher glides are subject to a higher heat transfer penalty. The authors describe the method as simplified and conservative, referring to experimental research for which the predicted HX area was up to 100 % more than calculated area. The method was implemented in the project work and combined with the pure fluid correlation for condensation of steam by Boyko and Kruzhilin (1967).

To improve accuracy of the Bell and Ghaly model for hydrocarbon working fluids, a pure fluid correlation developed for hydrocarbons might be used. This was done by Macdonald and Garimella (2016a), who analyzed mixtures of ethane and propane with mid-range temperature glides (6-13°C), mass fluxes from 150 kg/m^2s to 450 kg/m^2s. Tube diameters of 7.75 and 14.45 mm were studied, and reduced pressure varied from 0.46 to 0.87. The authors emphasized a lack of research on mixtures with mid-range temperature glides, and reported that in the low

temperature glide region (up to 6℃), experimental research has demonstrated reductions in HTCs compared with pure fluids. They adopted the pure fluid correlation developed for propane and pentane by Macdonald and Garimella (2016c), and found that 100 % of the HTCs were predicted to within $\pm$ 25 % accuracy compared to the experimentally measured values. The average deviation for all data was + 3.4 %, with an absolute average deviation of 8.5 %. Their experimental measurements showed that mixture HTCs reduced the most compared to pure fluids at low mass fluxes and high temperature glides, where low mixing and high temperature differences, respectively, result in higher concentration gradients.

Alberto Cavallini et al. (2002b) developed a new, simplified pure fluid condensation method for halogenated fluids and combined it with the Bell and Ghaly model to predict mixture HTCs. The model divides the flow into two categories, "ΔT-dependent" and "ΔT-independent", where ΔT refers to the temperature difference between the fluid and the wall. ΔT-dependent flows are dominated by gravity forces (i.e. stratified flows), whereas ΔT-independent flows are dominated by vapor shear forces (i.e. annular flows). The model is valid for tube diameters between 3 and 21 mm, $p_R < 0.75$ and $\frac{\rho_v}{\rho_l} < 4$. The authors reported the relative contribution of the mass transfer resistance, $\frac{xc_{p,v}}{h_v} \cdot \frac{T_{bub}-T_{dew}}{i_{bub}-i_{dew}}$, to the total thermal resistance, $\frac{1}{h}$, for two mixtures. They condenser through a 8.52 mm tube at a vapor quality of 0.5, 200 kg/m^2s mass flux and a mean saturation temperature of 40℃. For the mixture R-407C with a temperature glide of 5℃, the term contributed between 10-15 % of the total resistance. For propane-butane (0.5/0.5), with more than double the temperature glide (12.8℃), the contribution was higher and in the range 25-28 %. Furthermore, comparison between experimental and predicted Nusselt numbers for R-407C demonstrated an underestimation at high Nusselt numbers. The Nusslet number is a function of HTC, and therefore the deviation between experimental and predicted Nusselt numbers is somewhat representative for the same deviation for the HTC. The average deviation was – 2.2 %, and absolute average deviation was 10.4 %. It was suggested by the authors that the Bell and Ghaly model might penalize the HTC at high mass fluxes, where mixture effects are less predominant.

Del Col et al. (2005) modified the Bell and Ghaly model to account for non-equilibrium effects in the stratified flow regime and interfacial roughness between the vapor and liquid phases. The modification was developed based on two experimental datasets of synthetic refrigerants and was combined with the pure fluid, flow pattern model by Thome et al. (2003). Thome considered stratified, stratified-wavy, intermittent, annular and mist flow regimes. The experiments were performed on a 8 mm diameter tube with mass fluxes ranging from 100

kg/m^2s to 750 kg/m^2s, and temperature glides from 5 to 22℃. The model predicted 98 % of the experimental datasets to within $\pm$ 20 % accuracy.

Del Col et al. (2005) also tested the model on two independent experimental datasets, one with three halogenated mixtures and another with three hydrocarbon mixtures between propane and butane. The hydrocarbon experiments were performed on a 8 mm diameter tube, with saturation temperatures between 44℃ and 55℃, temperature glides between 4.6℃ and 6.5℃ and mass fluxes between 56 kg/m^2s and 191 kg/m^2s. The model was less accurate for the independent datasets, and predicted 85 % of the HTCs to within $\pm$ 20 % accuracy. The hydrocarbon HTCs were slightly overestimated, with an average deviation of + 9.6 %. Overall, the predictive performance of the model did not vary significantly with vapor quality, mass flux, flow regime or temperature glide. It was also found that physical properties did not vary with changes in composition of vapor and liquid phases. The authors conclude that predicted values have satisfactory agreement with experimental results, and that the method is less computationally challenging than those involving solutions of conservation equations.

The experimental hydrocarbon data of the study by Del Col et al. originates from Chang et al. (2000). They measured significant reductions in HTCs for mixtures compared with pure fluids, caused by mass transfer resistance as well as nonlinear property variations. The authors modified a pure fluid correlation by Shah (1979) to fit their hydrocarbon data, which achieved an accuracy of $\pm$ 20 % for most data with an average deviation of + 6.4 % for the mixtures and + 8.9 % for pure fluids.

Han Deng (Deng 2016) did an in depth study of different design models for in-tube mixture condensation in her doctoral thesis on boiling and condensation of mixtures. She compared the equilibrium models by Alberto Cavallini et al. (2002b) and Del Col et al. (2005) to six experimental datasets with a wide range of operating conditions, including temperature glides from 3.5℃ and 48.5℃ and tube diameters from 0.96 mm to 8 mm. She found that the model by Del Col et al. (2005) predicted most HTCs with satisfactory accuracy, but underestimated data for hydrocarbons at high reduced pressure. The average prediction of the model by Alberto Cavallini et al. (2002b) was found to have high accuracy, but slightly overestimated low HTCs and underestimated high HTCs.

Han Deng developed a new, simplified condensation model for mixtures based on the models by Alberto Cavallini et al. (2002b) and Del Col et al. (2005). The model employs the pure fluid correlation by Alberto Cavallini et al. (2002b), as their flow pattern model is easier to implement than that of Del Col et al. (2005). The accuracy of the model by Alberto Cavallini et al. (2002b) is improved by applying the modified Bell and Ghaly resistance developed by

Del Col et al. (2005). The model was able to predict more than 85 % of the HTCs in the six datasets to within $\pm$ 20 % accuracy, with average deviations from – 9.3 % to + 8.5 %. The ratio of calculated to experimental HTC did not vary significantly with vapor quality, mass flux or flow pattern, and was mostly within 0.8 to 1.2. Like the model by Del Col et al. (2005), the model slightly overestimated the hydrocarbon data by Chang et al. (2000), for which it also had a poorer predictive performance for lower range mass fluxes. The model did, however, manage to better predict the hydrocarbon HTCs at high reduced pressure. The predictive performance with temperature glide was not tested, and the author stressed the empirical nature of the model and its inability to represent all working conditions and experimental setups.

Han Deng further tested her model by performing an experimental study on condensation of R32/R1234ze(E) (0.25/0.75) inside a 8 mm diameter tube. Mass fluxes ranged from 101 kg/m^2s to 595 kg/m^2s and vapor qualities ranged from 0.24 to 1. Most HTCs were predicted to within $\pm$ 20 % accuracy, but underestimation was observed for mass fluxes of 100 kg/m^2s and overestimation was observed for mass fluxes of 200 kg/m^2s. She found that her model did not predict the experimental data with a significantly improved accuracy compared to the model by Del Col et al. (2005) or Alberto Cavallini et al. (2002b).

In the model by Colburn and Drew, the equations of mass conservation, heat transfer and mass transfer are solved iteratively for a liquid film flowing uniformly around the tube wall. The method models non-equilibrium between the liquid and vapor phases, and calculates the mass transfer resistance in the vapor phase directly (and not though estimation). Webb et al. (1996) claimed that the film method is more generally applicable than the Bell and Ghaly method, and A. Cavallini et al. (2002a) referred to research showing that the Bell and Ghaly method, although accurately predicting average HTCs, does not satisfactorily predict local HTCs. However, the film method is described as more complicated than the Bell and Ghaly method due to coupling of equations, which results in a “cumbersome” code implementation (Macdonald 2015). Macdonald (2015) found that the accuracy of the Bell and Ghaly method was satisfactory for reduced pressures above 0.4, but the film method was necessary for lower reduced pressures, as the influence of temperature glide was overestimated by Bell and Ghaly in this region.

A. Cavallini et al. (2002a) studied the film method by Colburn and Drew, combined with the pure fluid correlation for annular flow by Alberto Cavallini and Zecchin (1974). The predictive performance of the model was investigated by comparing experimental HTCs to calculated HTCs. The experiment involved a mixture between R-125 and R236ea, condensing through a 8 mm diameter tube at different mixture compositions, mass fluxes of 400 kg/m^2s

and 750 kg/m^2s and temperature glides on the order of 20℃. Inlet pressures varied between 0.8 and 1.4 MPa and saturation temperature varied between 40℃ and 60℃. Most HTCs were predicted to within $\pm$ 20 % accuracy, with a mean absolute deviation of 8.7 %.

Other authors have made similar models to that of Colburn and Drew (1937), by formulating and solving the conservation equations. For instance, Jin et al. (2003) developed a non-equilibrium model for annular flow, accounting for mass transfer resistance in both liquid and vapor phases. The liquid film HTC was calculated with a correlation by Shah (1979), and the heat and mass transfer equations were formulated and solved iteratively. The model was evaluated for an experimental dataset of mixtures between R134a and R123, condensing in a 8.4 mm diameter tube with temperature glides of around 26.0℃. HTCs were measured for different mass fluxes (200 kg/m^2s and 300 kg/m^2s), mixture compositions and inlet pressures (0.5-1.4 MPa). The model was able to predict the experimental HTCs with a mean deviation of 10.3 %, and most data was predicted to within $\pm$ 20 % accuracy. The predictive performance was consistent for vapor qualities between 0.9 and 0, but the model appeared to underestimate HTC at vapor qualities higher than 0.9. Vapor side mass transfer resistance was found to dominate upstream in the heat exchanger, while liquid side mass transfer resistance dominated downstream. The author recommended that models should include the liquid side mass transfer resistance for improved predictive performance.

Kim (1998) solved the equations of continuity, momentum, energy and mass transfer for a turbulent, liquid film condensing along the tube wall. The problem formulation resulted in eleven equations with eleven unknowns, which were solved using the explicit finite difference method. The HTC calculated with this method was compared to an experimental value for a mixture between R22 and R114, with an inlet pressure of 1.22 MPa and a mass flux of 170 kg/m^2s. The HTC was calculated at a pressure of 1.08 MPa and a mass flux of 283 kg/m^2s, and obtained "good" agreement with the experimental results at varying mass quality. No record was given on the accuracy of the model, but from observation of a graph in the paper, the experimental HTC appears to be overestimated by around 75 %. The reason for the poor accuracy may be that the HTC was calculated for other operating conditions than the measured HTC. Nevertheless, the accuracy of this method is relatively low, despite its numerical complexity.

3.2 Evaporation

Chang et al. (2000), who developed an empirical correlation for condensation, also studied evaporation of hydrocarbon mixtures. They performed experiments on evaporation of propane, butane, isobutene and propylene, as well as mixtures between propane and butane/isobutane. Recall that the fluids evaporated through a 8 mm diameter tube, with saturation temperatures from 44 to 55℃, temperature glides from 4.6 to 6.5℃ and mass fluxes from 56 to 191 kg/m^2s. The authors modified a pure fluid correlation by Wattelet et al. (1993) to fit their experimental data, and incorporated a theoretically developed correction factor for mixtures as suggested by Thome (1989). The Thome correction factor was developed based on flow boiling inside vertical tubes at low quality. It has been shown to accurately predict HTCs for different mixtures, including hydrocarbons. The method achieved a mean deviation of 14.7 % for the mixtures. In both the study by Chang et al. (2000) and Thome (1989), the HTC was reduced compared with pure fluids, and Thome explained that this was mainly caused by the effect of mass transfer resistance on nucleate boiling.

Zou et al. (2015) studied the predictive performance of several models used to calculate HTCs of evaporating mixtures between ethane and methane. The calculated HTCs were compared to a database of evaporating ethane/methane mixtures at varying compositions, saturation pressures from 0.35 to 0.65 MPa, heat fluxes from 10 to 60 kW/m^2, and mass fluxes from 113 to 260 kg/m^2s. A model proposed by Zou et al. (2010) was adapted by the authors to better predict the experimental HTCs of the mixtures. In the model, the pure fluid HTC is calculated as a combination of a convective boiling contribution and a nucleate boiling contribution. An empirically developed mixture correction factor is multiplied with the nucleate contribution to account for mass transfer resistance. Of all the models studied by the authors, the adapted model achieved the lowest mean absolute deviation (27.8 %) and root mean square deviation (33.5 %) between the predicted and experimental data. Some of the higher HTCs were under predicted.

Zou et al. (2015) also tested the predictive performance of the pure fluid model of Gungor and Winterton (1986), combined with the Thome correction factor for mixtures (Thome 1996). The Gungor and Winterton correlation is a general correlation for forced convective boiling, developed based on data for seven different fluids, from 28 authors. The fluids considered were water, synthetic refrigerants and alcohols. The method achieved a mean average deviation as high as 91.8 %, and a root mean square deviation of 111.5 %. Most HTCs were over predicted, and significant portions of the calculated HTCs were more than 60 % higher than the measured

value. A similar approach was applied in the project work, where both Gungor and Winterton's model and the Thome correction factor was used. In addition to the Thome correction factor, the Bell and Ghaly condensation method was used to correct the pure fluid HTC, as suggested by Sardesai et al. (1982). This approach was described by Thome (1998) in his report on boiling and evaporation of refrigerants. There is no available data on the accuracy of this method compared to experimental values.

Shah (2015) also proposed a method that involves both the Bell and Ghaly correction factor and the Thome (1996) correction factor. The Bell and Ghaly correction is applied to the convective contribution of a pure fluid correlation, while the Thome correction is applied to the nucleate boiling contribution. The author explained that the phenomena involved in convective boiling are similar to those involved in condensation, and that therefore the Bell and Ghaly method could be applicable to convective boiling as well. He compared the new method with an approach where only the Thome correction factor was applied to the nucleate boiling contribution. The model was tested with several pure fluid correlations to study the effect on predictive performance. Calculated HTCs were compared to data from 21 studies on 45 different mixtures, including halocarbons, hydrocarbons, nitrogen and carbon dioxide. Tube diameter ranged from 0.19 to 14 mm, mass fluxes from 50 to 930 kg/m^2s, reduced pressure from 0.05 to 0.63 and temperature glides up to 156℃. For all experimental data except that on LNG, the proposed method had a lower mean deviation than that involving only the Thome correction factor. The pure fluid correlation yielding the lowest mean deviation was that of Shah (1982), with a mean deviation of 19.5 %. The pure fluid correlation is a "chart" correlation based on graphical data, and is not very straightforward to implement in computer codes.

Two other pure fluid correlations studied by Shah (2015) gave deviations in the same order as by Shah (1982); that of Liu and Winterton (1991) (20.4 %) and Gungor and Winterton (1987) (20.7 %). The former requires both the unknown quantities of heat flux and wall temperature, whereas the latter requires only heat flux, and is an improvement and simplification by Gungor and Winterton of the model they developed in 1986. The mentioned pure fluid correlations were recommended for mixtures with glides up to 30℃. The predictive performance of the model was insensitive to variations in different parameters, such as tube diameter and temperature glide.

Like Zou et al. (2015), Barraza et al. (2016) studied the predictive performance of several methods for calculating mixture HTCs. The methods were intended for use in cryogenic applications. They compared the calculated HTCs with experimental data for several mixtures; a binary mixture between methane and ethane, a tri-component mixtures between methane,

ethane and propane, and a tri-component mixtures of synthetic refrigerants. The binary mixtures evaporated through small tubes of 0.5, 1.5 and 3 mm diameter, with bubble point temperatures of 132 K and 155 K and a temperature glide of 53 K. The authors found that pure fluid correlations were unsuited to predict mixture HTCs. A mixed fluid correlation by Granryd (1991) predicted the experimental data most accurately, with an absolute average deviation of 16 %, and 83 % of the data predicted to within 25 % relative error. The correlation is based on annular flow and valid for different operating conditions. However, it is less accurate at low qualities where annular flow is less likely to be present. A relatively high error is observed for high Nusselt numbers, where partial dryout occurs. Furthermore, the model was validated for an evaporating mixture of R22 and R144.

3.3 Frictional pressure loss

Jung and Radermacher (1989) studied the influence of mixture composition on pressure loss during annular flow boiling, and found no dependence. In fact, studies on working fluid mixtures tend to use pure fluid pressure loss correlations. Two such correlations are discussed in the following.

According to Macdonald and Garimella (2016c), the most common techniques for modelling two-phase pressure loss is to calculate the frictional pressure loss gradient as a multiple or fraction of the single phase pressure loss gradient:

$$\frac{dp}{dz} = \phi_v^2 \left(\frac{dp}{dz}\right)_v = \phi_l^2 \left(\frac{dp}{dz}\right)_l = \phi_{lo}^2 \left(\frac{dp}{dz}\right)_{lo} \tag{3-2}$$

Several methods have been proposed to calculate the two phase multiplier, ϕ. The methods are either empirically developed, or developed based on physical principles and hence relatively tedious to implement in design codes. Older empirical methods performe poorly outside the conditions for which they were developed, whereas newer empirical methods include factors that make them more applicable over a broader range of operating conditions. Such a new empirical method was developed by Macdonald and Garimella (2016c) based on a database of condensing propane. Compared to two other models, the new model achieved the lowest average deviation (3 %) and absolute average deviation (18 %) between calculated and measured data. Furthermore, the model predicted pressure loss more accurately for changes in saturation pressure and tube diameter. The method was also validated for data on condensation of other pure fluids and mixtures, with absolute average deviations ranging from 16-26 %.

A similar pressure loss model, which was used in the project work, is that by Friedel (1979), who developed an empirical method for calculating the two-phase multiplier. In his model, the multiplier was curve-fitted to an experimental dataset of 25 000 measurements on pressure loss for air-water and air-oil flows. The model was developed for a dataset involving a broad range of operating conditions, including mass fluxes from 7 to 4500 kg/m^2s and tube diameters from 4 to 200 mm (Aakenes 2012).

Müller-Steinhagen and Heck (1986) compared the Friedel method to an experimental dataset of 9300 measurements on pressure loss for different flow conditions and fluids, including water, R12 and argon. The absolute mean deviation between measured and predicted data was 111.6 %, and was clearly higher than a number of other models studied by the authors. The high deviation was mainly caused by an over estimation of the pressure loss at low vapor qualities and a poor prediction for high viscosity ratios μ_l/μ_v. Filip et al. (2014) also tested the Friedel method, and found that it predicted most of the data on pressure loss of condensing isobutene to within $\pm$ 30 % of the measured value. The latter study included a limited number of experiments (8), over a narrow range of flow conditions.

3.4 Acceleration pressure loss

Acceleration pressure loss represents the change in kinetic energy of the fluid during phase change. As with frictional pressure loss, the acceleration pressure loss of a fluid is not affected by the presence of a second component. During evaporation, the kinetic energy increases, resulting in a corresponding acceleration pressure loss from inlet to outlet. During condensation, the kinetic energy decreases, resulting in a corresponding pressure increase from inlet to outlet. Not all the kinetic energy change is realized in pressure increase during condensation, and therefore this effect is normally ignored, which achieves a conservative condenser design (Thome 2006). It is also common to neglect the acceleration pressure loss during evaporation, as frictional pressure loss typically dominates (Radermacher and Hwang 2005). A method for calculating the acceleration pressure loss during phase-change has been outlined by Thome (2006).

3.5 Summary

The different methods for predicting condensation HTCs are summarized in Table 5.2. Section 5.1.2.1 includes a brief evaluation of which correlations to implement, and the equations for the two top candidates are given in Table 5-3.

A number of the studies on condensation have demonstrated decreases in HTCs compared to pure fluids, and some suggest a greater heat transfer penalty for higher temperature glides. In general, there are quite a few methods for predicting HTCs of working fluid mixtures, and they are developed on different theoretical grounds. Some are empirical, whereas others are "physical" and developed based on conservation equations. The latter are more tedious to implement, and in some cases need to be solved numerically. Moreover, some methods are developed and tested for a broad range of tube diameters, mass fluxes, temperature glides and pressures, while others consider few tube diameters and operating conditions. Common for many of the methods is that a significant number of HTC are predicted to within $\pm$ 20 % accuracy compared to experimental values. Furthermore, there is no apparent connection between correlation complexity and predictive performance, and there is no broad consensus for the most suitable method to apply.

One of the most common methods for condensation, the Bell and Ghaly method, has been proven inaccurate under certain operating conditions. Several authors have modified and applied the method, without significant improvement in predictive performance compared to previous studies on the same method. The numerical method by Colburn and Drew has been suggested as an alternative to the Bell and Ghaly method where this fails to predict HTCs.

The different methods for predicting evaporation HTCs are summarized in Table 5-4. Section 0 includes a brief evaluation of which correlations to implement, and the equations for the two top candidates are given in Table 5-5.

The studies on evaporations consider different methods for predicting mixture HTCs. The Thome correction factor is used in 4 out of 6 studies, and appears to be a common method for predicting HTCs during evaporation of mixtures. By analogy with condensation, some studies apply the Bell and Ghaly correction factor to a convective boiling contribution term in the correlation. In general, predictive performance appears to be poorer for evaporation models that

for condensation models, which could be explained by the complex physical nature of nucleate boiling.

Frictional pressure loss and acceleration pressure loss is calculated similarly for mixtures and pure fluids. A common way of calculating the frictional pressure loss gradient is to multiply the one-phase pressure loss gradient with a two-phase multiplier. Newer empirical methods have been modified to predict the pressure loss gradient accurately across a range of operating conditions, and serve as feasible alternative to more tedious, physical models. Furthermore, it is common to neglect acceleration pressure loss, as this typically accounts for a low fraction of total pressure loss.

4 CASES AND CYCLE STATE POINTS

4.1 Cases and constraint conditions

Different cases are defined that determine the inlet and outlet temperatures of a water heat sink and an air heat source, and whether or not an option for IHX is included in the cycle. The cases are given in Table 4-1 to Table 4-4.

Table 4-1 Case 1:
Low temperature heat source with fixed heat sink outlet temperature.

	Heat source	Heat sink
T_{in}	100°C	10°C
T_{out}	Optimized	25°C

Table 4-2 Case 2:
Low temperature heat source with optimized heat sink outlet temperature.

	Heat source	Heat sink
T_{in}	100°C	10°C
T_{out}	Optimized	Optimized

Table 4-3 Case 3:
"High" temperature heat source with lower limit on heat source outlet temperature.

	Heat source	Heat sink
T_{in}	200°C	10°C
T_{out}	80°C	25°C

Table 4-4 Case 4:
"High" temperature heat source with lower limit on heat source outlet temperature and IHX.

	Heat source	Heat sink
T_{in}	200°C	10°C
T_{out}	80°C	25°C

Case 1 and 2 both have heat source inlet temperatures of 100°C, and no lower limit is set on heat source outlet temperature. In case 1, inlet and outlet temperatures of the heat sink is fixed, whereas in case 2, the outlet temperature of the heat sink is allowed to vary. Case 2 is only briefly studied, as the condenser model is developed based on fixed heat sink outlet temperature. Case 1 and 2 may resemble present applications of Rankine cycles in offshore gas processing, where compressed gas can be cooled in a Rankine cycle with no lower limit on heat source outlet temperature. The cases can also be relevant for present applications of ground heat sources.

Case 3 and 4 has a heat source inlet temperature of 200°C, and the heat source can be cooled to 80°C. The use of an internal heat exchanger is particularly relevant for cases with lower limits on heat source outlet temperature, and is studied in case 4. Case 3 and 4 may be relevant for

future applications of Rankine cycles is aluminum production, where the heat source temperature has been upgraded to a higher temperature but still has a lower limit on outlet temperature to obtain efficient gas cleaning and to avoid temperatures below acid dew point.

4.2 Calculating cycle state points

An Excel model received by SINTEF Energy has been modified and used to calculate cycle state points, and REFPROP is used to calculate working fluid properties. Calculation of state points is necessary to calculate work output for the different cases, and to be able to maximize that work output with the Excel problem solver.

State points 1 through 12 in Figure 4-1 are determined from the parameters in Table 4-5, in combination with component energy balances. Heat loss is neglected throughout. A detailed outline of this procedure, as well as calculation of heat loads and pump work can be found in the project thesis. The work output is given by the following equation:

$$\dot{W}_{net} = \dot{W}_{expander} - \dot{W}_{pump,wf} - \dot{W}_{pump,sink} \quad (4\text{-}1)$$

For the inclusion of IHX, the cycle state points are modified in the following way:

- Expander outlet state point becomes IHX (LP) inlet state point.
- Condenser inlet pressure is reduced with the IHX (LP) pressure loss.
- Condenser inlet enthalpy is reduced with the IHX enthalpy change.
- Condenser outlet state point becomes IHX (HP) inlet state point.
- HRHE inlet pressure is reduced with the IHX (HP) pressure loss.
- HRHE inlet enthalpy is increased with the IHX enthalpy change.

Table 4-5 Parameters for calculating cycle state points.

Working fluid	Heat source	Heat sink	Efficiencies
$\dot{m}_{wf}$ $p_{in,HRHE}$ $T_{out,condenser}$ $i_{out,HRHE}$ $\dot{Q}_{IHX}$ Δp_{HRHE}, Δp_{cond} $\Delta p_{IHX,HP}$, $\Delta p_{IHX,LP}$	Air $\dot{m}$ = 5 kg/s T_{in}: Case dependent T_{out}: Case dependent p_{in}= 1 bar Δp = 0 bar	Water T_{in} = 10°C T_{out} = Case dependent p_{in}= 3 bar Δp = 0.1 bar	$\eta_{is,pump}$ = 0.7 $\eta_{is,expander}$ = 0.85 η_{mech} = 0.95

The current work includes the following modifications of the state point calculation model received by SINTEF:

- HRHE outlet temperature is replaced with HRHE outlet enthalpy to improve optimization stability (optimization method is covered in Chapter 6).
- IHX pressure loss is calculated for both high and low pressure side (as opposed to assuming equal pressure loss on both sides).

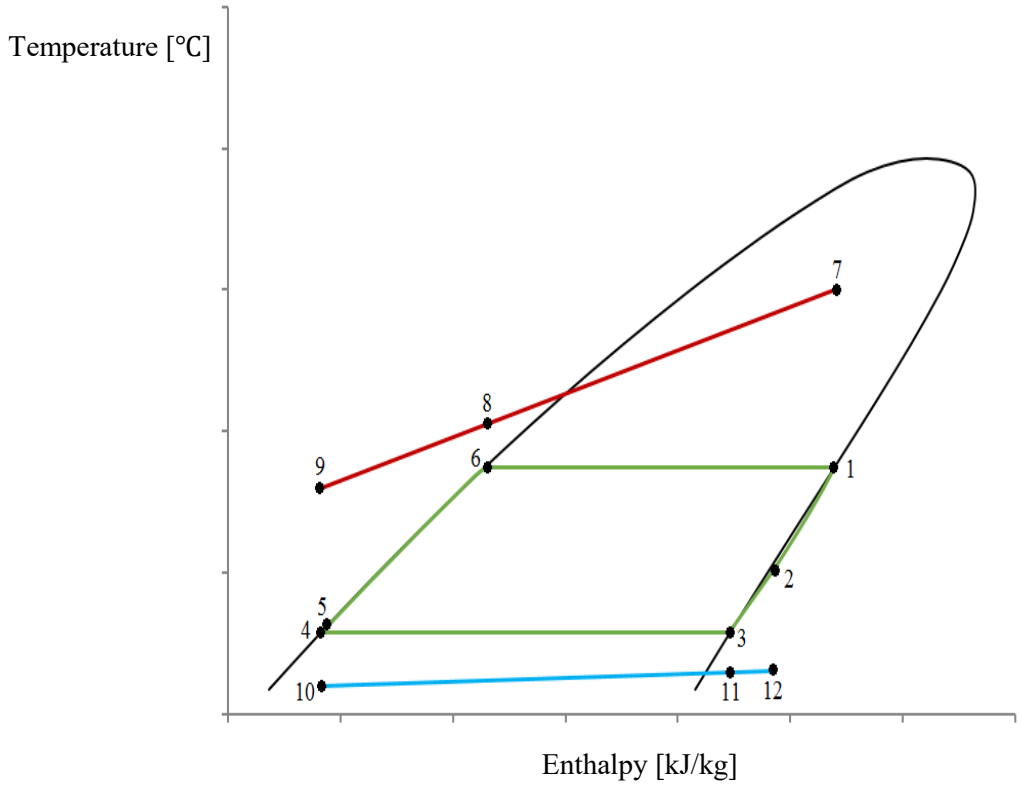

Figure 4-1 Cycle state points

5 HEAT EXCHANGER MODEL

5.1 Heat transfer correlations

5.1.1 Single phase heat transfer coefficient

Single-phase heat transfer coefficients are found in the same way for both pure fluids and mixtures, as mixtures only affect the single-phase heat transfer coefficient through changes in transport properties (Radermacher and Hwang 2005). The correlations are found in the book on heat and mass transfer by Incropera et al. (2013).

Table 5-1 Single phase heat transfer coefficient.

The heat transfer coefficient for single-phase flow is given by the Nusselt correlation:

$$h = \frac{Nu \cdot k}{d} \tag{5-1}$$

The Nusselt number for turbulent flow, $Re_D \geq 10\ 000$, is calculated with the Dittus-Boelter correlations for cooling and heating:

Cooling:

$$Nu = 0.0265 Re_D^{0.8} Pr^{0.3} \tag{5-2}$$

Heating:

$$Nu = 0.0243 Re_D^{0.8} Pr^{0.4} \tag{5-3}$$

The Reynolds and Prandtl numbers are given by Equation 5-10 and 5-11:

$$Re_D = \frac{\rho V d}{\mu} \tag{5-4}$$

$$Pr = \frac{c_p \mu}{k} \tag{5-5}$$

5.1.2 Two-phase heat transfer coefficient

5.1.2.1 Condensation

Evaluating correlations for implementation

As the objective of the current work is screening of hydrocarbon mixtures in Rankine cycles, simplicity in calculation and ability to predict hydrocarbon HTCs are used as decision criteria for choosing correlations. The iterative methods, such as the Colburn and drew method, are discarded due to their calculation complexity and since they do not appear to predict HTCs with improved accuracy compared to the simpler methods. Table 5-2 lists the remaining relevant models discussed in the literature survey, as well as their accuracy and suitability for determining hydrocarbon HTCs.

Table 5-2 Relevant models for calculating HTCs of condensing mixtures, including their accuracy and suitability for determining hydrocarbon HTCs. The correlations chosen for further study are marked with *.

	Model	Accuracy	Suitability
1*	Bell and Ghaly model with pure fluid correlation by Boyko and Kruzhilin (1967). *Applied in project work.*	No data.	Developed for steam. Code already implemented from project work.
2	Bell and Ghaly model with pure fluid correlation by Macdonald and Garimella (2016c). *Authors: Macdonald and Garimella (2016a).*	100 % of data predicted to within ± 25 %. Average and absolute average deviation of + 3.4 % and 8.5 %, respectively.	Developed for propane and pentane, and tested for ethane and propane. Mid-range temperature glides. Complex flow pattern model.
3	Bell and Ghaly model with pure fluid correlation by Alberto Cavallini et al. (2002b). *Authors: Alberto Cavallini et al. (2002b).*	Average and absolute average deviation of – 2.2 % and 10.4 %, respectively (Nusselt number prediction).	Developed for synthetic fluids. Simplified flow model.
4	Modified Bell and Ghaly with pure fluid correlation by Thome et al. (2003). *Authors: Del Col et al. (2005).*	85 % of data predicted to within ± 20 %. with an average deviation of + 9.6 %.	Flow pattern model developed for synthetic fluids. Slightly overestimates hydrocarbon HTCs, but underestimates at high reduced pressure.
5	Modified Bell and Ghaly developed by Del Col et al. (2005) with pure fluid correlation by Alberto Cavallini et al. (2002b). *Author: Han Deng (Deng 2016).*	85 % of dataset including hydrocarbons predicted to within ± 20 %, with average deviations from – 9.3 % to + 8.5 %.	Developed for a dataset including hydrocarbons. Poorer predictive performance for low mass flux hydrocarbons, and slightly overestimates the hydrocarbon data of Chang et al. (2000). Simplified flow model.
6*	Empirical method modifying the pure fluid correlation by Shah (1979). *Authors: Chang et al. (2000).*	Most data predicted to within ± 20 %, with an average deviation of + 6.4 %.	Developed and tested for propane and butane. Low-range temperature glides. Simple to implement. Pure and mixture HTC calculated similarly.

- Correlation 1 is chosen as a top candidate because it is already implemented form the project work.
- Correlation 2 was attempted implemented as it was developed for hydrocarbons over a suitable temperature glide, but was discarded as the HTC was discontinuous and increased exponentially with vapor quality (which is not a physically representative development of HTC during condensation).
- Correlation 3 and 4 were not chosen as they were developed for synthetic fluids.
- Correlation 5 was discarded as its implementation required iteration to find several unknown quantities. It was attempted implemented, but proved relatively complicated.
- Correlation 6 is as a top candidate as it was developed based on a dataset including hydrocarbons and simple to implement due to its empirical nature.

Top candidates for condensation correlations

The correlations for the two top candidates for implementation are given in Table 5-3.

Table 5-3 Condensation: the correlations for the two top candidates for implementation.

Correlation 1:	Correlation 6:
Pure fluid HTC: $$h_{pure} = h_l \left[1 + x\left(\frac{\rho_l}{\rho_v} - 1\right)\right]^{0.5} \quad (5\text{-}6)$$ h_l is the single-phase liquid HTC. Mixture HTC found with Bell and Ghaly correction method: $$h_{mixture} = \left(\frac{1}{h_{pure}} + \frac{xc_{p,v}}{h_v} \cdot \frac{\Delta T}{\Delta i}\right)^{-1} \quad (5\text{-}7)$$ $\frac{\Delta T}{\Delta i}$ is the temperature glide of the fluid and h_v is the vapor phase HTC.	Pure fluid and mixture HTC are calculated similarly with: $$h_{pure} = h_{mixture} = h_l\left(1 + \frac{2.5}{X_c^{0.912}}\right) \quad (5\text{-}8)$$ Where the correlation factor X_c is given by: $$X_c = \left(\frac{1-x}{x}\right)^{0.8}\left(\frac{p}{p_{crit}}\right)^{0.5} \quad (5\text{-}9)$$

Evaporation

Evaluating correlations for implementation

Table 5-4 Models for calculating HTCs of evaporating mixtures, including their accuracy and suitability for calculating hydrocarbon HTCs. The correlations chosen for further study are marked with *.

	Model	Accuracy	Suitability
1	Mixture correction factor by Thome (1989) and modified pure fluid correlation by Wattelet et al. (1993). *Authors:* Chang et al. (2000).	Mean deviation of 14.7 %.	Empirical pure fluid correlation and theoretical mixture correction factor. Developed for mixtures of propane and butane/isobutane, and based on experimental data from only one study.
2	Mixture correction factor and modified pure fluid correlation both by Zou et al. (2010). *Authors:* Zou et al. (2015)	Absolute mean deviation of 27.8 % and root mean square deviation of 33.5 %.	Empirically developed mixture correction factor. Developed for mixtures between methane and ethane. Based on few experimental datasets.
3	Thome (1996) correction factor for mixtures and pure fluid model by Gungor and Winterton (1986). *Authors:* Zou et al. (2015).	Mean average deviation of 91.8 % and root mean square deviation of 111.5 %.	General pure fluid correlation developed from data from several studies, but not hydrocarbons. Analytically developed mixture correction factor. Tested for methane/ethane mixtures.
4*	Thome (1996) and Bell and Ghaly (1973) correction factor for mixtures and pure fluid model by Gungor and Winterton (1986). *Author:* Thome (1998).	Not compared with experimental data.	Same pure fluid correlation as above. Little available information on accuracy and theoretical basis of mixture calculation method. Easy to apply as it was used in project work.
5*	Thome (1996) and Bell and Ghaly (1973) correction factor for mixtures combined with different pure fluid models. *Author:* Shah (2015).	Mean deviation of 19.5 % for pure fluid correlation by Shah (1982).	Method compared to database with broad range of fluids (including hydrocarbons) and operating parameters. Suitable for glides up to 30°C.
6	Mixture correlation developed by Granryd (1991).	Absolute mean deviation of 16 %,	Correlation for annular flow valid for different operating conditions.

6	*Authors:* Barraza et al. (2016).	and 83 % of data predicted to within 25 % relative error.	Predictive performance tested for binary and tri-component hydrocarbon and synthetic refrigerant mixtures. High-glide fluids. Cryogenic applications in small tube diameters.

- Correlation 1 was implement, but showed an exponential increase in HTC with vapor quality, and was discarded.
- Correlation 2 is relatively straightforward and adapted for hydrocarbons, but required the input of an “ideal temperature difference”, which was not defined anywhere in the text or elsewhere in available literature.
- Correlation 3 was tested for hydrocarbons, but had a relatively high deviation between measured and predicted HTCs and is therefore discarded.
- Correlation 4 is chosen as a top candidate because it is already implemented form the project work.
- Correlation 5 is chosen as a top candidate as it is straightforward to implement and verified for hydrocarbon data over a broad range of operating parameters, with an “acceptable” mean deviation of 19.5 %.
- Correlation 6 was discarded as it was developed for other conditions (cryogenic applications, higher glides and smaller tube diameters) than the current study.

Top candidates for evaporation correlations

The correlations for the two top candidates for implementation are given in Table 5-5.

Table 5-5 Evaporation: The correlations for the two top candidates for implementation.

Correlation 4:	Correlation 5:
Pure fluid HTC: $h_{pure} = Eh_l + Sh_{nb}$ (5-10) Nucleate boiling HTC: $h_{nb} = 55p_r^{0.12}(-\log p_r)^{-0.55}M^{-0.5}q^{0.67}$ (5-11) Enhancement and suppression factors: $E = 1 + 2400Bo^{1.16} + 1.37\left(\frac{1}{X}\right)^{0.86}$ (5-12) $S = \frac{1}{1 + 1.15 * 10^{-6}E^2Re_l^{1.17}}$ (5-13) Martinelli parameter and boiling number: $X = \left(\frac{1-x}{x}\right)^{0.9}\left(\frac{\rho_v}{\rho_l}\right)^{0.5}\left(\frac{\mu_l}{\mu_v}\right)^{0.1}$ (5-14) $Bo = \frac{q}{i_{fg}G}$ (5-15) Mixture HTC: $h_{mixture} = \left(\frac{1}{h_{pure}F_c} + \frac{xc_{p,v}}{h_v}\cdot\frac{\Delta T}{\Delta i}\right)^{-1}$ (5-16) F_c is a mass transfer factor, given by: $F_c = \left\{1 + \frac{h_{pure}}{q}(T_{dew} - T_{bub})\cdot \mathrm{Z}\right\}^{-1}$ (5-17) $Z = \left\{1 - exp\left(-\frac{q}{0.0003\rho_l i_{fg}}\right)\right\}^{-1}$ (5-18)	Pure fluid HTC: $h_{pure} = h_{cb} + h_{nb^*}$ (5-19) Convective and nucleate HTCs: $h_{cb} = FF_2h_l$ (5-20) $h_{nb^*} = S^*\,S_2h_l$ (5-21) where: $F = 1.12\left(\frac{x}{1-x}\right)^{0.75}\left(\frac{\rho_l}{\rho_v}\right)^{0.41}$ (5-22) $F_2 = \begin{cases} Fr_{lo}^{\frac{1}{2}}\ if\ Fr_{lo} < 0.05 \\ 1\ otherwise \end{cases}$ (5-23) $S^* = 1 + 3000Bo^{0.86}$ (5-24) $S_2 = \begin{cases} Fr_{lo}^{(0.1-2Fr_{lo})}\ if\ Fr_{lo} < 0.05 \\ 1\ otherwise \end{cases}$ (5-25) $Fr_{lo} = \frac{G^2}{gd\rho_l^2}$ (5-26) Mixture HTC: $h_{mixture} = F_ch_{nb^*} + \left(\frac{1}{h_{cb}} + \frac{Y}{h_{vo}}\right)^{-1}$ (5-27) where: $Y = xc_{p,v}\frac{\Delta T}{\Delta i}$ (5-28) $h_{vo} = 0.023\left(\frac{Gxd}{\mu_v}\right)\frac{Pr_v^{0.4}k_v}{d}$ (5-29) $F_{TS} = \left\{1 + \left(\frac{h_{nb}}{q}\right)(T_{dew} - T_{bub})Z\right\}^{-1}$ (5-30)

The heat flux, q, is required in both correlations. This is an unknown quantity, and dependent on the HTC. An iterative procedure is implemented to calculate the correct heat flux.

5.1.3 Choosing which correlations to implement

In the previous sections, the two top candidates for correlations to implement were given in Table 5-2 for condensation and Table 5-4 for evaporation. Rather arbitrarily, the correlations implemented in the project work were one of the top candidates for both condensation and evaporation.

It is difficult to decide which correlations have the better predictive performance. Still, two factors favor implementation of the correlations that were not used in the project work (5 for evaporation and 6 for condensation). First, no studies have been found that compare the correlations used in the project work with experimental data. This has been done for both the "new" alternatives, which verified the methods for mixture condensation. Moreover, the new correlations have been either developed based on hydrocarbon data (condensation) or tested and verified for hydrocarbons (condensation and evaporation). Consequently, the project work correlations are rejected, and correlation 6 for condensation and correlation 5 for evaporation are chosen for implementation in the current work. Note that correlation 6 for condensation does not have a separate method for calculating mixture HTCs, but one method that covers both pure fluids and mixtures.

The condensation correlation that was implemented in the project work is compared to correlation 6 Appendix B. For both correlations, HTCs are plotted for different mass fluxes, HX tube diameters and reduces pressured. Condenser area is also calculated with both correlations, using the method in Section 5.3.1 for a fixed heat sink/source, HX design and operating conditions. This allows comparison of the correlations on the same basis. This is not a comparison between pure and mixed fluid correlations, but a comparison between the two pure fluid correlations, and between the two mixed fluid correlations. The different condensation correlations are discussed in Section 9.6.

5.2 Pressure loss correlations

The pressure loss is calculated with the frictional pressure loss gradient according to Equation 5-37. Acceleration pressure loss is neglected for reasons mentioned in the literature survey.

$$\Delta p = \left(\frac{dp}{dz}\right)\Delta z \tag{5-31}$$

Δz is the tube length.

The single-phase pressure loss gradient is found in the book on heat and mass transfer by Incropera et al. (2013). The two-phase pressure loss gradient by Friedel (1979) is chosen over that by Macdonald and Garimella (2016c), due to a relatively high calculation complexity for the latter.

Table 5-6 Single-phase pressure loss gradient.

The single-phase pressure loss gradient is given by:

$$\frac{dp}{dz} = \frac{f\rho V^2}{2d} \tag{5-32}$$

The Darcy friction factor for turbulent flow is determined from the Retukhov correlation for turbulent flow in smooth tubes and is valid for $3000 \leq Re_D \leq 5 \cdot 10^6$:

$$f = (0.79\log(Re_D) - 1.64)^{-2} \tag{5-33}$$

Table 5-7 Two-phase pressure loss gradient.

The two-phase pressure loss gradient is found with the Friedel method as explained in the conference paper by Wilson et al. (2000).

The pressure loss gradient is estimated by multiplying the single-phase liquid pressure loss gradient with a two-phase multiplier:

$$\frac{dp}{dz} = \phi_{lo}^2 \left(\frac{dp}{dz}\right)_l \tag{5-34}$$

The single-phase liquid pressure loss gradient, $\left(\frac{dp}{dz}\right)_l$, is evaluated at total mass flux.

ϕ_{lo}^2 is the two-phase multiplier and is given by:

$$\phi_{lo}^2 = A_1 + \frac{3.24 A_2}{Fr^{0.045} We^{0.035}} \tag{5-35}$$

$$A_1 = (1-x)^2 + x^2 \left(\frac{\rho_l}{\rho_v}\right)\left(\frac{f_v}{f_l}\right) \tag{5-36}$$

$$A_2 = x^{0.78}(1-x)^{0.24}\left(\frac{\rho_l}{\rho_v}\right) \tag{5-37}$$

f_l and f_v are the pure liquid and vapor friction factors evaluated at total mass flux. We and Fr are the two-phase Weber and Froude numbers, given by:

$$We = \frac{G^2 d}{\rho_{tp}\sigma} \tag{5-38}$$

$$Fr = \frac{G^2}{\rho_{tp} d g} \tag{5-39}$$

ρ_{tp} is the homogeneous density and is given by:

$$\rho_{tp} = \left(\frac{x}{\rho_v} + \frac{1-x}{\rho_l}\right)^{-1} \tag{5-40}$$

5.3 Condenser and HRHE model

The condenser and HRHE are modeled as illustrated in Figure 5-1. The working fluid flows through N circular tubes of length L and diameter d. The water heat sink and air heat source flow counter-currently on the tube outside.

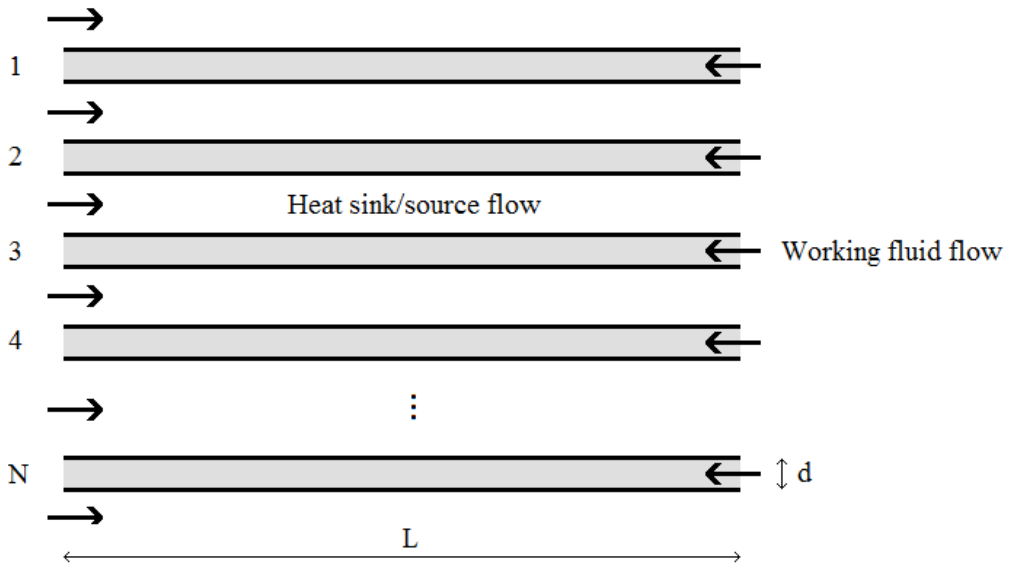

Figure 5-1 Heat exchanger model.

The inner surface area is given by Equation 5-1:

$$A_i = N\pi dL = \frac{(UA)}{U_i} \tag{5-41}$$

Overall heat transfer coefficient

For negligible resistance through the tube wall and across fins, the overall heat transfer coefficient based on the tube inside is given by:

$$U_i = \left(\frac{1}{h_i} + \frac{1}{h_o \cdot R}\right)^{-1} \tag{5-42}$$

$$R = \frac{A_o}{A_i} \tag{5-43}$$

h_i is the heat transfer coefficient of the working fluid flowing on the tube inside, and h_o is the heat transfer coefficient of the heat sink or heat source flowing on the tube outside. h_o is assigned constant values for both heat sink and heat source of 1500 $\frac{W}{m^2K}$ and 60 $\frac{W}{m^2K}$,

respectively. The relative sizes reflect the differences in heat transfer coefficients of water and air.

R is the ratio between the outer and inner tube area and accounts for fin area on the tube outside. The ratio is set to 1 in the condenser and 10 in the HRHE. The HRHE fin area will reduce the dampening effect that the low air heat transfer coefficient has on the overall heat transfer coefficient.

5.3.1 Calculating HX area, overall HTC and pressure loss

The condenser and HRHE are modeled by dividing the total enthalpy change into $n = 10$ equally spaced enthalpy intervals. The HX operating conditions and geometry (diameter and tube length) are determined from the cycle optimization model (as explained in Section 6.1.4 and 0). In the current section, operating conditions and geometry can be assumed known.

A pre-defined pressure loss is divided equally between the intervals, such that pressure and enthalpy can be estimated at 11 points throughout the HX. The state points resulting from this discretization is illustrated with dots in Figure 5-2.

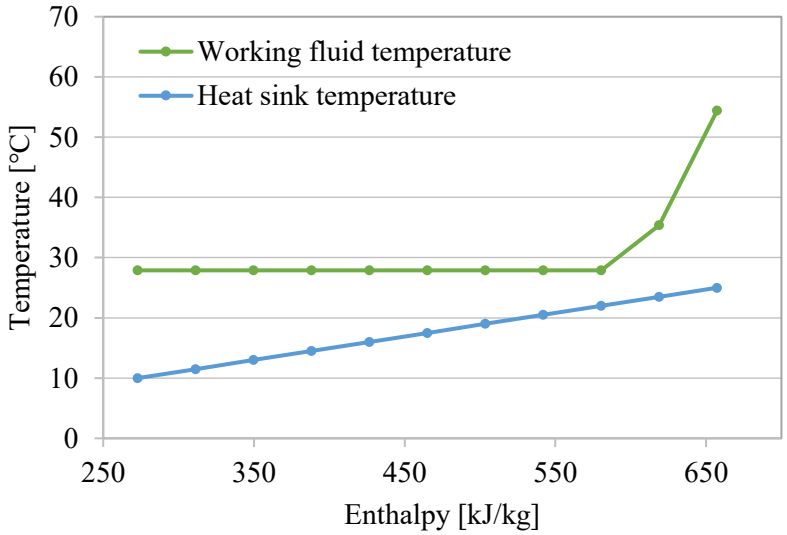

Figure 5-2 Example discretization of condenser into enthalpy intervals.

The assumption of equal pressure loss distribution in the enthalpy intervals is illustrated in Figure 5-3, and the corresponding actual pressure loss distribution is illustrated in Figure 5-4 (as calculated from pressure loss gradients based equal pressure loss distribution). As seen by comparing the figures, assuming equal pressure loss is a significant simplification of the actual pressure loss distribution. Actual pressure loss is unevenly distributed because the velocity changes during phase change, which affects the value of the pressure loss gradient. The challenge of predicting the actual pressure loss distribution is that the distribution varies with working fluid and operating conditions. Iterative procedures could be used, but would require relatively significant computing power.

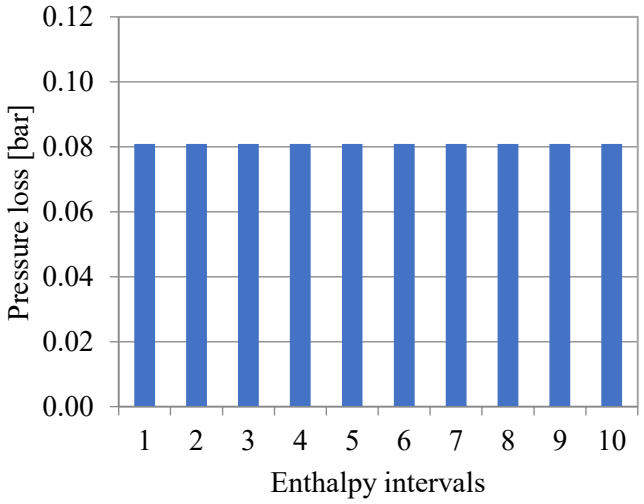

Figure 5-3 Estimated pressure loss distribution in the enthalpy intervals of a condenser.

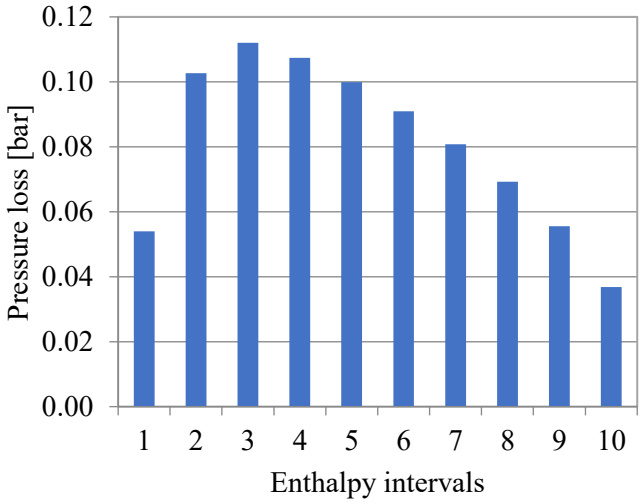

Figure 5-4 Calculated pressure loss distribution in the enthalpy intervals of a condenser.

The method for calculating HX area, overall HTC and pressure loss based on enthalpy discretization is outlined in Table 5-8.

Table 5-8 Method for calculating condenser and HRHE area, overall HTC and pressure loss.

Interval HTCs:

$$h_n = h(p_n, T_n) \tag{5-44}$$

$$U_n = \left(\frac{1}{h_{i,n}} + \frac{1}{h_o \cdot R}\right)^{-1} \tag{5-45}$$

Tube diameter and number of tubes are inputs for calculating interval HTCs.

Interval area:

$$A_n = \frac{(UA)_n}{U_n} = \frac{\dot{Q}_n}{U_n AMTD_n} \tag{5-46}$$

Total area:

$$A_{tot} = \sum_{n=1}^{10} A_n \tag{5-47}$$

Overall heat transfer coefficient:

$$U = \frac{(UA)_{tot}}{A_{tot}} = \frac{\sum_{n=1}^{10}(UA)_n}{A_{tot}} \tag{5-48}$$

Interval pressure loss:

$$\left(\frac{dp}{dz}\right)_n = \left(\frac{dp}{dz}\right)_n (p_n, T_n) \tag{5-49}$$

$$\Delta p_n = \left(\frac{dp}{dz}\right)_n L_n \tag{5-50}$$

where:

$$L_n = \frac{A_n}{\pi N d} \tag{5-51}$$

Total pressure loss

$$\Delta p_{tot} = \sum_{n=1}^{10} \Delta p_n \tag{5-52}$$

5.3.2 Internal heat exchanger model

The internal heat exchanger is modeled as illustrated in Figure 5-1. The hot side (red) and cold side (blue) of the working fluid flow counter-currently through N_{layers} layers of tubes. The tube diameter and number of tubes on the cold side are given by d_1 and N_1, and the corresponding values on the hot side are given by d_2 and N_2. The hot side is the "low pressure" (LP) side and the cold side is the "high pressure" (HP) side.

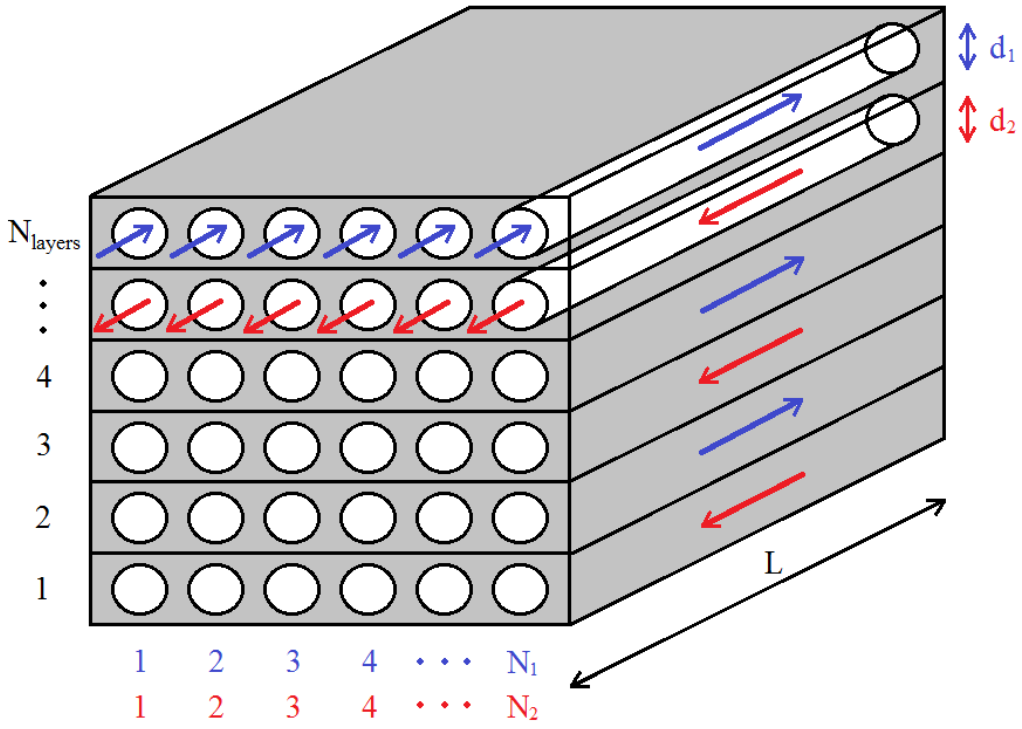

Figure 5-5 Internal heat exchanger model.

The inner surface area is calculated as the average of low pressure and high pressure side area:

$$A_i = \frac{A_{HP} + A_{LP}}{2} = \frac{\frac{N_{layers}}{2}\pi L(N_1 d_1 + N_2 d_2)}{2} \tag{5-53}$$

As all of the above design parameters are set by the optimization tool (as explained in Section 0) except for tube length, another equation for IHX area is necessary to solve for the inner area. The high and low pressure side areas are found with the following alternative equations:

$$A_{HP} = \frac{\dot{Q}_{IHX}}{U_{HP} LMTD} \tag{5-54}$$

$$A_{LP} = \frac{\dot{Q}_{IHX}}{U_{LP} LMTD} \tag{5-55}$$

For negligible resistance through the wall, the overall heat transfer coefficient for high and low pressure side is given by:

$$U_{HP} = \left(\frac{\mathrm{R}}{h_{LP}} + \frac{1}{h_{HP}}\right)^{-1} \tag{5-56}$$

$$U_{LP} = \left(\frac{1}{h_{HP} \cdot R} + \frac{1}{h_{LP}}\right)^{-1} \tag{5-57}$$

Where:

$$R = \frac{A_{HP}}{A_{LP}} = \frac{N_1 d_1}{N_2 d_2} \tag{5-58}$$

6 OPTIMIZATION MODEL

The model is similar to that explained in the project work, and is only briefly outlined in the following. A more detailed description can be found in the project thesis. The model calculates maximum work output for a pre-defined value of total HX area.

An attempt was made to optimize HX geometry and cycle parameters simultaneously, but the optimization had difficulties reaching the global optimum solution due too many variables. As an alternative, the overall HTC of the condenser and HRHE are estimated, such that condenser and HRHE area can be approximated from cycle parameters (UA-value).

The optimization model can be thought of as a three step process. In the first step, optimum HX operating conditions for a given pinch point are obtained by maximizing work output for a fixed pinch point. In the second step, HX area is calculated for a fixed pinch point and pressure loss. Performing steps 1 and 2 several times allows the construction of a "composite" equation for overall HTC on the form; $U = f(\Delta p, T_{pinch})$. In the final step, work output is maximized and areas are calculated from the equations for overall HTC, giving $A_{cond} = \frac{(UA)_{cond}}{U_{predicted,cond}}$ and $A_{HRHE} = \frac{(UA)_{cond}}{U_{predited,HRHE}}$. In this step, UA-values are available from the cycle simulation.

The 3 steps are illustrated in Figure 6-1, with color codes listed in Table 6-1.

Table 6-1 Color codes for Figure 6-1.

Color codes:
Optimization objective
Constraint
-> Result of operation

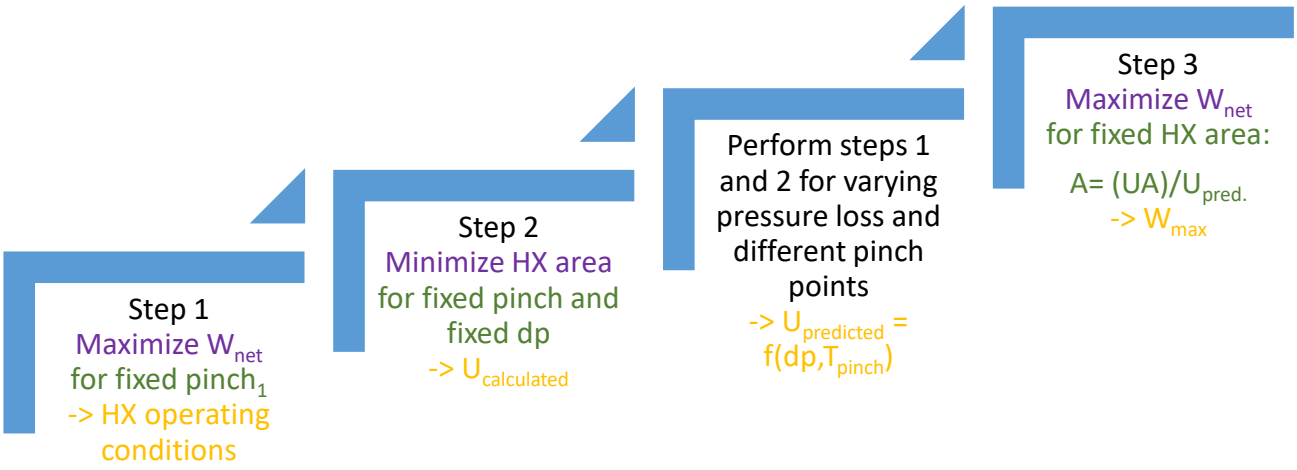

Figure 6-1 Steps in optimization model.

Improvements from previous model:

- New heat transfer correlations

- Making U vary with pinch point as well as pressure loss, $U = f(\Delta p) \rightarrow U = f(\Delta p, T_{pinch})$.

- Calculating a more accurate evaporating heat flux through iteration, instead of estimating a constant value.

6.1.1 Step 1: Obtaining optimum HX operating conditions for a fixed pinch point

Table 6-2 Optimization procedure for obtaining optimum HX operating conditions for a fixed pinch point.

Optimization procedure: Maximizing cycle work output		
Optimization variables	Optimization constraints	Output
$\dot{m}_{working\ fluid}$ $p_{in,HRHE}$ $T_{out,cond}$ $i_{out,HRHE}$	For condenser optimization: $T_{pinch,HRHE} = 10℃$ $T_{pinch,cond} = 3/13/23℃$(1) For HRHE optimization: $T_{pinch,cond} = 5℃$ $T_{pinch,HRHE} = 3/13/23℃$ No wet expansion	HX operating conditions: HX heat load Temperature profile Pressure levels Working fluid mass flow Heat sink mass flow

(1) For ethane this is set to $3/8/13℃$ to avoid transcritical condensation (which would require condensation pressure as an optimization variable as well).

6.1.2 Step 2: Calculating overall HTC (and area) for a fixed pinch point and fixed pressure loss

Table 6-3 Optimization procedure calculating overall HTC (and area) for a fixed pinch point and fixed pressure loss.

Optimization procedure: Minimizing HX area			
Input	Optimization variables	Optimization constraints	Output
HX operating conditions	Number of tubes, N Tube diameter, d	HX pressure loss: Δp	(HX area: A) Overall HTC: U

6.1.3 Obtaining the "composite" function for overall HTC

Three sets of HX operating conditions are obtained for three HX pinch points; 3℃ 13℃ and 23℃, with the procedure given in Table 6-1Table 6-2. These serve as inputs to the optimization procedure for calculating overall HTC in Table 6-3. Now, several HTCs are calculated for each "pinch point" (and corresponding HX operating parameters) by varying HX pressure loss, giving curves for overall HTC versus pressure loss as illustrated in Figure 6-2.

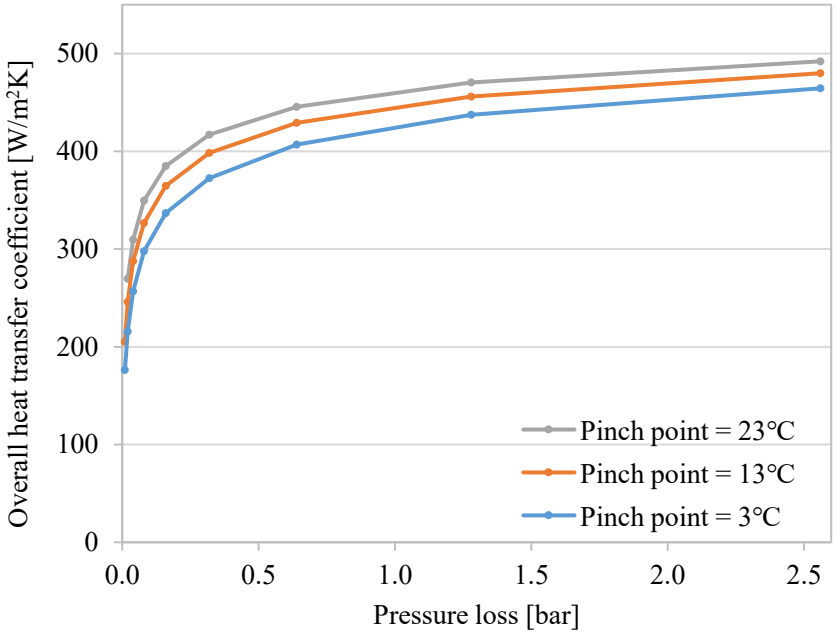

Figure 6-2 Overall heat transfer coefficient versus pressure loss for pinch points 3, 13 and 23℃.

To obtain the composite function for overall HTC, an optimization procedure is first performed to construct an equation for overall HTC as a function of pressure loss; $U = f(\Delta p)$. The equation represents a "composite equation" for all the pinch points. The procedure is described in Table 6-4.

Table 6-4 Optimization procedure for constructing $U = f(\Delta p)$

Optimization procedure: Minimizing sum of squares; $\Sigma[\Delta p_{range}(U_{predicted} - U_{calculated})]^{2}$ (1)		
Input	Optimization variables	Output
<u>Datasets on the form:</u> (x,y,z) $(\Delta p_1, T_{pinch,1}, U_{max,1})$ $(\Delta p_2, T_{pinch,1}, U_{max,2})$ $(\Delta p_3, T_{pinch,1}, U_{max,3})$ $(\Delta p_J, T_{pinch,1}, U_{max,J})$ $(\Delta p_1, T_{pinch,2}, U_{max,1})$ $(\Delta p_2, T_{pinch,2}, U_{max,2})$ $(\Delta p_3, T_{pinch,2}, U_{max,3})$ $(\Delta p_J, T_{pinch,2}, U_{max,J})$ $(\Delta p_1, T_{pinch,3}, U_{max,1})$ $(\Delta p_2, T_{pinch,3}, U_{max,2})$ $(\Delta p_3, T_{pinch,3}, U_{max,3})$ $(\Delta p_J, T_{pinch,3}, U_{max,J})$	a b c Optimization constraints <u>Predicted overall HTC:</u> $U_{predicted} = U(\Delta p)$ where $U(\Delta p) = \frac{a \cdot \Delta p}{b + \Delta p} + c \cdot \Delta p$	<u>Equation for overall HTC:</u> $U = U(\Delta p)$

(1) $(U_{predicted} - U_{calculated})$ is weighed with a pressure range, Δp_{range}, to account for non-uniform distance between pressure loss data points (as seen in Figure 6-2, more data points are included in the lower range of pressure loss. The reason for this is that most of the change in U occurs in this region).

The equation for overall HTC as a function of pressure loss, $U = U(\Delta p)$, is illustrated in Figure 6-3. The overall HTCs for the different pinch points are also given.

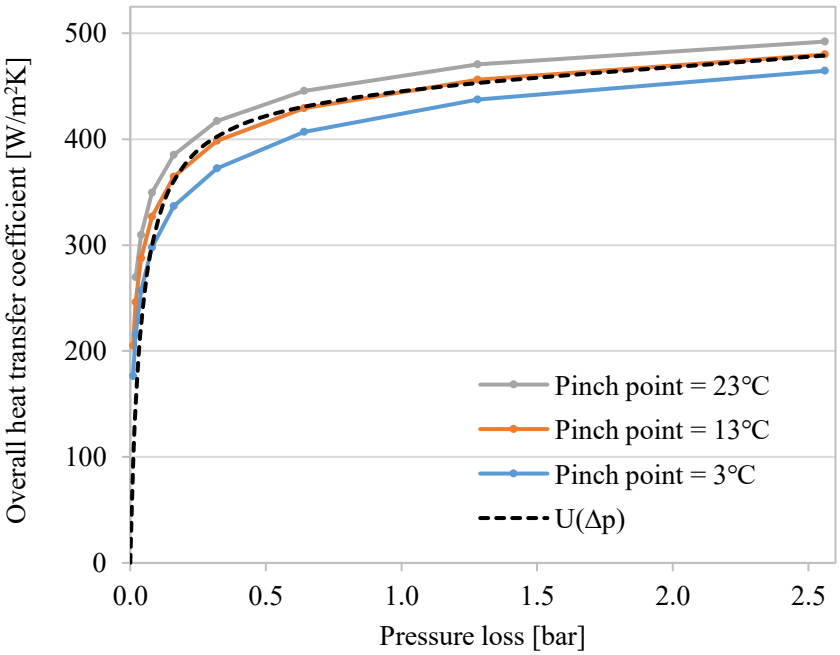

Figure 6-3 Constructed function for overall HTC, $U = U(\Delta p)$, as well as overall HTCs for pinch points 3, 13 and 23°C.

Next, the equation for overall HTC is adjusted to account for variation in pinch point. A factor is added to $U = U(\Delta p)$ that allows for overall HTC to decrease for lower pinch points and increase for higher pinch points. The result is an equation for overall HTC on the form $U = U(\Delta p) + U(T_{pinch})$. The value of $U(T_{pinch})$ is calculated as follows:

$$U(T_{pinch}) = \frac{\Delta U}{2} \cdot y \tag{6-1}$$

$$\Delta U = U_{av}(T_{pinch} = 23) - U_{av}(T_{pinch} = 3) \tag{6-2}$$

$$y = \frac{T_{pinch} - 13}{23 - 13} \tag{6-3}$$

Predicted overall HTCs for different pressure losses and pinch points are illustrated in Figure 6-4. The figure shows that the equation allows overall HTC to increase with higher pressure loss and pinch point, and decrease with lower pinch points.

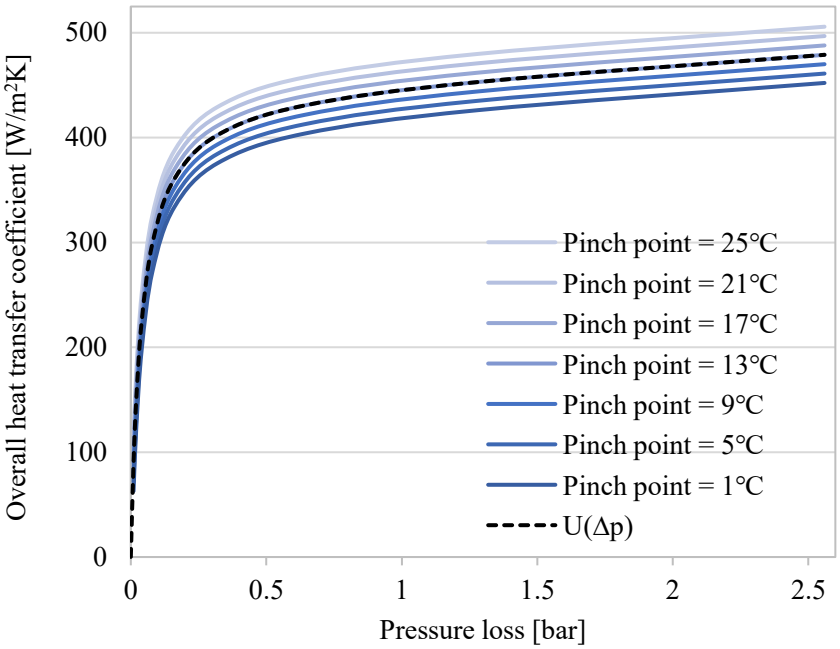

Figure 6-4 Predicted overall heat transfer coefficients for different pressure losses and pinch points, as well as $U = U(\Delta p)$.

6.1.4 Step 3.1: Maximizing cycle work output with pre-defined HX area

Table 6-5 Maximizing work output with pre-defined total HX area

Optimization procedure: Maximizing cycle work output		
Input	Optimization variables	Optimization constraints
<u>Equations for overall HTC for condenser and HRHE:</u> $U_{cond} = f(\Delta p, T_{pinch})$ $U_{HRHE} = f(\Delta p, T_{pinch})$ <u>Condenser/HRHE area:</u> $\rightarrow A_{cond/HRHE} = \frac{\sum_n (\dot{Q}_n / LMTD_n)}{U_{cond/HRHE}}$	$\dot{m}_{working\ fluid}$ $p_{in,HRHE}$ $T_{out,condenser}$ $i_{out,HRHE}$ $\Delta p_{HRHE}, \Delta p_{cond}$ $T_{out,sink}$ (2)	<u>Total HX area:</u> $A_{tot} = A_{cond} + A_{HRHE}$ Output <u>Maximum work output:</u> W_{max}

Table 6-6 Optimization procedure for maximizing work output with pre-defined total HX area

(1) HX areas are estimated based on the constructed equation for overall HTC. Inner surface area is used for both condenser and HRHE.

(2) Heat sink outlet temperature is included as an optimization variable in case 2.

The optimization procedure is performed over a range of pre-defined total HX area, giving a curve of work output vs. total HX area, where each point on the curve is optimized.

In the final step, the saturated liquid state in the HRHE and the saturated vapor state in the condenser are estimated from the assumption that pressure loss divides uniformly in the enthalpy intervals. The purpose of calculating the saturated states is to calculate LMTD more accurately and to capture the high UA-values that occur in the region around these states for high values of pre-defined area. The HX's are divided into 5 equally sized enthalpy intervals before and after these states (except the HRHE for transcritical fluids which is divided into 10 equally sized intervals as before), as illustrated in in Figure 6-5.

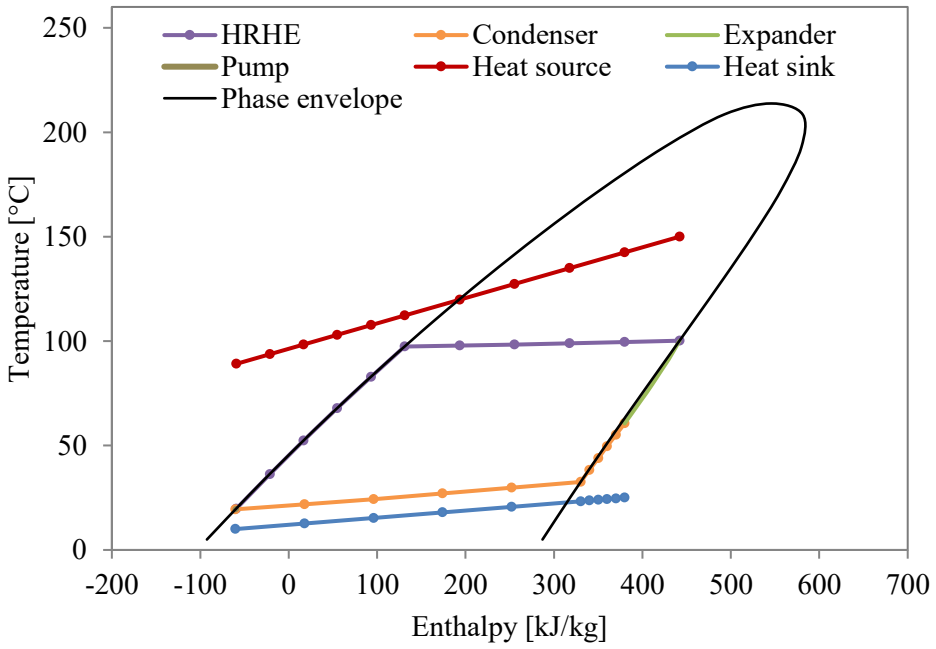

Figure 6-5 Modified HX discretization.

6.1.5 Step 3.2: Maximizing cycle work output with pre-defined HX area and IHX

IHX area is calculated directly during the optimization of work output, as opposed to condenser and HRHE area which are estimated from the equations for overall HTCs.

Table 6-7 Maximizing work output with internal heat exchanger and pre-defined total HX area

Optimization procedure: Maximizing cycle work output		
Input	Optimization variables	Optimization constraints
Equations for overall HTC for condenser and HRHE: $U_{cond} = f(\Delta p, T_{pinch})$ $U_{HRHE} = f(\Delta p, T_{pinch})$ Condenser/HRHE area: $\rightarrow A_{cond/HRHE} = \frac{\sum_n (\dot{Q}_n / LMTD_n)}{U_{cond/HRHE}}$	$\dot{m}_{working\ fluid}$ $p_{in,HRHE}$ $T_{out,condenser}$ $i_{out,HRHE}$ $\Delta p_{HRHE}, \Delta p_{cond}$ IHX heat load/design: $\dot{Q}_{IHX}$, $N_1, N_2, N_{layers}, d_1, d_2$	Total HX area: $A_{tot} = A_{cond} + A_{HRHE} + A_{IHX}$ Output Maximum work output: W_{max}

7 WORKING FLUID SCREENING

Pinch point analysis is used to choose which working fluids to investigate with the current method, meaning that work output is optimized at fixed HX pinch points (5℃ in condenser and IHX, and 10℃ in HRHE). This is the same optimization procedure as described in Table 6-2.

7.1 Case 1 and 2

Case 1, as described in Section 4.1, is used to screen working fluids for both case 1 and 2. Maximum work output of different pure fluids and mixtures is shown in Figure 7-1.

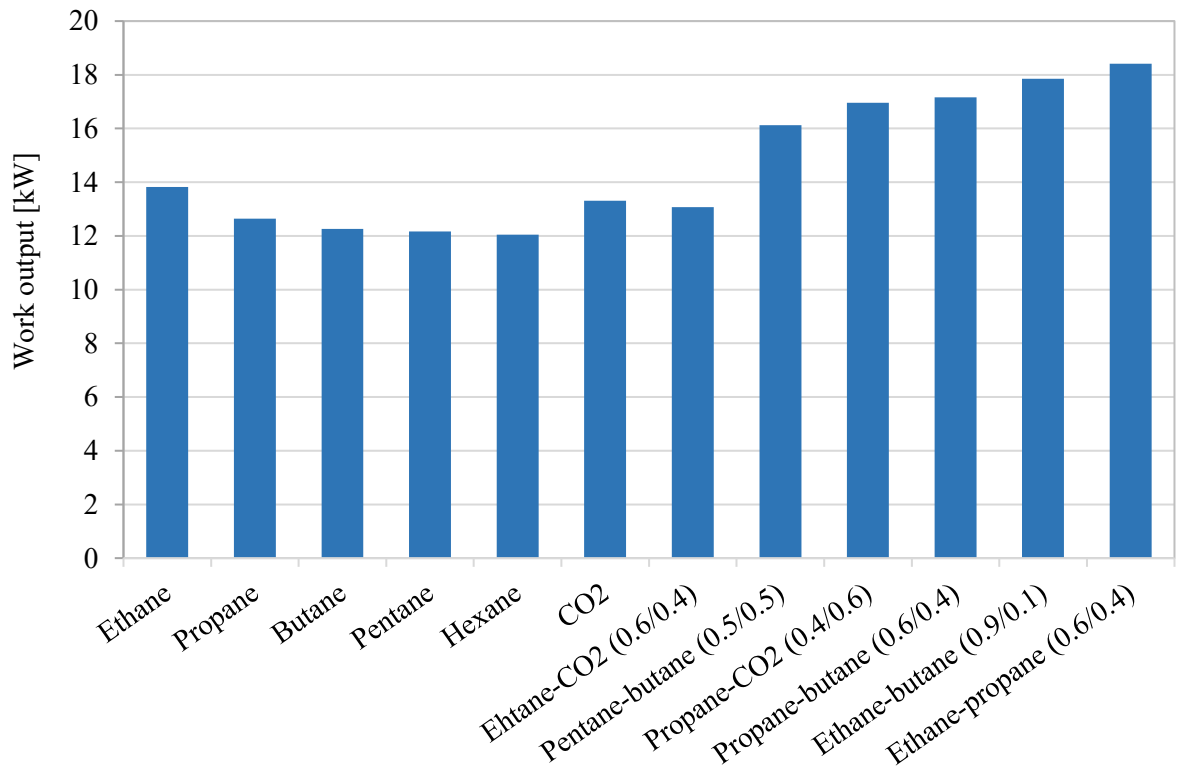

Figure 7-1 Maximum work output of different pure fluids and mixtures from a pinch point analysis of case 1.

Four hydrocarbon mixtures are screened; the "best" pure fluid, ethane, is combined with propane and butane, as they are the second and third best fluids. For the same reason, propane and butane are themselves mixed. Also, the third and fourth best fluids, butane and pentane, are mixed. Moreover, CO_2 is mixed with the two best hydrocarbons, ethane and propane. Ethane-

CO_2 has such a low critical point that the process becomes supercritical, which required a significant amount of computing time and therefore only a few compositions were tested. The optimum composition of this mixture is probably not found.

To save simulation time, optimum mixture compositions are found from the assumption that compositions that achieve temperature match in the condenser (temperature change of working fluid matches temperature change of heat sink), gives the highest work outputs. This was indicated by both previous research (as documented in project thesis) and in a summer project performed at SINTEF. A few nearby compositions are tested to find the optimum composition.

As seen in Figure 7-1, ethane is the highest performing pure fluid, and is in addition to CO_2 the only transcritical fluid under the heat source conditions set in case 1. Propane-ethane (0.4/0.6) is the highest performing mixture, with 33.2 % higher work output than pure ethane. These two fluids are chosen for further study. Butane is also chosen, such that one of the investigated fluids are subcritical. It was chosen because it is the only subcritical fluid operating above atmospheric pressure. Butane has relatively low operating pressures compared to ethane ($P_{HRHE} = 6.5$ bar vs. $P_{HRHE} = 74.2$ bar). The three chosen fluids are shown together in Figure 7-2.

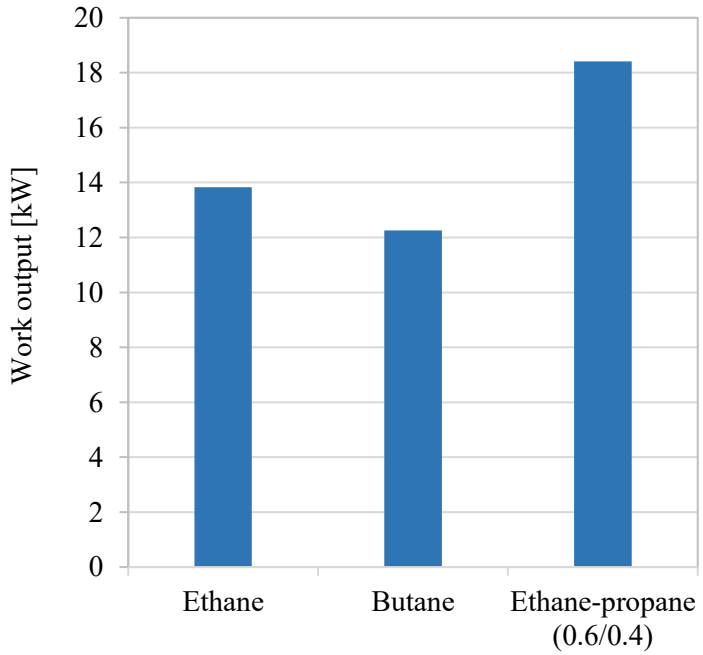

Figure 7-2 Maximum work output ethane, butane and ethane-propane (0.6/0.4) from pinch point analysis for case 1.

7.2 Case 3 and 4

Case 3 and 4 are described in Section 4.1. Optimum work output of different pure fluids and mixtures, including absolute (light blue column) and percentage improvement with IHX, is shown in Figure 7-3.

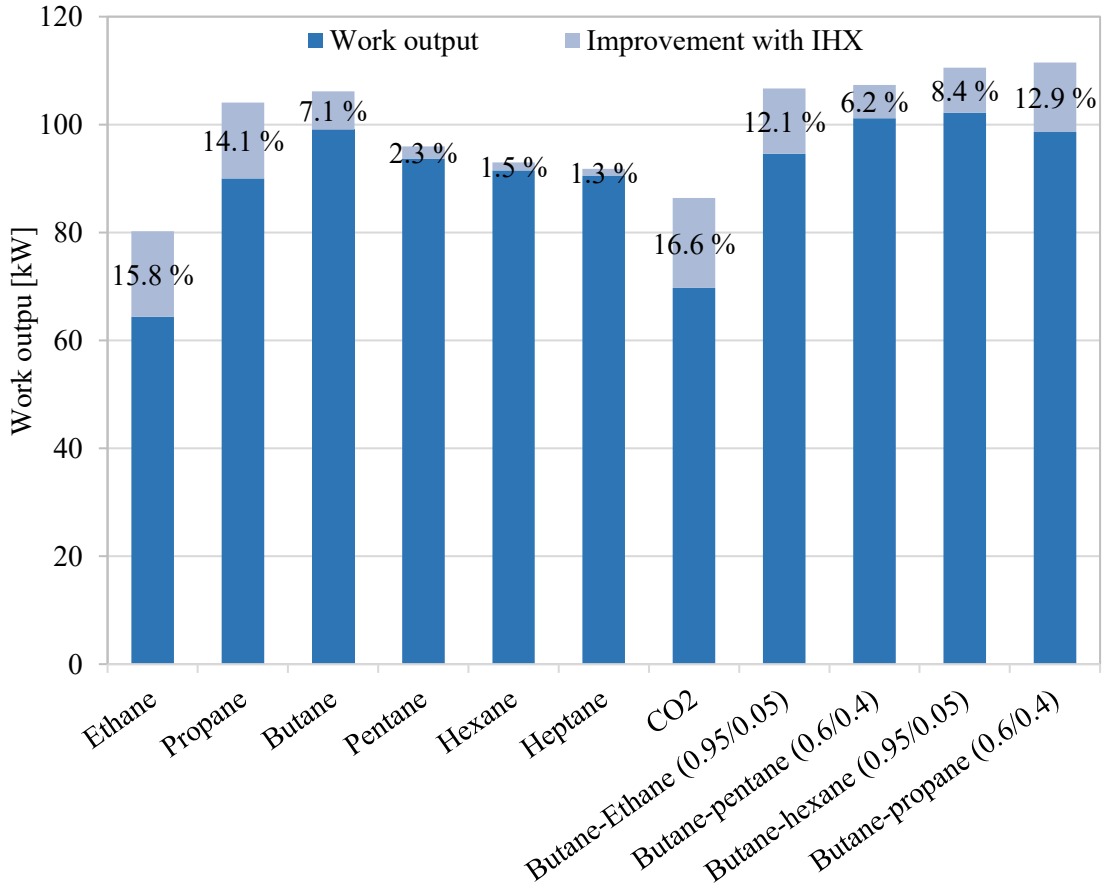

Figure 7-3 Maximum work output of different pure fluids and mixtures in case 3, including improvement with IHX in case 4. Results are found from pinch point analysis.

The highest performing pure fluid, butane, is mixed with ethane, propane, pentane and hexane. It is not mixed with heptane, as this would result in excessive glides compared to the heat sink. The pure fluid and the mixture achieving the highest work output *with IHX* are chosen for further study; Butane and butane-propane (0.6/0.4). The improvement from butane with IHX to butane-propane (0.6/0.4) with IHX is 6.1 %. Without IHX, butane-propane (0.6/0.4) actually has slightly lower work output than pure butane. The chosen fluids are shown together in Figure 7-4. Optimum mixture compositions are found in the same way as with case 1.

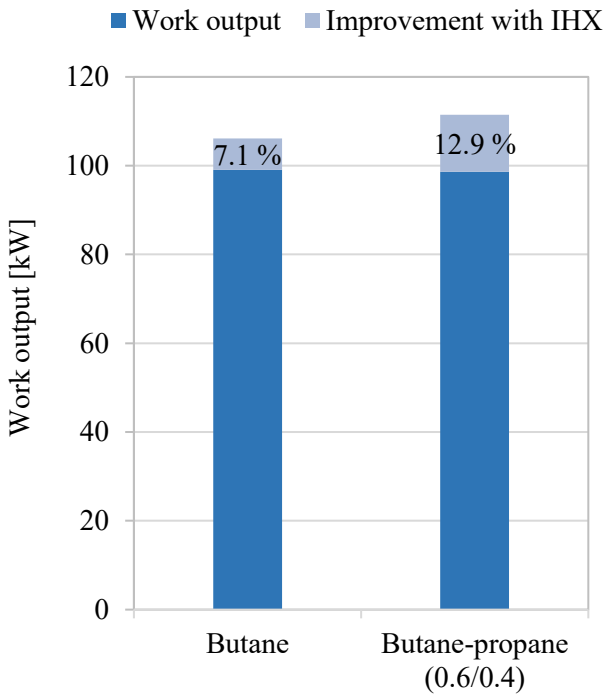

Figure 7-4 Maximum work output of butane and butane-propane (0.6/0.4), including improvement with IHX. Results are found from pinch point analysis for case 3 and 4.

Mixtures between CO_2 and propane were tested, and variation in work output with molar fraction of CO_2 as plotted in Figure 7-5. The figure shows that no mixture compositions achieve higher work output than pure propane.

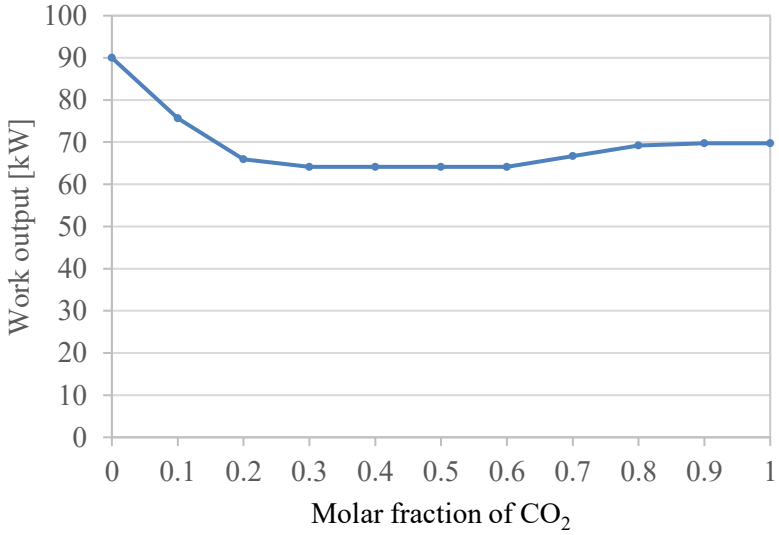

Figure 7-5 Maximum work output vs. molar fraction of CO_2 in propane.

8 RESULTS

In the results section, curves are given for work output versus total HX area for the different fluids. Following these curves are plots of work output that include the improvement with mixture compared to pure fluid (for case 1 and 2), or the improvement with IHX (for case 4). Temperature-enthalpy diagrams at selected values of total HX area are given for the fluids to illustrate how the different cycles look. Finally, plots are given that show the distribution between condenser and HRHE (and IHX) area for the different fluids.

The results for case 1, 2 and 3 are found from step 3 in the optimization model, as explained in Section 6.1.4. The results for case 4 with IHX are found from the method in Section 0. In addition to determining maximum work output for a pre-defined value of total HX area, step 3 determines the optimum distribution of HX area, HX pressure loss, pressure levels and other operating parameters.

A subsection of the results is termed “HX design”, in which the different fluid HX pressure losses, pinch points and geometries (tube diameters, number of tubes, tube lengths) are listed for a given value of total HX area. HX geometry is determined from the optimization procedure described in Section 6.1.2.

8.1 Case 1 and 2

Recall that both case 1 and 2 involve a heat source at 100°C, with no lower limit on heat source outlet temperature. Figure 8-1 and Figure 8-2 plot maximum work output as a function of total HX area for the different fluids in case 1 and case 2, respectively. Both plots show that the mixture has higher work output than both pure fluids for all values of total HX area. Moreover, ethane has higher work output than butane for areas higher than 75 m^2.

Work output increases from case 1 to case 2, as heat sink outlet temperature is allowed to optimize. However, the pure fluids achieve a greater increase in work output from case 1 to case 2 than the mixture. This decreases the amount of improvement from pure fluid to mixture in case 2 compared to case 1, as seen by comparing the two figures.

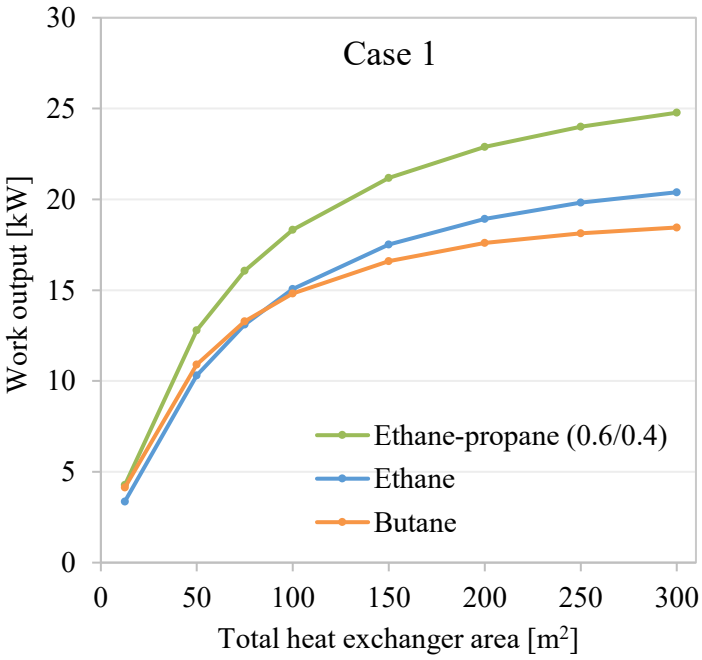

Figure 8-1 Case 1: Work output vs. total heat exchanger area.

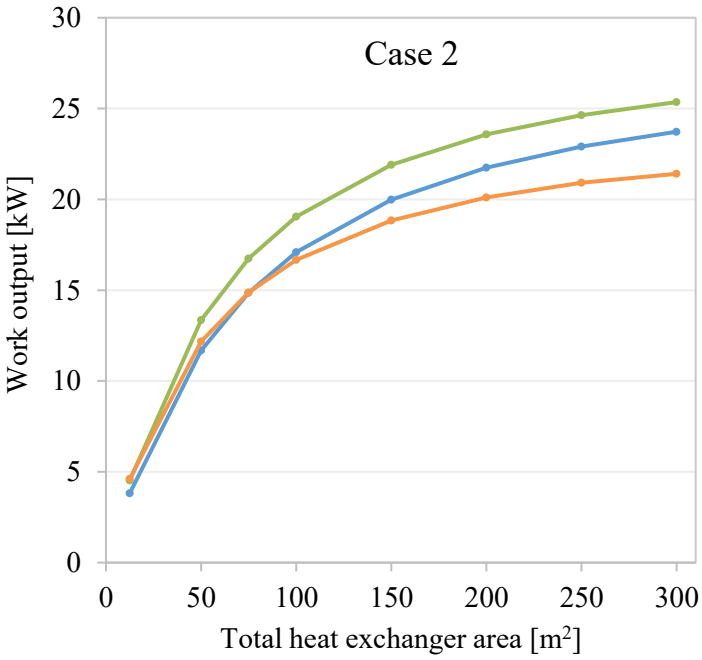

Figure 8-2 Case 2: Work output vs. total heat exchanger area.

Figure 8-3 plots the work output of ethane in case 1 for the different values of total HX area, along with improvement with the ethane-propane (0.6/0.4) mixture. Similarly, Figure 8-4 plots the work output of butane in case 2, and the improvement with the ethane-propane (0.6/0.4) mixture. The average improvement in work output from both ethane and butane to mixture is 22.5 %. The improvement from butane to mixture is concentrated to the high area region, where the percentage improvement from mixture to pure fluid reaches almost 34 %.

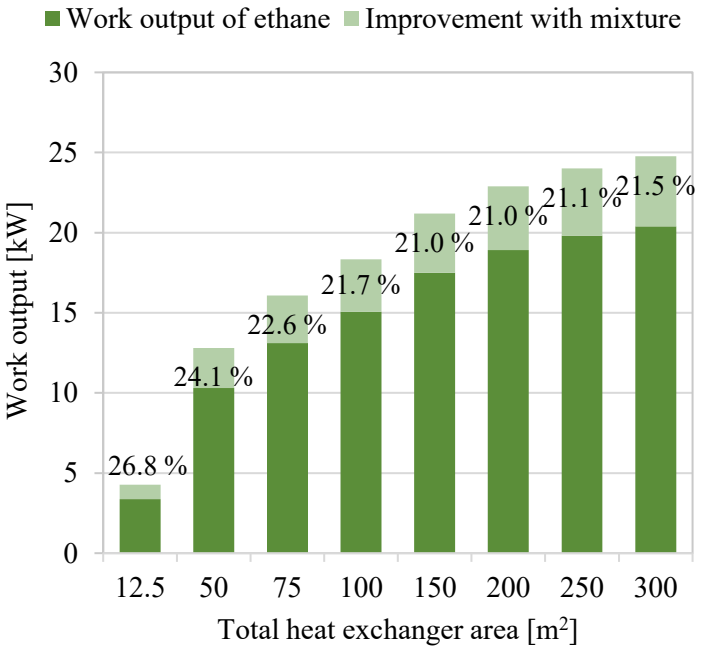

Figure 8-3 Case 1: Work output of ethane and improvement with ethane-propane (0.6/0.4) mixture.

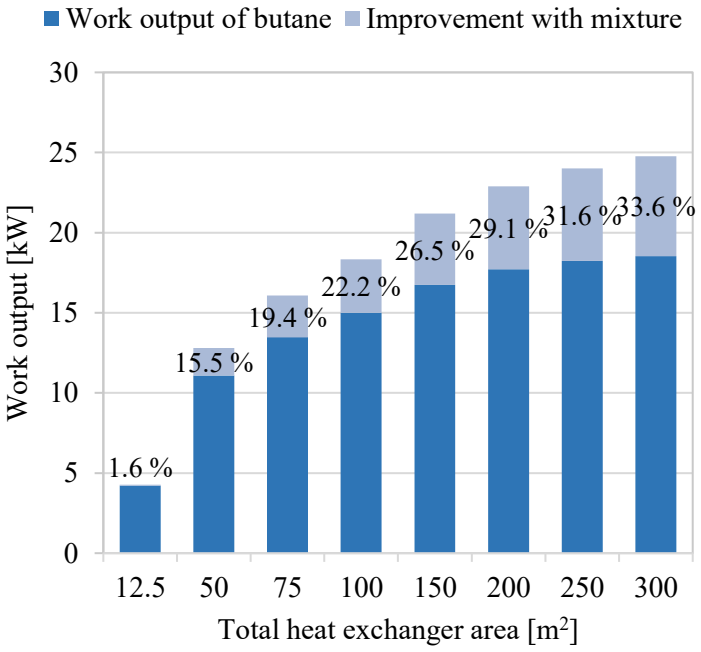

Figure 8-4 Case 1: Work output of butane and improvement with ethane-propane (0.6/0.4) mixture.

Figure 8-5 and Figure 8-6 respectively show the improvement in work output of mixture compared to ethane and butane for case 2. Compared to case 1, the average improvement from butane to mixture has dropped from 22.5 % to 13.1 %, and the average improvement from ethane to mixture has dropped from 22.5 % to 11.2 %. This illustrates that the work outputs of the pure fluids increase more from case 1 to case 2 than that of the mixture.

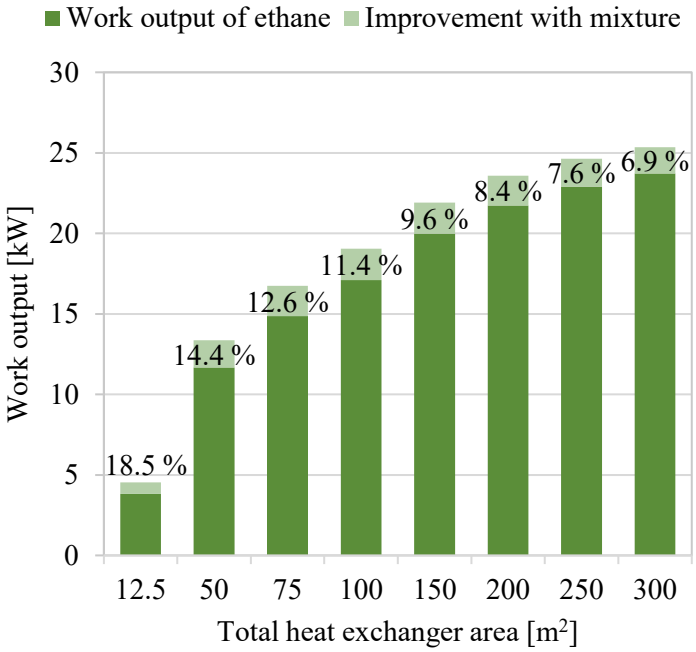

Figure 8-5 Case 2: Work output of ethane and improvement with ethane-propane (0.6/0.4) mixture.

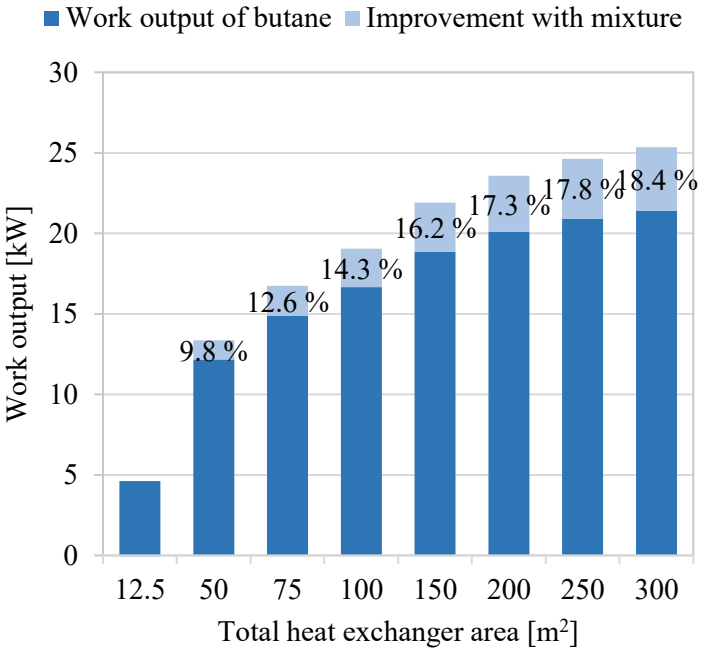

Figure 8-6 Case 2: Work output of butane and improvement with ethane-propane (0.6/0.4) mixture.

Figure 8-7 to Figure 8-12 plot the temperature-enthalpy diagrams for the different fluids and cases at a total HX area of 100 m^2. Work outputs and HX inlet pressures are also given in the plots, which illustrates how work outputs compare at this total HX area, as well as differences in operating pressures. Butane has operating pressure below 10 bar, and ethane has approximately ten times higher working pressures. Ethane-propane (0.6/0.4) allows for significant decreases in operating pressure compared ethane, but they are still well above that of butane.

As can be observed in Figure 8-7, butane has a high critical temperature compared to the heat source temperature, which gives rise to a subcritical heating process. The temperature profile in the HRHE is characterized by a pinch point "knee" at saturated liquid, which gives a poor temperature match between the heat source and working fluid, and relatively high temperature differences in the HRHE. Ethane and ethane-propane (0.6/0.4) have significantly lower critical temperatures than butane, which allows for a transcritical heating process. This enables an improved temperature match between the heat source and the working fluid in the HRHE, and lower HRHE temperature differences.

Both butane and ethane have pinch point knees at saturated vapor in the condenser, limiting the condenser temperature differences. Ethane has a significant desuperheating region in the condenser, which also contributes to a poor condenser temperature match. Ethane-propane (0.6/0.4), on the other hand, has a gliding temperature change during condensation, which allows for an improved temperature match between heat sink and working fluid, and low condenser temperature differences.

From case 1 to 2, heat sink outlet temperature decreases, and outlet pressure and temperature from the expander decreases for the same total HX area. It can be observed that condenser temperature match of the pure fluids has improved. The mixture, on the other hand, now has a poorer match between heat sink and working fluid temperatures.

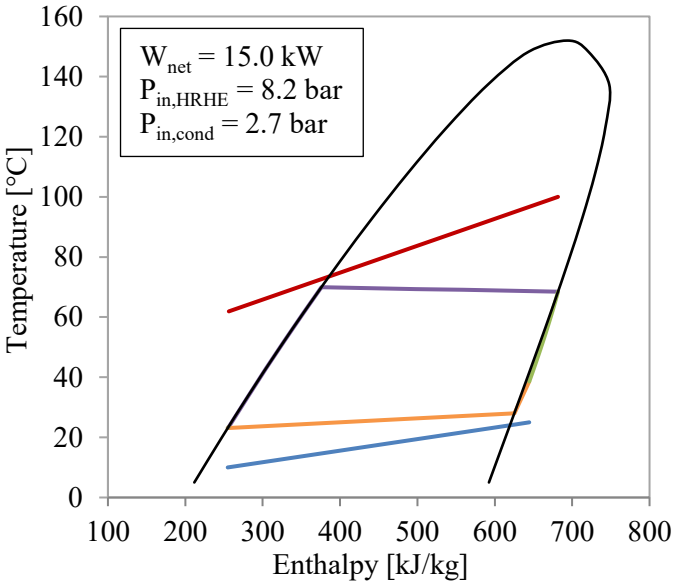

Figure 8-7 Case 1: Temperature-enthalpy diagram for Butane.

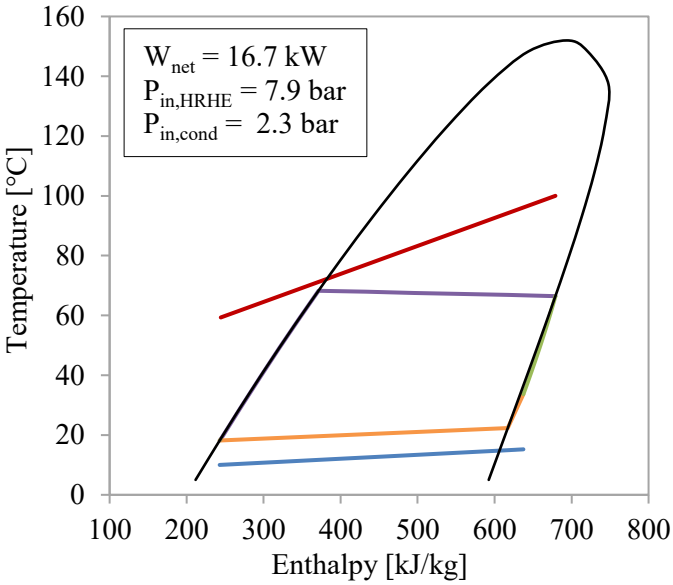

Figure 8-8 Case 2: Temperature-enthalpy diagram for Butane.

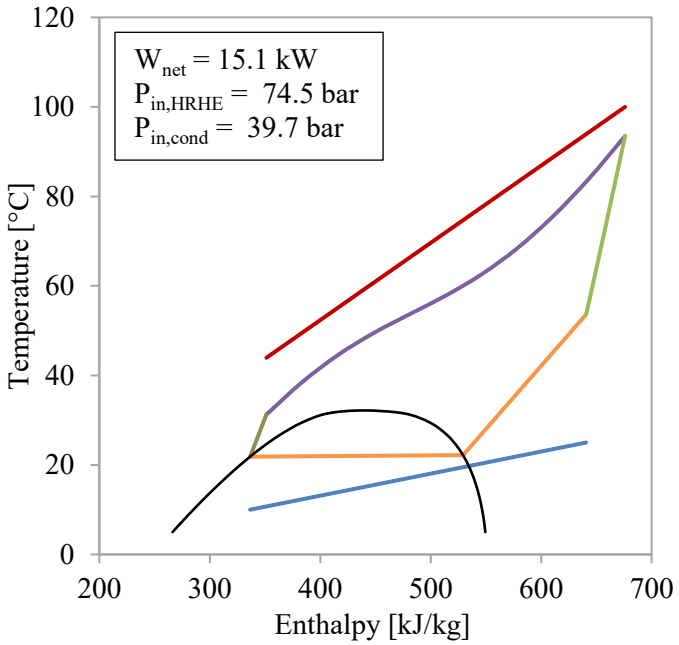

Figure 8-9 Case 1: Temperature-enthalpy diagram for Ethane.

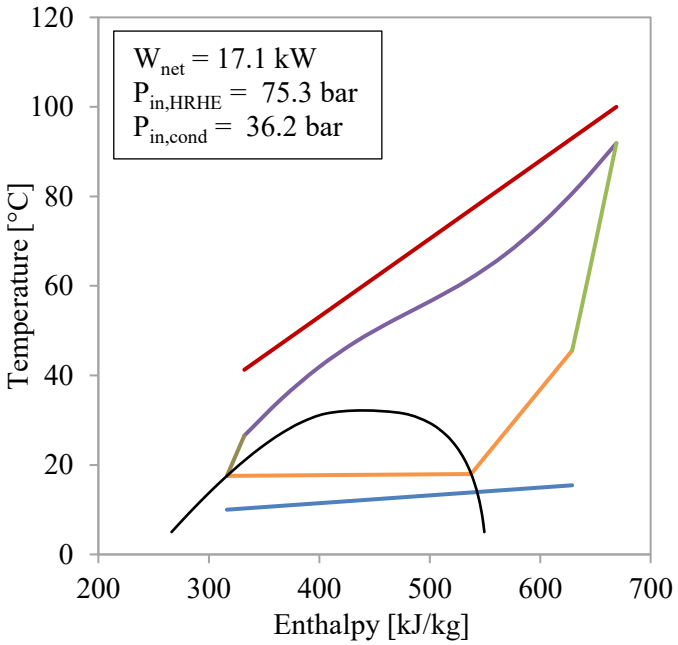

Figure 8-10 Case 2: Temperature-enthalpy diagram for Ethane.

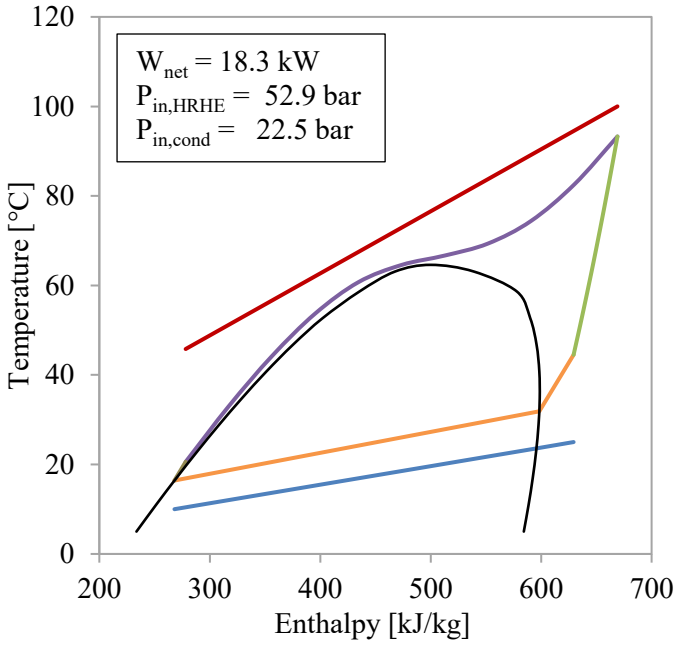

Figure 8-11 Case 1: Temperature-enthalpy diagram for Ethane-propane (0.6/0.4).

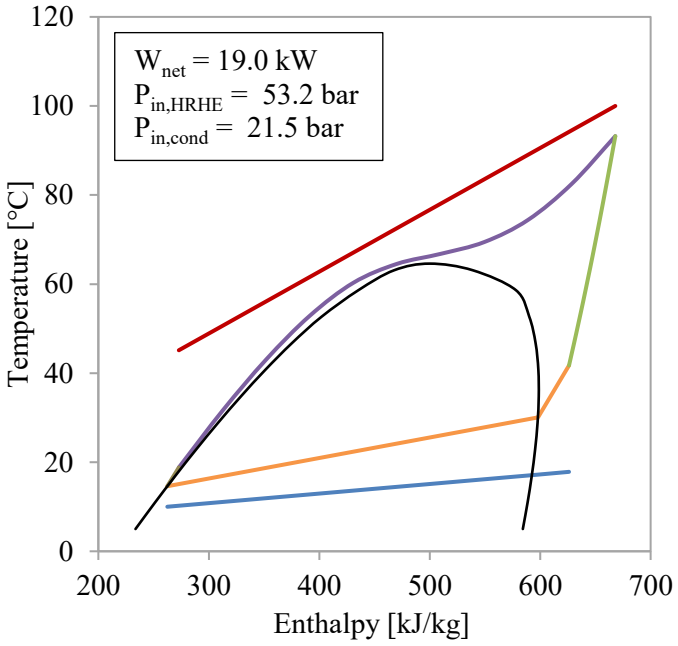

Figure 8-12 Case 2: Temperature-enthalpy diagram for Ethane-propane (0.6/0.4).

Figure 8-13 to Figure 8-15 show the distributions between condenser and HRHE for the different fluids in case 1. For butane, condenser area dominates, whereas ethane has a higher HRHE area. For the mixture, HX areas are more balanced, with slightly higher HRHE area.

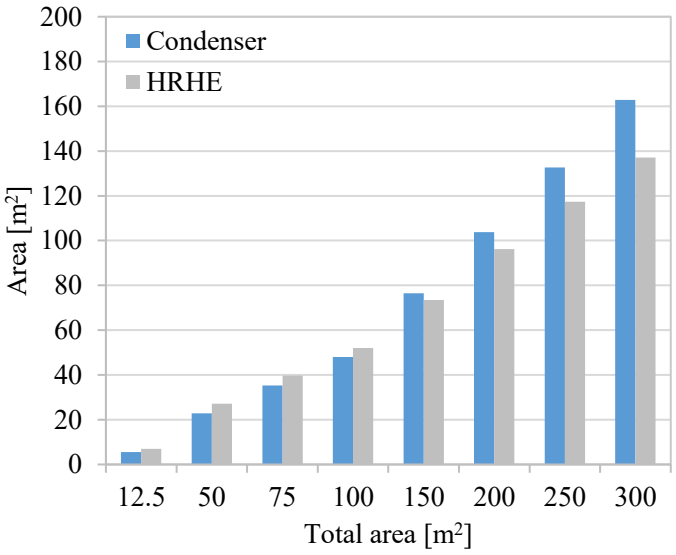

Figure 8-13 Case 1: Condenser and HRHE area for Butane.

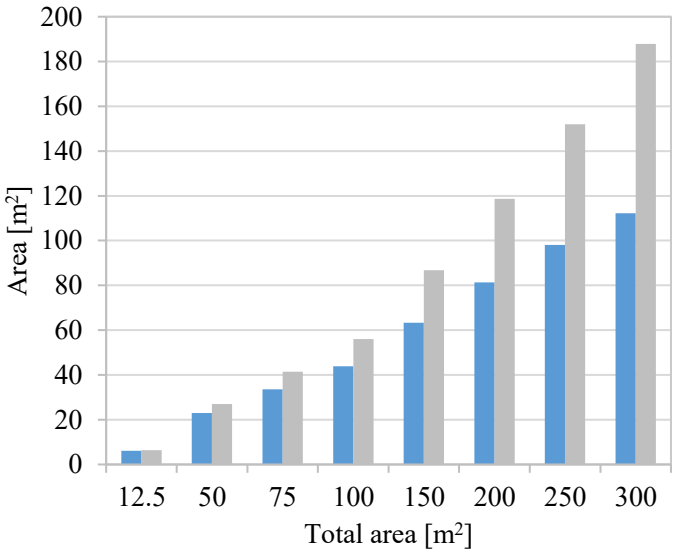

Figure 8-14 Case 1: Condenser and HRHE area for Ethane.

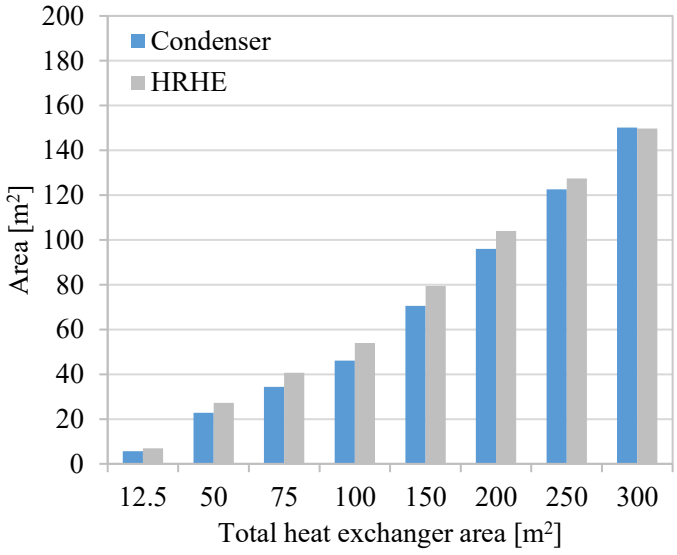

Figure 8-15 Case 1: Condenser and HRHE area for Ethane-propane (0.6/0.4).

8.1.1 Heat exchanger design for case 1

Total HX areas of 50 m^2 and 150 m^2 are chosen for comparison of HX design. Table 8-1 and Table 8-2 list different HX design parameters at the respective areas. Work outputs, HX pressure loss and percentage of condenser and HRHE area are the optimum values as calculated from step 3, Section 0. The number of tubes, tube diameter and length is found with the optimization procedure outlined in Table 6-3. Furthermore, Table 8-3 and Table 8-4 compare the estimated areas from step 3 (calculated with the equations for overall HTC), with the "actual" areas calculated with the method in Section 5.3.1 and Table 6-3. HX operating conditions are given in Appendix A.1.

At 50 m^2, condenser and HRHE areas are relatively equal for the different fluids, and HRHE area is greater than condenser area. At a total HX area of 150 m^2, condenser and HRHE areas differ more, and show higher condenser area for butane, higher HRHE area for ethane, and more distributed areas for the mixture.

Most diameters optimize at 4 mm, with the exception of the butane condenser, with has higher tube diameters. At 50 m^2, the number of tubes is between 200 and 400, also with the exception of the butane condenser. The number of tubes is higher at 150 m^2, and the level of pressure loss and pinch points are lower.

The absolute average deviation between estimated and calculated area for all fluids is 6.2 %. However, the average deviation is skewed by the high deviations for the butane HRHEs, with average deviations of 13.7 % and 28.6 %.

Table 8-1 HX design at a total HX area of 50 m^2.

Working fluid	W_{net}	HX	Area [%]	Pressure loss [bar]	Pinch point [°C]	d [mm]	N	L [m]
Butane	11.1 kW	Condenser	46.6	0.45	7.0	12.0	77	7.1
		HRHE	53.4	0.62	6.2	4.0	395	4.7
Ethane	10.3 kW	Condenser	44.0	0.58	5.0	4.0	346	5.2
		HRHE	54.0	0.66	9.3	4.0	260	7.8
Ethane-propane (0.6/0.4)	12.8 kW	Condenser	45.1	0.81	10.0	4.0	371	4.7
		HRHE	54.6	0.68	9.5	4.0	224	9.6

Table 8-2 HX design at a total HX area of 150 m^2.

Working fluid	W_{net}	HX	Area [%]	Pressure loss [bar]	Pinch point [°C]	d [mm]	N	L [m]
Butane	16.7 kW	Condenser	51.9	0.38	2.1	19.3	66	17.3
		HRHE	48.0	0.41	1.2	4.3	681	6.1
Ethane	17.5 kW	Condenser	42.4	0.39	1.6	4.0	737	6.6
		HRHE	57.8	0.52	4.4	4.0	513	12.8
Ethane-propane (0.6/0.4)	21.2 kW	Condenser	47.0	0.52	4.7	4.0	892	6.3
		HRHE	53.0	0.62	4.2	4.0	402	16.1

Table 8-3 Estimated area (step 3) versus calculated area (step 2) at a total HX area of 50 m^2.

Working fluid	HX	Estimated area [m^2]	Calculated area [m^2]	Deviation [%]
Butane	Condenser	22.9	21.6	+ 5.8
	HRHE	27.0	23.8	+ 13.7
Ethane	Condenser	23.0	22.7	+ 1.3
	HRHE	27.0	25.5	+ 5.9
Ethane-propane (0.6/0.4)	Condenser	22.7	21.8	+ 4.1
	HRHE	27.3	27.2	+ 0.4

Table 8-4 Estimated area versus calculated area at a total HX area of 150 m^2.

Working fluid	HX	Estimated area [m^2]	Calculated area [m^2]	Deviation [%]
Butane	Condenser	76.5	73.4	+ 4.2
	HRHE	73.5	57.1	+ 28.6
Ethane	Condenser	63.3	61.3	+ 3.1
	HRHE	86.7	82.7	+ 4.9
Ethane-propane (0.6/0.4)	Condenser	70.5	71.0	- 0.6
	HRHE	79.5	81.5	- 2.5

8.2 Case 3 and 4

Figure 8-16 plots the work output of case 3 (without IHX) and 4 (with IHX) versus of total HX area. Recall that both case 3 and 4 involve a heat source cooled from 200°C to 80°C. The plot shows that the mixture has lower work output than the pure fluid for all values of total HX area; the work output of butane is on average 3.7 % higher than the work output of the mixture.

When the option of internal heat exchanger is introduced, the pure fluid starts assigning area to the IHX at a total HX area of 150 m^2, and the mixture does so at 100 m^2. From 150 m^2 to 400 m^2, the average improvement with IHX is 8.4 % for the mixture and 4.6 % for the pure fluid. Consequently, the work output of the mixture is now comparable to that of the pure fluid.

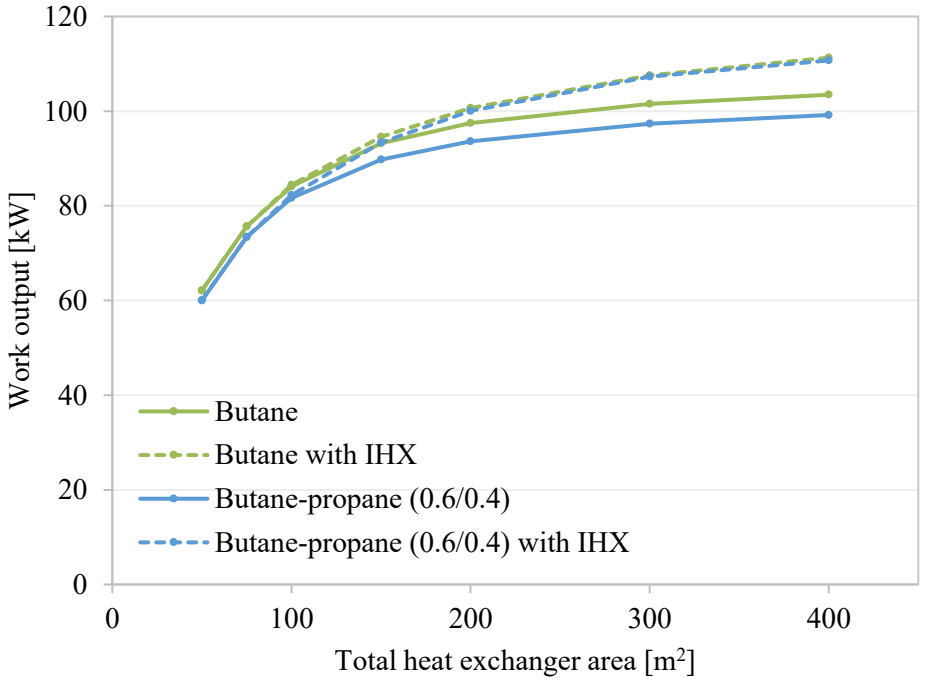

Figure 8-16 Work output vs. total heat exchanger area for case 3 and 4.

Figure 8-17 and Figure 8-18 show the work outputs at 150 m^2 to 400 m^2 for butane and butane-propane (0.6/0.4), respectively. The improvement with IHX is also shown in the figure, both the absolute value improvement and the percentage improvement with IHX. The figures illustrate that improvement with IHX is greater for higher values of total HX area. Moreover, they show that improvement is higher for the mixture and that work outputs of both fluids with IHX is relatively similar.

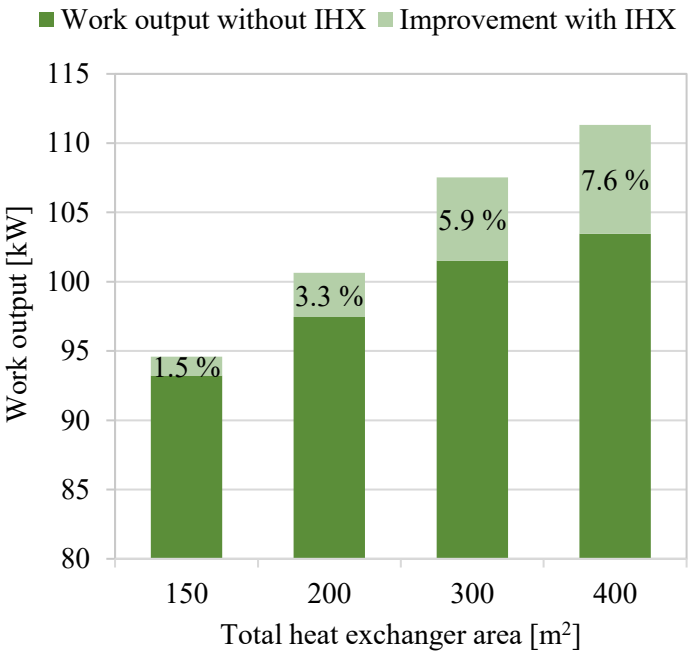

Figure 8-17 Butane: Work output at 150 m^2 to 400 m^2 for case 3, along with improvement with IHX in case 4.

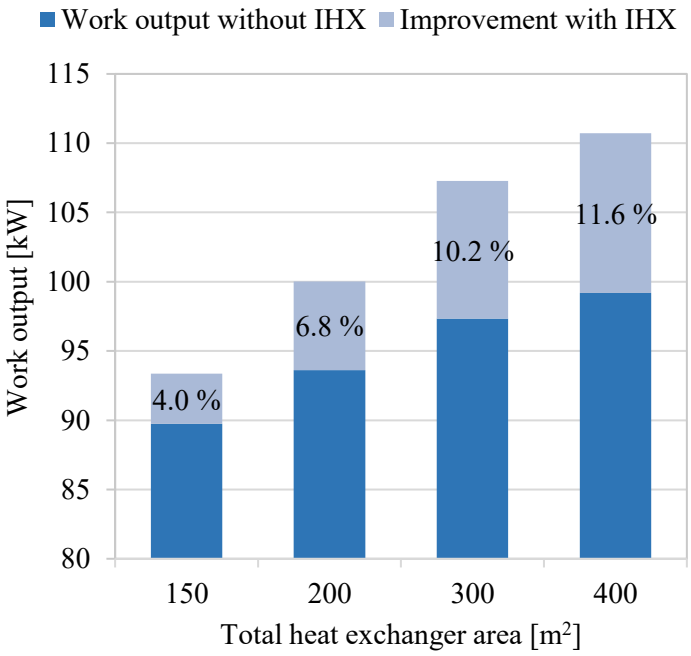

Figure 8-18 Butane-propane (0.6/0.4): Work output at 150 m^2 to 400 m^2 for case 3, along with improvement with IHX in case 4.

Figure 8-19 to Figure 8-22 plot the temperature-enthalpy diagrams for the different cases and fluids at a total HX area of 200 m^2. Work outputs and operating pressures are also given in the figure, where the latter are higher for the mixture. Figure 8-19 and Figure 8-20 show that butane and butane-propane (0.6/0.4) have similar temperature profiles in the HRHE, but are distinguished by the temperature glide of butane-propane (0.6/0.4) in the condenser. Average logarithmic temperature differences (not given here) actually show that the mixture has higher HRHE temperature differences and, despite the gliding temperature of change during condensation, higher temperature differences in the condenser. As is slightly visible by comparing Figure 8-19 and Figure 8-20, the higher mixture condenser temperatures occur in the desuperheating region of the condenser.

Figure 8-22 Figure 8-21 demonstrate that the IHX allows lower HRHE and condenser temperature differences. In particular, the IHX has “relieved” the relatively high temperature differences in the desuperheating region of the condensers.

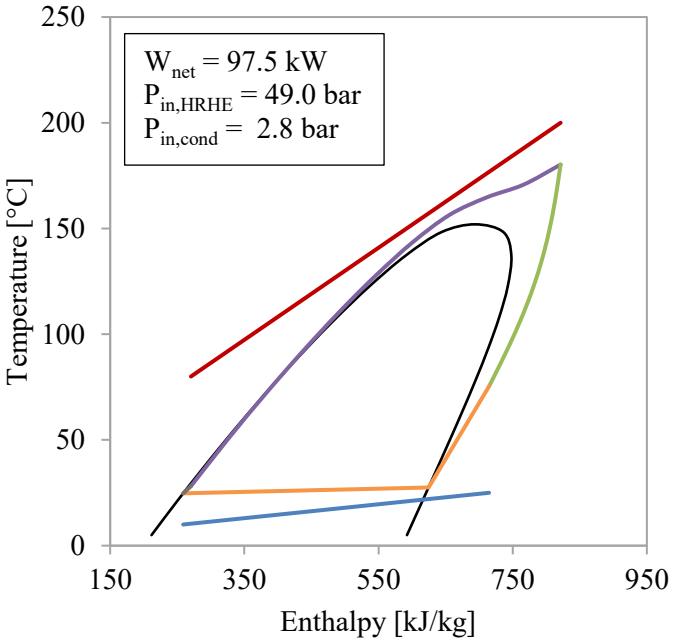

Figure 8-19 Case 3: Temperature-enthalpy diagram for Butane without IHX.

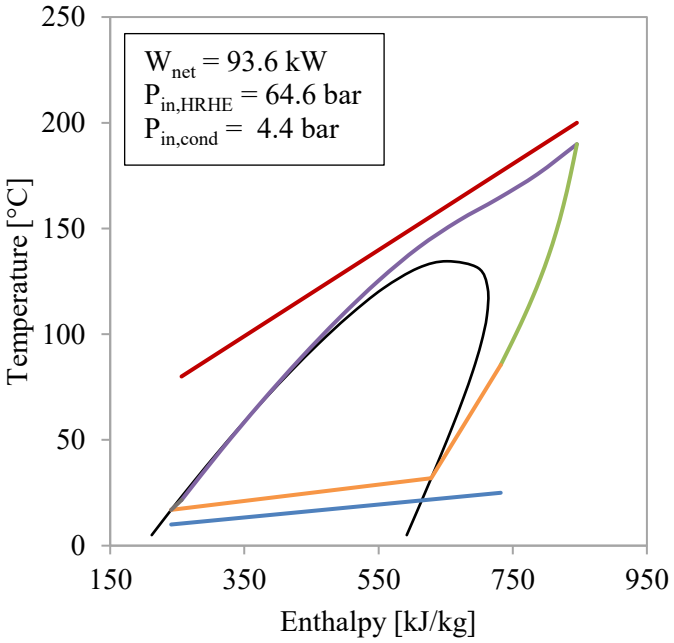

Figure 8-20 Case 3: Temperature-enthalpy diagram for Butane-propane (0.6/0.4) without IHX.

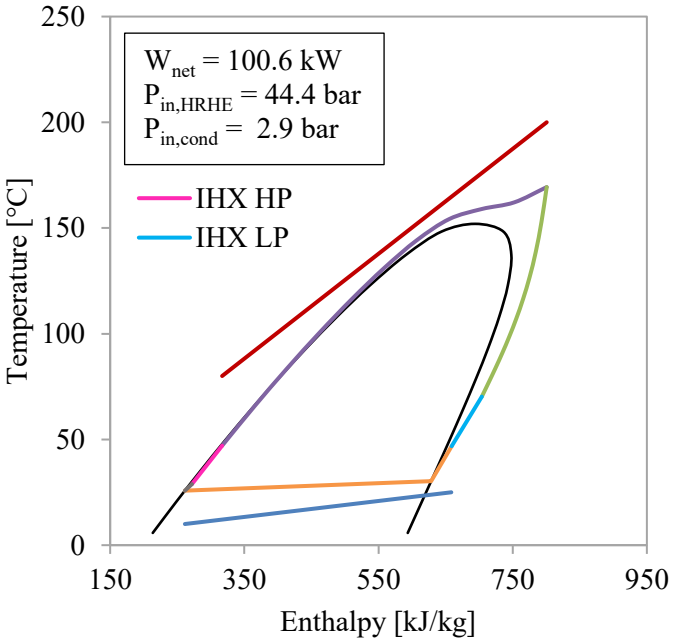

Figure 8-21 Case 4: Temperature-enthalpy diagram for Butane with IHX.

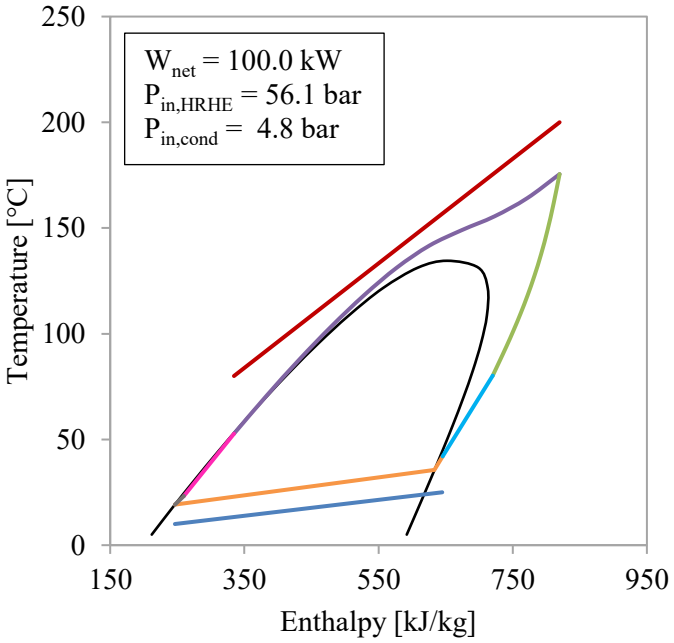

Figure 8-22 Case 4: Temperature-enthalpy diagram for Butane-propane (0.6/0.4) with IHX.

Figure 8-23 and Figure 8-24 show the distribution of area between condenser and HRHE for butane and the mixture without IHX. The distributions are relatively equal, with a slightly higher weight of mixture condenser area. Figure 8-25 and Figure 8-26 show the distribution of area between condenser, HRHE and IHX for the fluids in case 4. The fraction of IHX area

increases with total HX area, and gives rise to a more evenly distributed condenser and HRHE area. The fraction of IHX area increases "exponentially" for the pure fluid, whereas the increase in fraction of IHX area stagnates for the mixture.

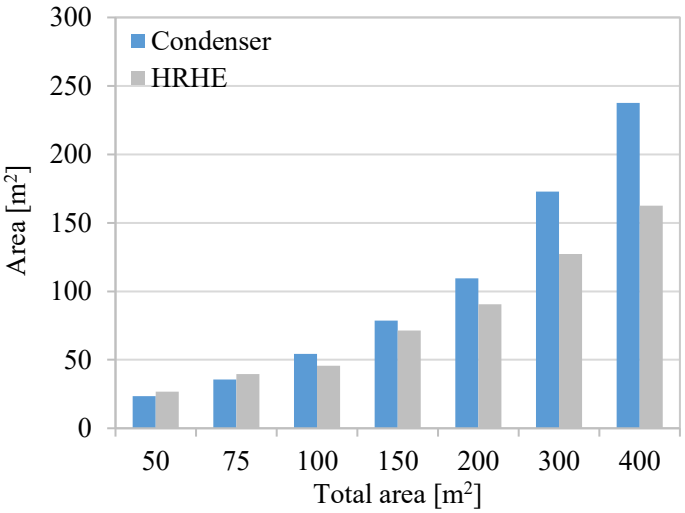

Figure 8-23 Case 3: Condenser and HRHE area for butane without IHX.

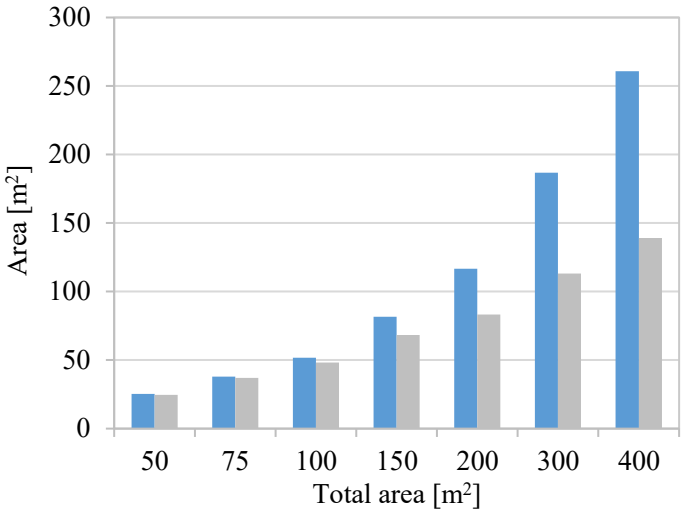

Figure 8-24 Case 3: Condenser and HRHE area for butane-propane (0.6/0.4) without IHX.

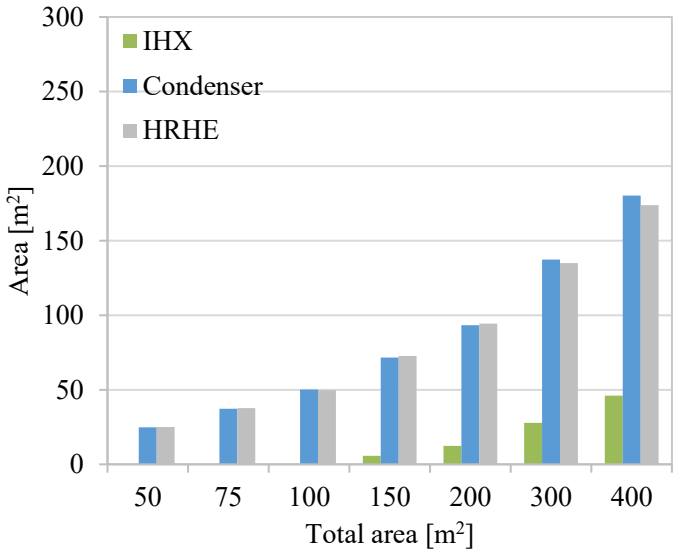

Figure 8-25 Case 4: Condenser, HRHE and IHX area for butane.

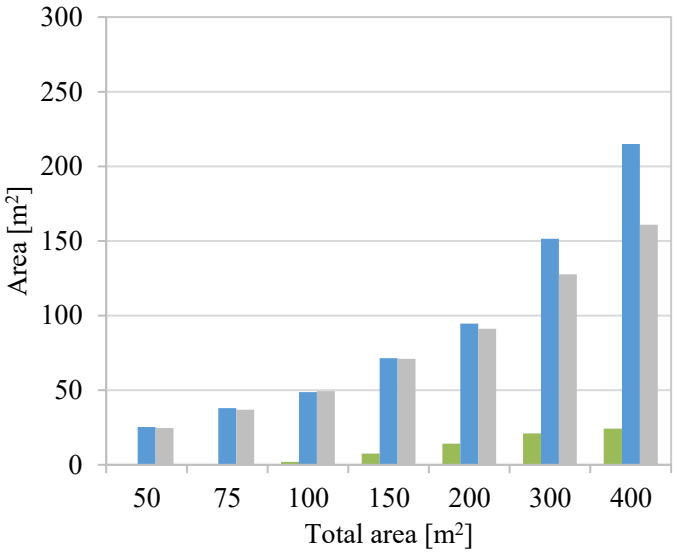

Figure 8-26 Case 4: Condenser, HRHE and IHX area for butane-propane (0.6/0.4).

8.2.1 Heat exchanger design for case 3 and 4

A total HX area of 200 m^2 is chosen for comparison of HX design. Table 8-5 lists different HX design parameters for case 3 and 4, including HX pressure loss and percentage of condenser and HRHE (and IHX) area. The work outputs, number of tubes, tube diameter and lengths are also given. Moreover, Table 8-6 lists different parameters for the IHX in case 4, including high and low side pressure loss, tube diameters, number of tubes per layer (N_1 and N_2), number of layers and tube length. Lastly, Table 8-7 compares the estimated areas with the calculated areas. HX operating conditions are given in Appendix A.2.

The distribution between condenser and HRHE area is relatively similar, and even more so for the fluids with IHX, for which fraction of IHX area is 6-7 %. For both cases, pressure loss optimizes at a lower level in the condenser, and pressure loss is in general lower for the fluids with IHX. Moreover, pinch points in the IHX is high compared to condenser and HRHE pinch points. Condenser tube diameter is higher than HRHE diameter, and the number of tubes in the condenser is generally lower.

For both fluids with IHX, pressure loss on the high pressure side optimizes approximately ten times higher than the pressure loss on the low pressure side. High pressure side tube diameters (d_1) optimize at 4 mm, and the low pressure side tube diameters (d_2) optimize between 12 and 16 mm. The mixture has higher pressure loss, lower tube diameter on the low pressure side, fewer tubes per layer, and more layers.

The absolute average deviation between estimated and calculated area is 3.3 %, with no significant outliers.

Table 8-5 HX design for case 3 and 4 at a total HX area of 200 m^2.

Working fluid	W_{net}	HX	Area [%]	Pressure loss [bar]	Pinch point [°C]	d [mm]	N	L [m]
Butane	97.5	Condenser	54.8	0.27	5.5	16.6	190	11.9
		HRHE	45.3	1.42	7.5	4	353	19.8
Butane-propane (0.6/0.4)	93.6	Condenser	58.4	0.30	6.9	13.4	226	12.0
		HRHE	41.7	1.23	10.1	4.0	361	18.3
Butane with IHX	100.6	Condenser	46.7	0.40	6.5	12.2	306	8.4
		HRHE	47.2	1.97	7.8	4	338	21.3
		IHX	6.1	-	17.7	-	-	-
Butane-propane (0.6/0.4) with IHX	100.0	Condenser	47.1	0.45	9.2	9.3	417	7.5
		HRHE	45.6	2.07	8.8	4	339	21.5
		IHX	7.1	-	18.4	-	-	-

Table 8-6 IHX design for case 4 (1: HP-side, 2: LP-side) at a total HX area of 200 m^2.

Working fluid	Pressure loss, HP [bar]	Pressure loss, LP [bar]	d_1 [mm]	d_2 [mm]	N_1	N_2	N_{layers}	L [m]
Butane	0.37	0.03	4	15.8	7	6	61	2.0
Butane-propane (0.6/0.4)	0.44	0.05	4	12.6	4	4	110	2.5

Table 8-7 Estimated area versus calculated area for case 3 and 4 at a total HX area of 200 m^2.

Working fluid	HX	Estimated area [m^2]	Calculated area [m^2]	Deviation [%]
Butane	Condenser	109.5	118.5	- 7.6
	HRHE	90.5	87.1	+ 3.2
Butane-propane (0.6/0.4)	Condenser	116.7	114.5	+ 1.9
	HRHE	83.3	82.8	+ 0.6
Butane with IHX	Condenser	93.3	97.8	- 4.6
	HRHE	94.4	90.3	+ 4.5
Butane-propane (0.6/0.4) with IHX	Condenser	94.5	91.0	+ 3.9
	HRHE	91.2	91.6	- 0.4

8.3 Project work results

The main results from the project work are given in this section. The results will be compared to the results of the current work in the discussion, Section 9.4.

The project work case involved a heat source at 150°C, cooled to 80°C, with a similar heat sink as in case 1, 3 and 4. Based on pinch analysis, the pure working fluid with the highest work output for this case was transcritical propane, and the mixture with the highest work output was transcritical propane-butane (0.8/0.2). Subcritical pentane and pentane-hexane (0.6/0.4) were also studied. The level of total HX area was higher compared to the current work because HRHE outside area was calculated, which is ten times higher than the inner area. Plots of work output versus total HX area are given in Figure 8-27 to Figure 8-29.

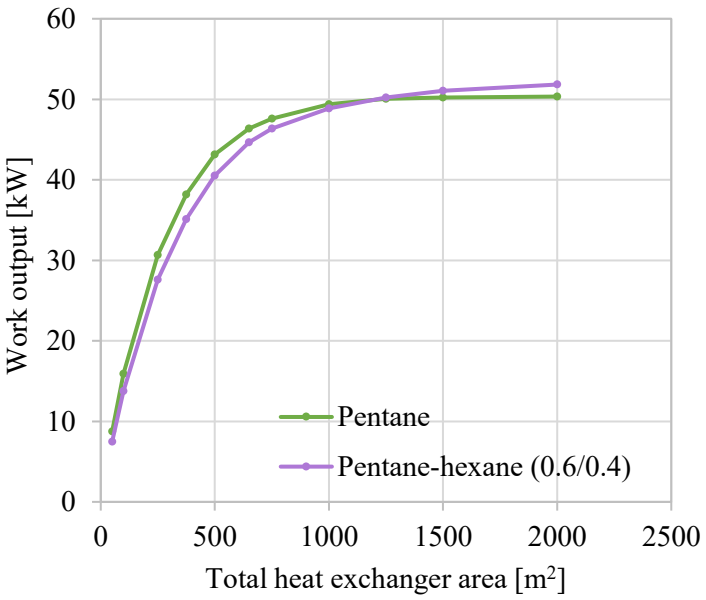

Figure 8-27 Work output vs. total heat exchanger for pentane and pentane-hexane (0.6/0.4)

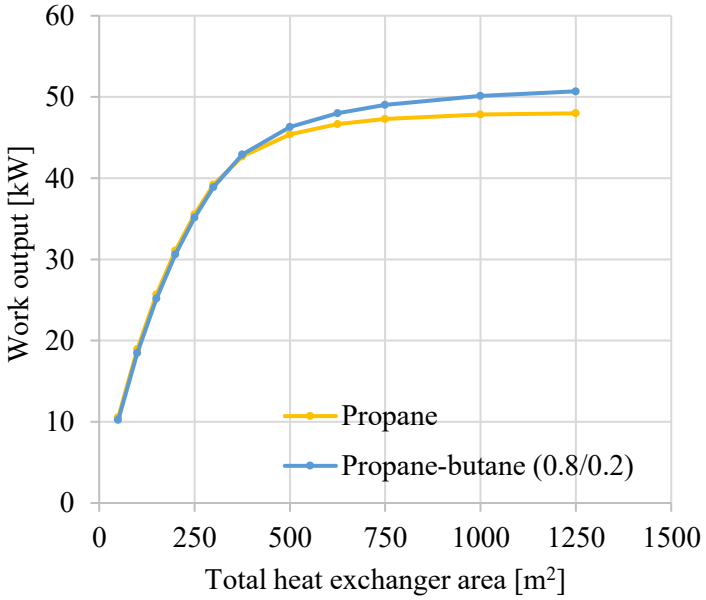

Figure 8-28 Work output vs. total heat exchanger for Propane and propane-butane (0.8/0.2)

Figure 8-27 shows that in the lower range of HX area, pentane achieves higher work output than pentane-hexane (0.6/0.4), whereas the opposite is the case for higher areas. Percentage increase in work output from pure fluid to mixture is 3.0 % at a total HX area of 2000 m^2, but pinch points at this area are less than 1°C.

Figure 8-28 shows that propane-butane (0.8/0.2) has approximately the same work output as propane for low values of total area, but outperforms propane for higher areas (5.6 % at 1250 m^2). However, pinch points also need to be very low for the propane-butane (0.8/0.2) to outperform propane (condenser pinch point is lower than 1°C at 1250 m^2). Consequently, neither the subcritical mixture nor the transcritical mixture shows significant improvement compared to pure working fluids in this case.

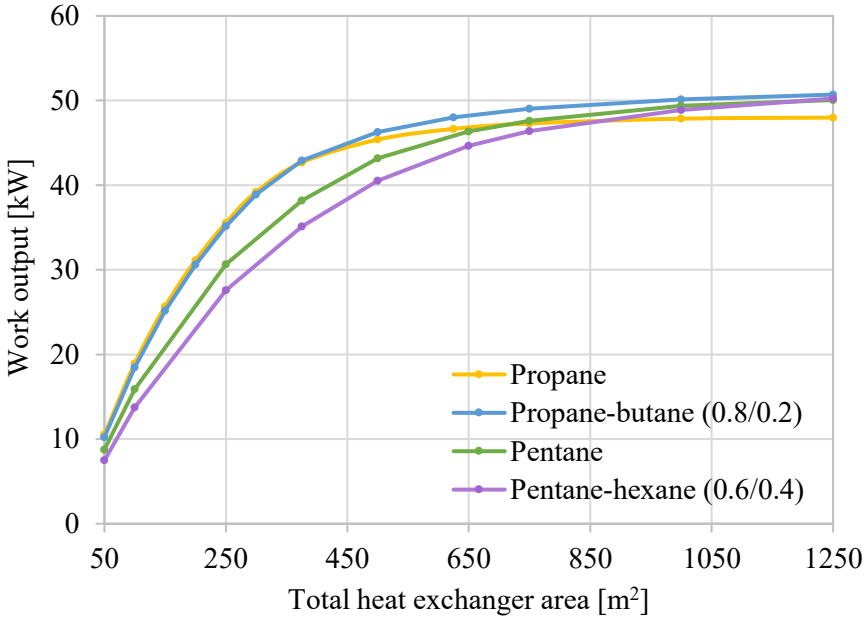

Figure 8-29 Work output vs. total heat exchanger for all working fluids

Figure 8-29 plots the work outputs for all fluids versus total HX area. The figure shows that the subcritical fluids have lower work output than the transcritical fluids in the lower range of total HX area, and that the differences in work output decrease for high areas.

9 DISCUSSION

For all cases, the variation in work output with total HX area for the different fluids is compared and explained. A special focus is given to HX temperature differences, and the possibility of increased work output through reduced HX temperature differences and exergy losses. Moreover, the underlying nature of the distributions between condenser and HRHE is explored for the different fluids in case 1. For case 3 and 4, the distribution between condenser and HRHE (and IHX) area is also discussed, but in less detail and on the background of the same arguments as case 1. For case 1, 3 and 4, differences in optimum HX design is explained and discussed. After the case results have been discussed, the different cases are compared with focus on potential for increased work output using mixtures. Furthermore, the cycle model is evaluated in terms of strength and weaknesses, and the "new" and "old" condensation correlations are compared. Some general remarks are given on the use of correlations in the current work.

9.1 Case 1

9.1.1 Work output versus total HX area

Recall that the mixture achieved the highest work output in case 1, and that the case involves a heat source at 100°C. For areas above 75 m^2, butane achieved the lowest work outputs, and ethane achieved work outputs between that of butane and the mixture.

The differences between the fluid work outputs can be explained with the different factors that contribute to increased area. As work output is optimized for increasing values of pre-defined area, the optimization tool has the choice between increasing the UA-value, $\sum_n(\dot{Q}_n / LMTD_n)$, or reducing overall HTC to achieve increased area. The former will typically contribute to an increase in work output through lower HX temperature differences, and the latter will contribute to an increase in work output through lower HX pressure loss. Lower HX temperature differences is particularly effective in increasing work output, as this will enable lower HX losses, and a greater enthalpy change across the expander; $\dot{W}_{exp} = \dot{m}_{wf}\left(h_{in,exp} - h_{out,exp}\right)$.

The ability of the fluids to decrease HX temperature differences with increasing area is related to the shape of their HX temperature profiles. As observed in Figure 8-6, the ability of butane to decrease HX temperature differences is limited by pinch points at both saturated liquid in the HRHE and saturated vapor in the condenser. Instead of lowered HX temperature differences, its HX pressure loss is reduce instead. Consequently, butane achieves a relatively low value of work outputs with increasing area. Ethane, limited only by a pinch point at saturated vapor in the condenser, achieves higher work outputs with increasing area compared to butane. Even better, ethane-propane (0.6/0.4) with condenser and HRHE temperature profiles well matched with the heat sink and heat source, achieves the highest work outputs.

The validity of the above argumentation can be investigated by comparing average logarithmic mean temperature differences in the condenser and HRHE, which are plotted against total HX area for the different fluids in Figure 9-1 and Figure 9-2. Subcritical butane has significantly higher average temperature differences in the HRHE compared to the transcritical fluids. At the same time, butane actually has the lowest temperature differences in the condenser. However, the difference between the fluids in the condenser is relatively low, and butane is approached by the mixture at high areas. Thus, temperature differences in the HRHE appears to dominate differences in work output.

Temperature differences are relatively equal for ethane and the mixture, which indicates that temperature differences are not sufficient to explain differences in work output between these two fluids. In fact, the pumping power required for ethane is a relatively high compared to ethane-propane (0.6/0.4), as seen in Figure 9-3. Butane pumping power is even lower, but this does not weigh up for its low expander work, limited by an “un-matched” HRHE temperature profile.

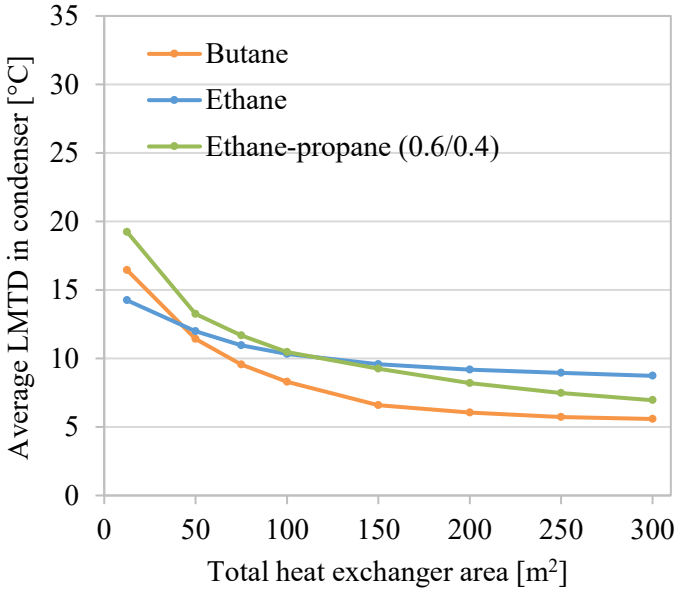

Figure 9-1 Average logarithmic temperature differences in the condenser.

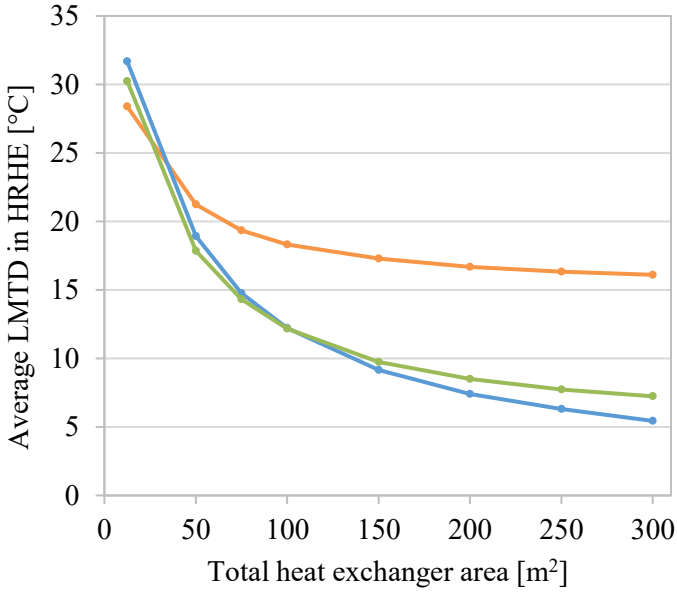

Figure 9-2 Average logarithmic temperature difference in the HRHE.

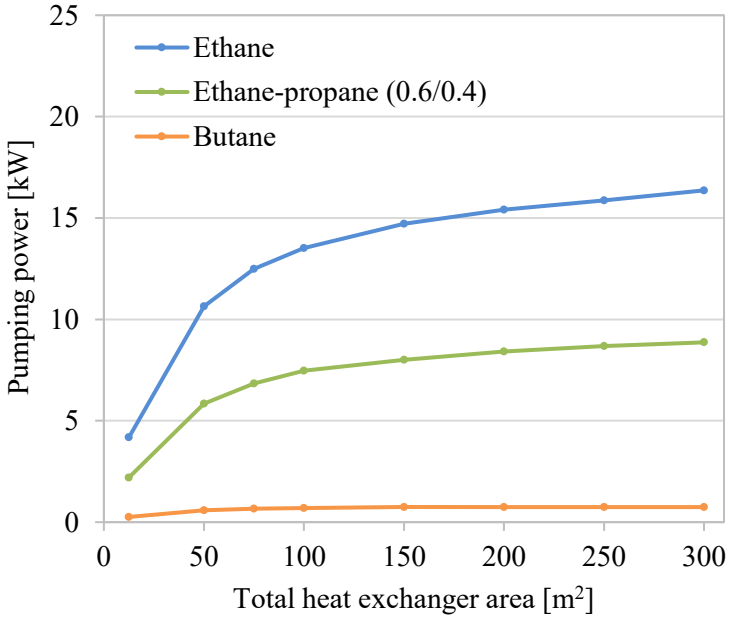

Figure 9-3 Pumping power for the different fluids.

The average improvement in work output from ethane to ethane-propane (0.6/0.4) is 22.5 %, compared to 33.2 % improvement with pinch point analysis. Mixtures typically require greater HX area than pure fluids for the same pinch point, as their temperature glide causes lower average temperature differences. This may explain why improvement from pure fluid to mixture is not as high when comparison is made on the basis of equal total HX area.

The average improvement from butane to ethane-propane (0.6/0.4) is also 22.5 %, but the improvement potential is focused in the higher area region, where the mixture can reach improvements in work output of almost 34 %, as seen in Figure 8-4. This indicates that the potential of transcritical ethane-propane (0.6/0.4) at high values of total HX area is significant compared to a more "conventional" subcritical pure working fluid. However, optimum operating pressures of ethane-propane (0.6/0.4) can reach as high as 50-60 bar, while that of butane optimizes below 10 bar. This may infer higher costs and safety requirements related to high-pressure components for the mixture. Operating pressures of ethane can reach 70-80 bar, which means that the transcritical mixture achieves both an increase in work output and a decrease in operating pressures compared to the transcritical pure fluid.

As an alternative to the transcritical mixture, one may consider the use of a subcritical mixture, which can have the benefit of increased work output compared to butane, but lower operating pressures than ethane-propane (0.6/0.4). However, a subcritical mixture will still be limited by a HRHE pinch point at saturated vapor, and thus it is unlikely that it will achieve as high work outputs as the transcritical mixture.

Butane is not the poorest performing fluid for all values of total HX area. At a total area of 50 m^2, butane has 5.8 % higher work output than ethane. Below 75 m^2, the HRHE temperature differences of butane are not significantly high compared to those of ethane. Coupled with lower pumping power, butane is able to outperform ethane below 75 m^2. In fact, butane archives the highest values of work output per unit area of the two pure fluids. With the analogy between HX areas and costs, this means that work output per unit costs can be higher for butane, which might make butane the more desirable pure fluid in some cases.

9.1.2 Distribution of area between condenser and HRHE

The distribution of area between the condenser and HRHE is plotted for the different fluids in Figure 8-13, Figure 8-14 and Figure 8-15.

HX area is governed by the equation:

$$A = \frac{\sum_n (\dot{Q}_n / LMTD_n)}{U_{predicted}} = \frac{UA}{U_{predicted}} \quad (9\text{-}1)$$

The distribution of HX area between the condenser and HRHE is determined by the relative sizes of UA-values and overall HTCs in the condenser and HRHE.

As previously indicated, logarithmic mean temperature differences are coupled with the shape of temperature profiles in the HXs. Well-matched temperature profiles between heat source/sink and working fluid enable temperature differences to reduce, contributing to an increase in area. Moreover, HRHE heat load is higher than condenser heat load, and the difference between the two increases for higher areas. The effect is higher HRHE UA-value and area compared to the condenser. This effect is typically negligible compared to the effect of temperature differences and overall HTC in the current work, and is neglected in the following discussion.

9.1.2.1 Butane

The condenser and HRHE overall HTCs of butane are plotted against total HX area in Figure 9-4, and the UA-value is plotted against total HX area in Figure 9-5. The plots show that both the overall HTC and the UA-value is higher in the condenser. Higher UA-value in the condenser can be attributed to the fact that the condenser temperature profile, as observed in Figure 8-7, is slightly better matched than the HRHE temperature profile, allowing for lower logarithmic temperature differences. Now, higher condenser overall HTC contributes to *lower* condenser area compared to HRHE area, whereas higher UA-value in the condenser contributes to *higher* condenser area. As seen in Figure 8-13, for areas lower than 150 m^2, the effect of higher HTC dominates and condenser area is lower than HRHE area. For areas of 150 m^2 and above, the effect of higher UA-value dominates and condenser area increases beyond HRHE area. As observed in Figure 9-5, this is caused by the stagnation in the UA-value for the HRHE at 150 m^2, where pinch point in the HRHE reaches 1.2°C and logarithmic temperature differences can no longer decrease at the same rate. Consequently, the increase in HRHE area stagnates as well.

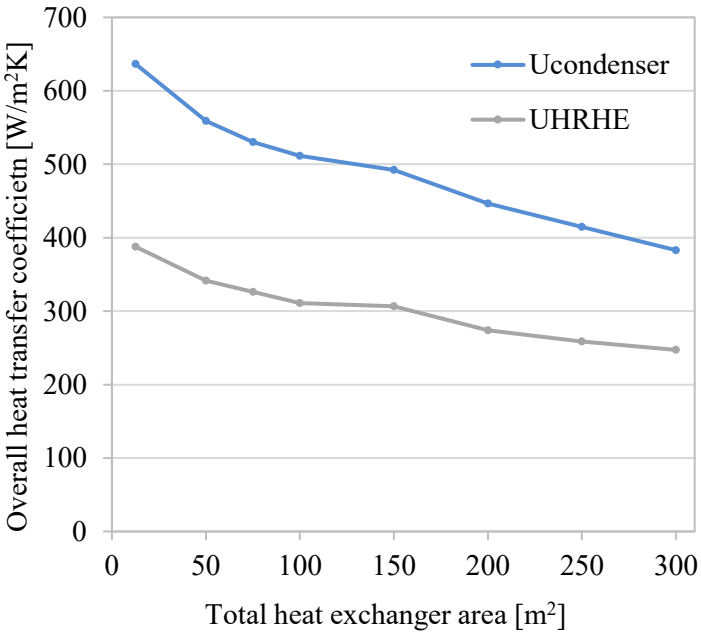

Figure 9-4 Overall heat transfer coefficient versus total HX area for butane.

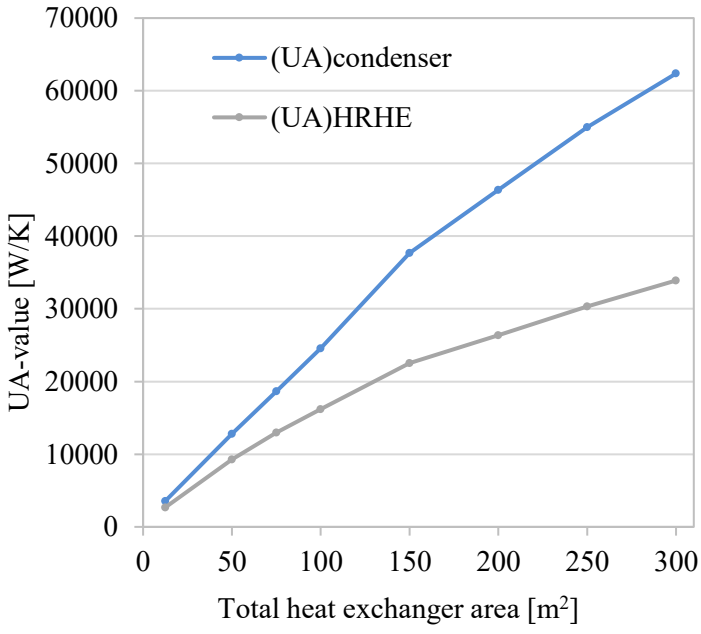

Figure 9-5 UA-value versus total HX area for butane.

9.1.2.2 Ethane

The same plots are given for ethane in Figure 9-6 and Figure 9-7. The plots show, as with butane, that both overall HTC and UA-value are higher in the condenser. Yet, as observed in Figure 8-14, condenser area is lower for all values of total HX area, contrary to what was the case for butane. For ethane. The condenser overall HTC is much higher compared to the HRHE overall HTC, which weighs more strongly towards less condenser area. Moreover, UA-value increases more rapidly in the HRHE (only slightly visible in the Figure 9-7), owing to the smooth temperature profile in the HRHE. This causes HRHE area to increase faster than condenser area, outweighing the faster decrease in condenser overall HTC that can be observed in Figure 9-6.

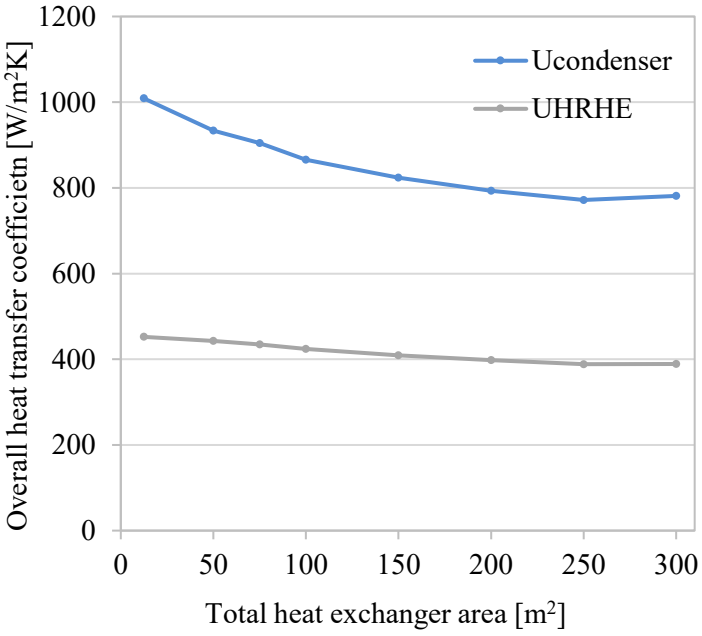

Figure 9-6 Overall heat transfer coefficient versus total HX area for ethane.

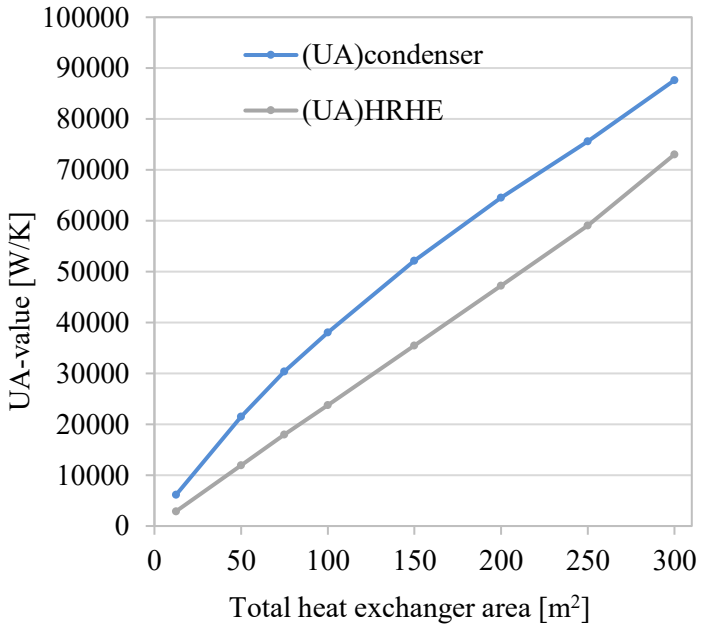

Figure 9-7 UA-value versus total HX area for ethane.

9.1.2.3 Ethane-propane (0.6/0.4)

The plot of area distribution in Figure 8-15 for ethane-propane (0.6/0.4) shows that condenser and HRHE area are more evenly distributed. Figure 9-8 and Figure 9-9 show that the effect of higher condenser overall HTC (and *lower* condenser area) appears to balance the effect of higher condenser UA-value (and *higher* condenser area); whereas the overall HTCs approach similar values for increased area, UA-values depart from each other. UA-value increases more rapidly in the condenser, causing condenser area to "catch" up with HRHE area for high values of total HX area, as shown in Figure 8-15.

The decrease in overall HTC with area is higher for the condenser because the pressure losses chosen by the optimization represent a region of high curvature of the function $U_{cond} = f(\Delta p, T_{pinch})$ (this region is illustrated in Figure 6-4 for low pressure losses). The reason why the UA-values depart from each other is that HRHE pinch point approaches zero faster than the condenser pinch point, owing to a well matched condenser temperature profile, illustrated in Figure 8-11.

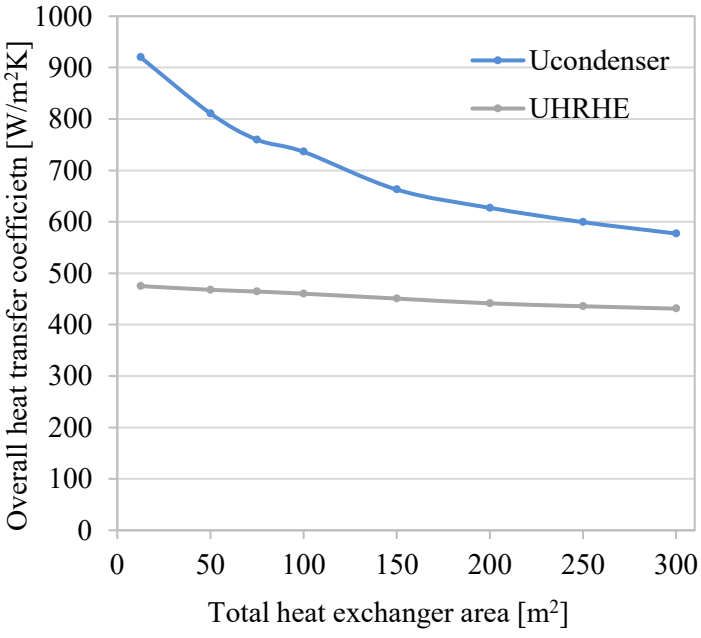

Figure 9-8 Overall heat transfer coefficient versus total HX area for ethane-propane (0.6/0.4).

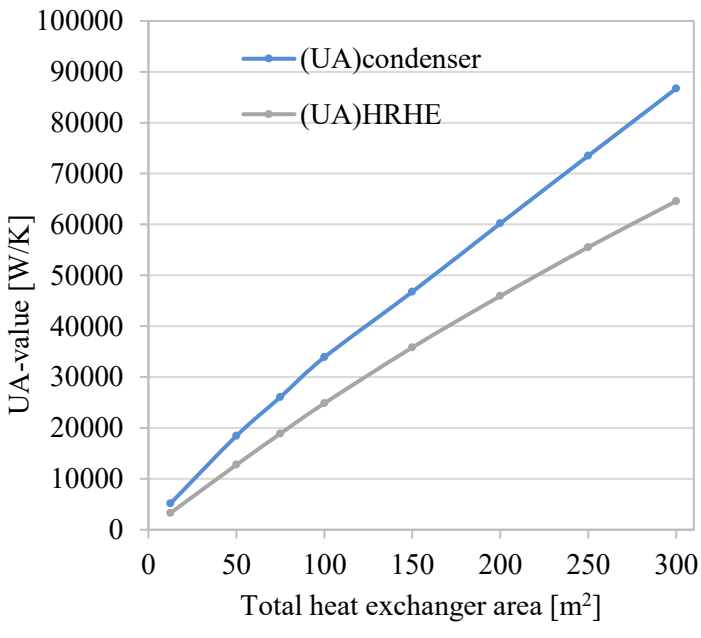

Figure 9-9 UA-value versus total HX area for ethane-propane (0.6/0.4).

9.1.3 HX design

In Section 8.1.1, HX designs are compared for total HX areas of 50 m^2 and 150 m^2. At 50 m^2, condenser and HRHE areas are relatively equal for the different fluids, and HRHE area is greater than condenser area. Higher HRHE area reflects the lower overall HTC in the HRHE, and the dominance of this effect over UA-values (or temperature differences) in the low-area region.

Pressure loss optimizes between 0.45 and 0.81 bar. In particular, the butane pressure losses are lower than the pressure loss of the other fluids, which is probably owed to the fact that the pressure levels of butane are relatively low, as shown in Table 12-1 in Appendix A.1. Low pressure levels mean that the pressure ratio across the expander, and consequently work output, is more sensitive to pressure loss in the HXs.

At a total HX area of 50 m^2, pinch points optimize between 5°C and 10°C for the different fluids. Due to the gliding temperature change of the mixture in the condenser, it has twice as high pinch point as ethane for approximately the same condenser area. Butane is characterized by a low HRHE pinch point, due to the pinch point "knee" at saturated liquid. The transcritical fluids, with gliding temperature change in the HRHE, have higher HRHE pinch points.

Most diameters optimize at 4 mm a total HX area of 50 m^2, with the exception of the butane condenser, which has a diameter of 12 mm. The pressure in the butane condenser is relatively low, as shown in Appendix A.1. Lower pressure levels mean relatively low densities, which gives rise to higher velocities and pressure loss than the other fluids for a diameter of 4 mm. In fact, when assigning butane the same HX design as ethane at a total HX area of 50 m^2, pressure loss increases from 0.38 bar to 1.63 bar, and the decrease in work output compared to zero condenser pressure loss increases from 21.0 % to 45.3 % (at the same time, condenser area reduces from 21.6 to 9.75 m^2). The higher condenser diameter causes the flow to be distributed between fewer number of tubes. For the other fluids, the number of tubes optimize at higher levels than butane due to higher pressures and lower tube diameters; between 200 and 400. For the same tube diameter, lower condenser pressure gives rise to a higher number of tubes relative to the HRHE. Thus, the choice of working fluid and its operating pressures appears to have a significant impact on HX geometry.

At a total HX area of 150 m^2, condenser and HRHE areas differ more, as the influence of temperature differences has started to take effect. This is especially true for butane, where relatively low temperature differences in the condenser gives rise to higher condenser area, despite the lower HRHE overall HTC (which contributes to higher HRHE area). For ethane, lower HRHE overall HTC outweighs the effect of lower condenser temperature differences, and HRHE area is higher. For the mixture, lower HRHE overall HTC is more balanced with the effect of lower condenser temperature differences, and HRHE area is only slightly higher than condenser area.

Pressure losses are lower at 150 m^2 than 50 m^2, caused by lower overall HTCs, which is coupled with lower pressure losses. Pinch points reflect the temperature profiles of the fluids; both pinch points for butane are low because of the pinch point knees at saturated liquid and vapor. The same is true for the ethane condenser, whereas the ethane HRHE pinch point is higher due to the transcritical HRHE process. For ethane-propane (0.6/0.4), both pinch points are relatively high due to the well-matched temperature profiles in both HXs. In fact, for this value of total HX area, the mixture may be the only applicable fluid in terms of pinch point feasibility. However, pinch points are also quite low for the mixture, so one may question whether this area is feasible for any of the fluids.

Tube diameter in the butane condenser is now even higher at 150 m^2 than 50 m^2, and the number of tubes lower, caused by an even lower condenser pressure. For the other fluids, the tube diameters still optimize at 4 mm, but mass flows and areas are higher, which increases the number of tubes.

Table 8-3 and Table 8-4 list the HX areas estimated with the functions for overall HTC as well as the areas calculated at the given pressure losses with the method in Section 5.3.1. The absolute average deviation between estimated and calculated area for all fluids is 6.2 %. However, the average deviation is skewed by the high deviations for the butane HRHEs, with average deviations of 13.7 % and 28.6 %. In general, deviation between estimated and calculated area can be partly accounted to the inability of the function $U = f(\Delta p, T_{pinch})$ to precisely estimate overall HTCs for different pressure loss and pinch points. Additionally, HTCs vary with other parameters than pinch point and pressure loss, as demonstrated in Appendix B for mass flux and reduced pressure. Moreover, deviations may be caused by LMTD being used for estimated area and AMTD being used for calculated area.

The relatively high deviation between estimated and calculated area in the butane HRHE can be explained by two factors. First of all, using LMTD in place of AMTD when finding estimated area gives a higher deviation in the HRHE for subcritical fluids than for transcritical fluids. This is because LMTD will better capture the low temperature differences that occur in the region around pinch for the subcritical fluid. Secondly, reduced pressure or mass flows chosen by the optimization procedure in "step 3" may differ from the corresponding values that the function $U = f(\Delta p, T_{pinch})$ was developed for (reduced pressure and mass flow calculated for optimum HX operating parameter in step 2, Section 6.1.2). The consequence is higher deviations between estimated and calculated area. This seems to be more so the case for the butane HRHE, as can be observed by comparing Figure 9-10 to Figure 9-13. Reduced pressure is calculated based on HX inlet pressures, and for the butane HRHE, reduced pressure optimize outside the range that the function for overall HTC were developed on. The same is mostly true for the working fluid mass flows of butane.

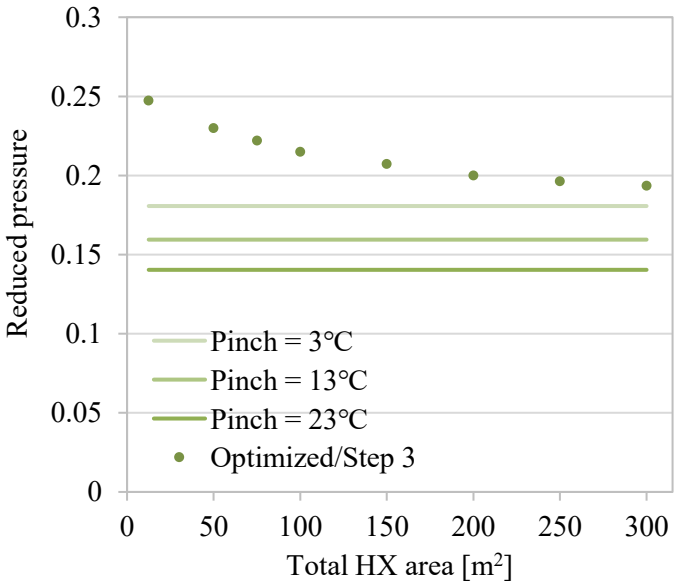

Figure 9-10 Butane HRHE: Reduced pressure versus total HX area for the different pinch point optimizations in step 1/2 and from results in step 3.

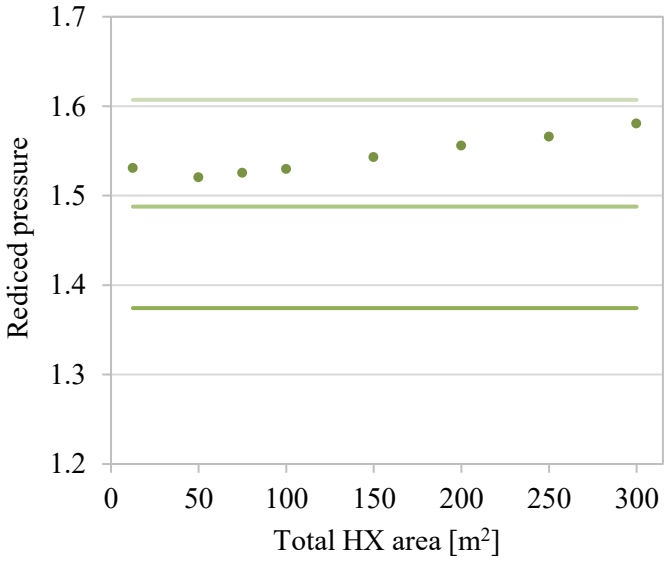

Figure 9-11 Ethane HRHE: Reduced pressure versus total HX area for the different pinch point optimizations in step 1/2 and from results in step 3.

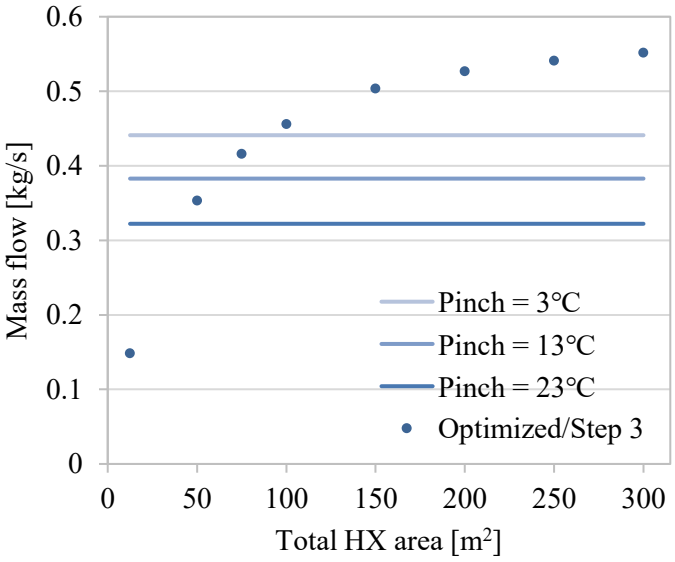

Figure 9-12 Butane: Mass flow versus total HX area for the different pinch point optimizations in step 1/2 and from results in step 3.

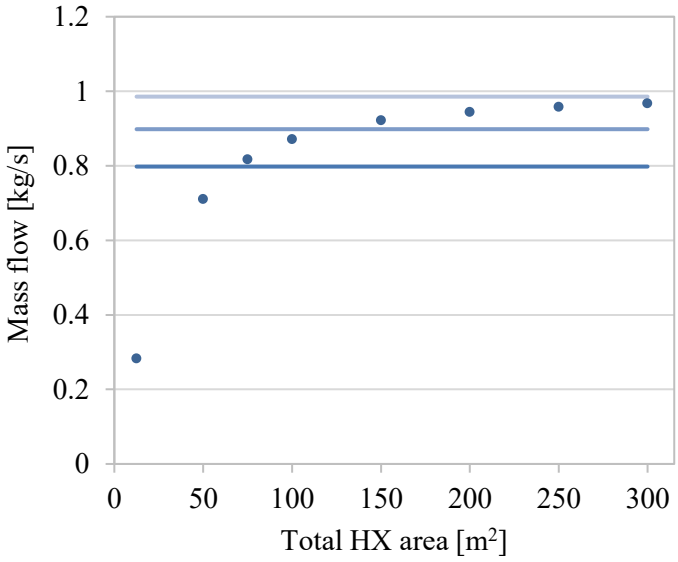

Figure 9-13 Ethane: Mass flow versus total HX area for the different pinch point optimizations in step 1/2 and from results in step 3.

Over-estimation of the butane HRHE area limits the fluids potential of increased work output for a given value of pre-defined area, and penalizes the fluid compared to ethane and ethane-propane (0.6/0.4). In contrary, for a total HX area of 150 m^2, the mixture HRHE area is under-estimated, and allows for use of more area to increase work output than what is actually available. In general, most of the areas are over-estimated and consequently, most of the work outputs at pre-defined area are under-estimated.

9.2 Case 2

Case 2 is similar to case 1, except that the heat sink outlet temperature is optimized. Work output versus total HX area is plotted in Figure 8-2, which shows that the mixture no longer outperforms the pure fluids by as much as in case 1. This can be seen by comparing Figure 8-3 and Figure 8-4 to Figure 8-5 and Figure 8-6, which demonstrate the fall in improvement potential from pure fluid to mixture. The average improvement from butane to mixture has dropped from 22.5 % to 13.1 %, and the average improvement from ethane to mixture has dropped from 22.5 % to 11.2 %. Thus, optimizing heat sink outlet temperature benefits the pure fluids more than the mixture. This is illustrated more clearly in Figure 9-14 to Figure 9-16.

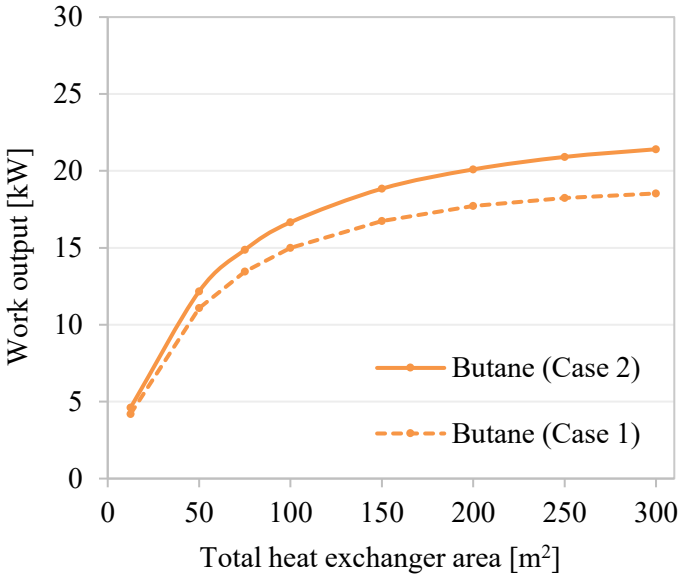

Figure 9-14 Butane: Work output versus total HX area for case 1 and 2.

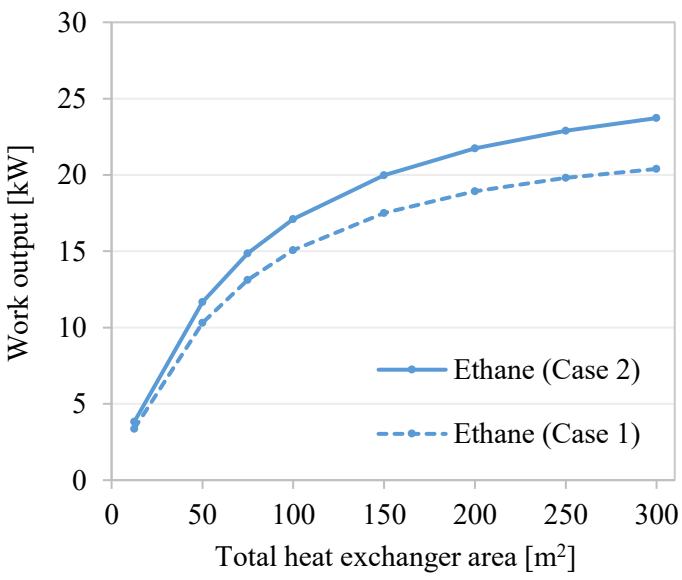

Figure 9-15 Ethane: Work output versus total HX area for case 1 and 2.

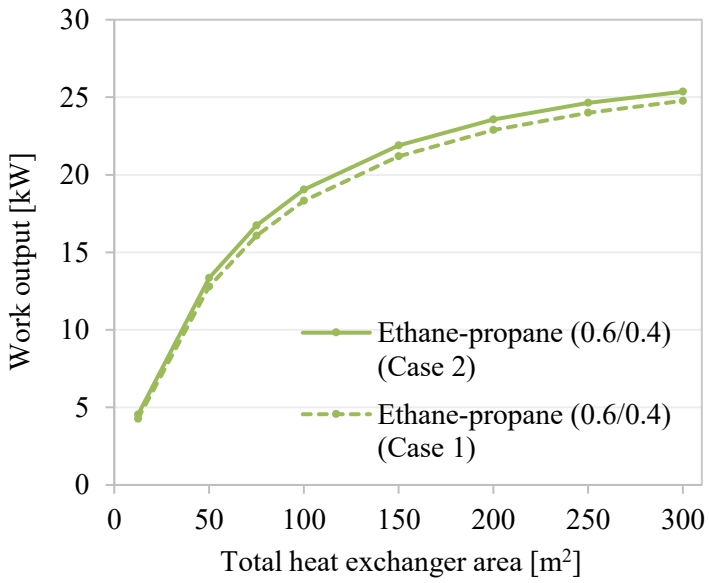

Figure 9-16 Ethane-propane (0.6/0.4): Work output versus total HX area for case 1 and 2.

The reason why optimized heat sink outlet temperature allows for increased work output appears to be that reducing heat sink outlet temperature allows for decreased expander outlet pressure for the same condenser area. This gives rise to a higher enthalpy drop across the expander, and a higher work output. Observe for instance Figure 8-7 and Figure 8-8 for butane, which show a decrease in expander outlet temperature (and pressure, not shown) from case 1 to case 2, and a simultaneous decreasing heat sink outlet temperature. Reducing heat sink outlet temperature maintains the same average temperature differences in the condenser and consequently, the same condenser area. In other words, optimized heat sink outlet temperature allows for an improved temperature match in the condenser, which is the case for both the pure fluids.

For the mixture, the gliding temperature change during condensation limits the potential to reduce expander outlet pressure with decreasing heat sink outlet temperature, without having to increase condenser area. Consequently, heat sink outlet temperatures optimize at higher levels for the mixture. Worth noting is that case 2 actually decreases temperature match in the mixture condenser, which increases condenser losses. Still, reduced expander outlet pressure contributes to increased work output.

Reducing heat sink outlet temperature increases heat sink pumping power due to an increase in heat sink mass flow. The heat sink pumping power is calculated with the following equation:

$$\dot{W}_{pump,sink} = \left(\frac{\Delta p \cdot \dot{m}}{\rho}\right)_{sink} \tag{9-2}$$

Heat sink pressure loss is set to a constant value of 1 bar, but pressure loss, and consequently pumping power, would typically increase with increasing heat sink mass flow.

Heat sink mass flow is plotted against total HX area for the different fluids in Figure 9-17. The figure shows that heat sink mass flow optimizes at higher levels for the pure fluids, which is related to the fact that heat sink outlet temperature optimizes at lower levels for the pure fluid. The consequence of higher mass flows is a more significant underestimation of pumping power for the pure fluids, and therefore a more significant overestimation of work outputs. Thus, optimizing heat sink outlet temperature unfairly favors the pure fluids over the mixture. In addition, the cost of heat sink water may be significant in geographic regions with low access to cold water, which would infer a higher cost for the pure fluids.

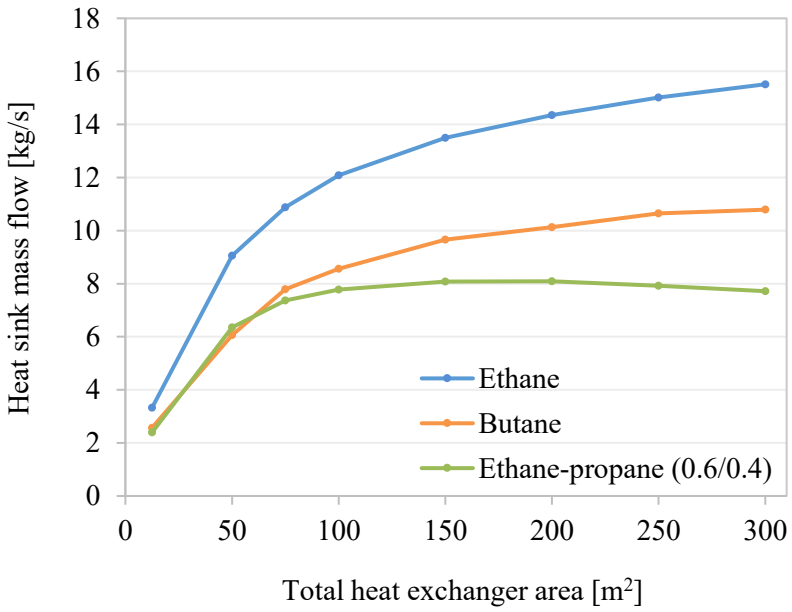

Figure 9-17 Heat sink mass flow versus total HX area.

Conclusively, case 2 suggests that pure fluids may benefit from optimized heat sink outlet temperatures more than mixtures. However, optimizing heat sink outlet temperature unfairly favors the pure fluids, both due to the failure of pumping power to account for increasing heat sink pressure loss with increasing heat sink mass flow, and because of the cost related to heat sink water. The heat exchanger models are not developed for variations in heat sink parameters,

and it is therefore difficult make conclusions about the effect of changing heat sink parameters. Furthermore, working fluid studied in case 2 are based on “pinch point” screening of working fluids for case 1. A corresponding screening of working fluids based on case 2 might have revealed other trends between pure fluids and mixtures than what was observed in Section 7.1

9.3 Case 3 and 4

9.3.1 Work output versus total heat exchanger area

Contrary to case 1 and 2, the mixture has lower work output than the pure fluid for all values of total HX area, as shown in Figure 8-16. The work output of butane is on average 3.7 %, or 3.2 kW, higher than the work output of the mixture. Working fluid pumping power is on the same order and on average 3.6 kW greater for the mixture, which is likely brought about by a higher pressure lift in the pump. This appears to account for some of the difference in work output between the two fluids. However, it does not explain why the mixture does not outperform the pure fluid in this case, as whit case 1 and 2.

The inability of the mixture to outperform the pure fluid may be related to the HX temperature differences. Despite the gliding temperature difference during condensation of propane-butane (0.6/0.4), it has higher average logarithmic temperature differences in both condenser and HRHE, as illustrated in Figure 9-18 and Figure 9-19. The discontinuity at 100 m^2 in the butane HRHE is owed to the fact the part of the HRHE process at this value of total HX area happens to take place in the two-phase region (as opposed to the other areas), giving rise to relatively high temperature differences. Higher HX temperature difference and exergy losses could explain the lower work output of the mixture in this case.

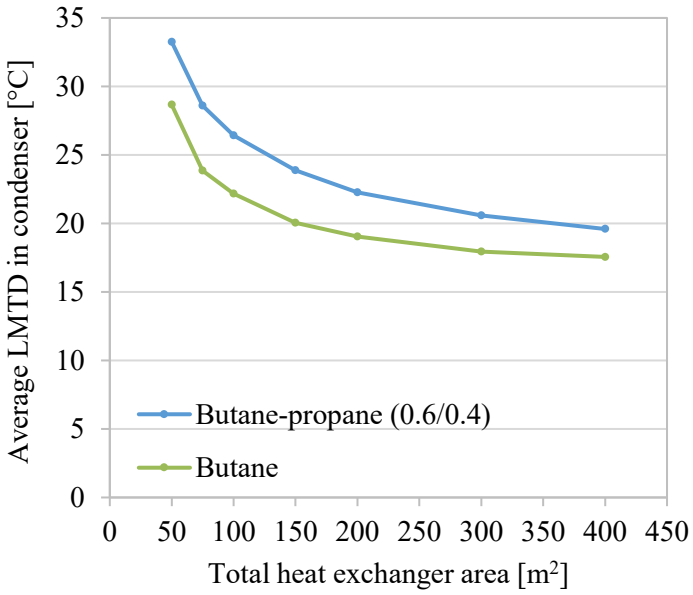

Figure 9-18 Case 3: Average logarithmic temperature differences in the condenser.

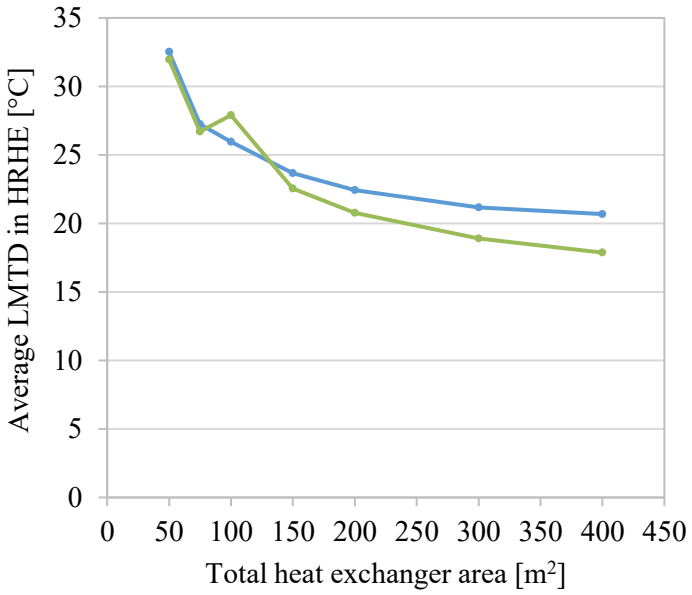

Figure 9-19 Case 3: Average logarithmic temperature differences in the HRHE.

When the option of internal heat exchanger is introduced, the pure fluid starts assigning area to the IHX at a total HX area of 150 m^2, and the mixture does so at 100 m^2. The IHX give rise to higher work output, which could be explained by increases in working fluid mass flow and reductions in HX temperature differences.

Condenser and HRHE temperature differences with and without IHX are plotted in Figure 9-20 and Figure 9-21, which show that the IHX enables continued reduction in temperature differences when these start approaching constant values without IHX. Thus, area is assigned to the IHX when increases in condenser and HRHE area no longer allow significant decreases in HX temperature differences.

From observation of the figures, it can be seen that the IHX enables a greater reduction in temperature differences for the mixture, explaining perhaps why the mixture achieves a greater increase in work output with IHX. Introducing an IHX significantly reduces temperature differences in the desuperheating region of the condenser, and allows the gliding temperature change of the mixture during condensation to facilitate relatively low condenser temperature differences.

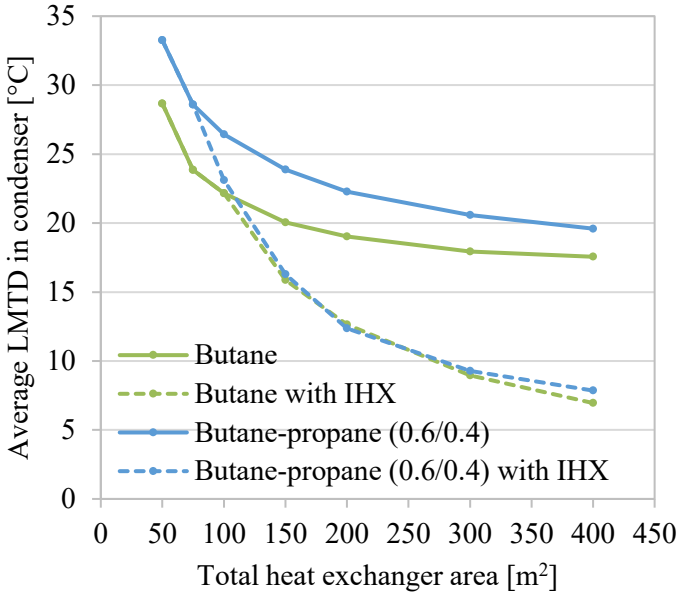

Figure 9-20 Case 3 and 4: Average logarithmic temperature differences in the condenser.

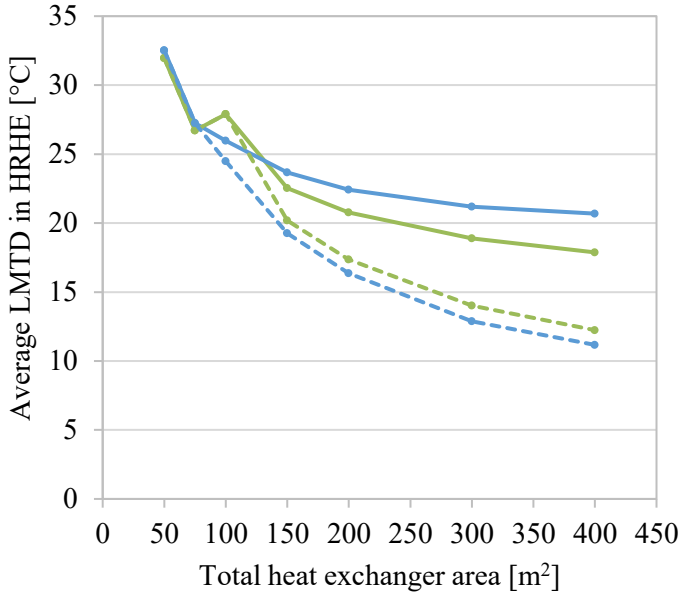

Figure 9-21 Case 3 and 4: Average logarithmic temperature differences in the HRHE.

In part, the results from the optimization model verify the results from working fluid screening, namely that the mixture does not provide higher work output than the pure fluid. However, the results differ in that the mixture is not able to achieve higher work outputs than the pure fluid *with* IHX. As with case 1, this may be explained with the inability of pinch point analysis to compare fluids on the basis of same total HX area.

In the working fluid screening, the mixture for further study was chosen based on the highest work output with IHX. As mentioned, the mixture had in fact lower work output than the mixture without IHX. Other fluids, such as butane-hexane (0.95/0.05), achieved higher work output than butane (+ 3.2 %), and would have been an interesting fluid to further study if more time were available.

9.3.2 Distribution of area between condenser, HRHE and IHX

As seen in Figure 8-23 and Figure 8-24 for case 3, condenser area is generally higher than HRHE area for both butane and butane-propane (0.6/0.4). This is caused by both slightly lower condenser temperature differences, as observed by comparing Figure 9-18 and Figure 9-19, as well as higher HRHE overall HTC. The percentage of condenser area is higher for the mixture, for which the mentioned factors weight a bit more strongly towards condenser area. It is worth noting that the distribution of area for the transcritical pure fluids is "opposite" that of case 1. This may be partly owed to the restriction on heat source outlet temperature in the current case, which limits the ability of HRHE temperature differences to decrease.

When introducing the option of internal heat exchanger, the pure fluid starts assigning a small percentage of area to the IHX at 150 m^2, while the mixture does so at 100 m^2. As illustrated in Figure 8-23 and Figure 8-24, fraction of condenser area has now decreased compared to HRHE area. This happens despite lower condenser temperature differences, as illustrated by comparing Figure 9-20 and Figure 9-21. An explanation for this is that, while HRHE heat loads remain the same when introducing IHX, condenser heat loads decrease, which decreases condenser area relative to HRHE area. Moreover, increases in condenser and HRHE HTCs keep the HX areas from increasing with reduced temperature differences.

The fraction of IHX area increases with increasing value of total HX area, as this allows continued decrease in condenser and HRHE temperature differences. More IHX area is assigned to the pure fluid, because the pure fluid achieves lower temperature differences in the IHX, as illustrated in Figure 9-22. In fact, temperature differences in the mixture IHX stagnate with increasing area, while that of the pure fluid continues to decrease, explaining the stagnation in IHX area for the mixture and the continued increase in IHX area for the pure fluid. However, this does not appear to significantly influence the potential of the mixture to increase work output with IHX, as improvement with IHX is higher for the mixture. This is probably because the increased work output with IHX is related to the ability of the IHX to facilitate decreases in condenser and HRHE temperature differences.

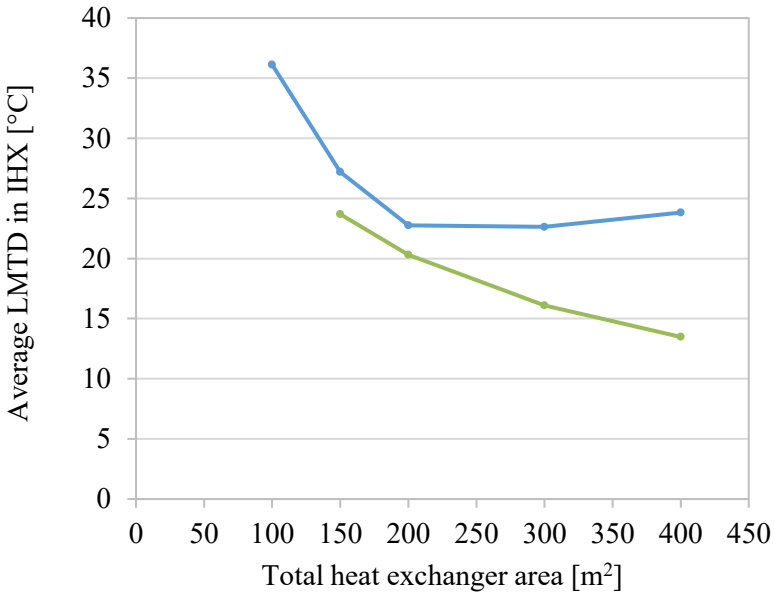

Figure 9-22 Case 4: Average logarithmic temperature differences in the IHX.

In the working fluid screening, an IHX heat load of 68.2 kW was assigned butane and an IHX heat load of 123.2 kW was assigned butane-propane (0.6/0.4). Condenser pinch point was 5°C and HRHE pinch point was 10°C. By linearly interpolating between the results in "step 3" at the given IHX heat load, condenser and HRHE pinch point are found as the values in Table 9-1. The interpolations show that, for the same heat load as in the pinch point (PP) analysis, lower condenser and HRHE pinch points, and probably higher condenser and HRHE areas, are found. Moreover, IHX pinch points in step 3 are low compared to the IHX pinch point set during the pinch-point analysis. Consequently, the fixed pinch points set in the pinch point analysis probably result in sub-optimum distribution of area. To ensure a more optimum distribution of IHX area (and higher work output for a "given area") with PP-analysis, IHX pinch point should be higher relative to condenser and HRHE pinch points.

Table 9-1 Pinch points for a given IHX heat load in "step 3" and in the pinch point analysis.

Working fluid	$\dot{Q}_{IHX}$	Step	Pinch condenser [°C]	Pinch HRHE [°C]	Pinch IHX [°C]
Butane	68.2	PP-analysis	5.0	10.0	5.0
	68.2	Step 3	5.1	6.3	14.8
Butane-propane (0.6/0.4)	123.2	PP-analysis	5.0	10.0	5.0
	123.2	Step 3	4.4	3.5	30.0

9.3.3 HX design

A total HX area of 200 m^2 is chosen for comparison of HX design. As observed in Figure 8-23 to Figure 8-26, this is an area where the distribution between condenser, HRHE and IHX area is relatively similar for the two fluids with IHX. The mixture has, as explained in the previous chapter, a slightly higher faction of condenser area. The pure fluid has 4.2 % higher work output than the mixture without IHX, but approximately the same work output with IHX. With IHX, the distribution between condenser and HRHE area is more similar, and the IHX accounts for 6-7 % of the total area.

For all fluids, pressure loss optimizes at a lower level in the condenser, where the pressure is lower than in the HRHE. Most notably, pressure loss is higher for the case with IHX, which is caused by higher HTCs, as explained in the previous section. As the mixture experiences a greater decrease in temperature differences with IHX, and consequently a greater increase in HTC (to enable lower condenser area despite lower temperature differences), pressure loss increases more for the mixture.

Pinch points are higher for the mixtures, as expected from the higher average temperature differences, coupled with the gliding temperature change during condensation. As with case 1, this possibly makes use of the mixture at high areas more feasible. Moreover, HRHE tube diameter and number of tubes optimize at approximately the same levels for all fluids (4 mm and ~ 350 tubes). Higher HRHE pressure loss with IHX causes a slightly lower number of tubes for case 4. For all cases, condenser pressure is relatively low compared to HRHE pressure, as shown in Table 12-3 in Appendix A.2. As with case 1, this means that densities are relatively low, and that velocities and condenser pressure loss in the condenser will be higher than in the HRHE for equivalent tube diameters. Consequently, tube diameters optimize at higher levels in the condensers. The relative condenser diameters for the different fluids reflect the relative condenser pressures. The higher condenser diameters give fewer number of tubes compared to the HRHE.

Table 8-6 list high and low side pressure loss, as well as the different design parameters for the IHX at 200 m^2. The pressure loss on the high pressure side optimizes approximately ten times higher than the pressure loss on the low pressure side. This suggests that the pressure loss on the low pressure side penalizes work output to a higher degree. Pressure loss is slightly higher

for the mixture, which is probably because the mixture has higher pressure levels and achieves a lower penalty in work output for the same pressure loss.

As with HRHE and condenser tube diameters, IHX tube diameters reflect the pressure levels of the fluids. Both high pressure side tube diameters, or d_1, optimize at 4 mm, and the low pressure side tube diameters, or d_2, optimize at higher levels. The number of tubes on the low pressure side is lower compared to the high pressure side for both fluids (not shown for the mixture because of rounded values), which is probably because of the higher diameters. The mixture probably has a smaller low pressure side tube diameter because of a higher pressure level. Furthermore, the mixture has less number of layers, but when multiplying the number of tubes with the number of layers, the total number of tubes on low and high pressure side do not differ by as much.

Table 8-7 shows estimated versus calculated area for case 3 and 4. The absolute average deviation is 3.3 % with no significant outliers, as was observed for case 1. The condenser area of butane is, opposite to most other areas, underestimated in the condenser. However, this underestimation is partly "balanced" by an overestimation in the butane HRHE. In general, the deviations are not excessive and do not appear to shift results in any significant direction.

9.4 Case comparison

Working fluid screening for the different cases was done with pinch point analysis, and showed that different pure fluids give the highest work output under the different constraint conditions. Ethane working fluid was optimum for the heat source at 100°C (case 1), propane was optimum for the heat source at 150°C (project work) and butane was optimum for the heat source at 200°C (case 3 and 4). Moreover, all the optimum working fluids are transcritical, and have relatively low critical temperatures compared to the subcritical fluids. The number of carbon atoms in the fluid, and consequently its critical temperature, increases with heat source temperature. This suggests that the optimum working fluid is in part decided by how its critical temperature compares with the heat source temperature.

The heat source temperature influences the level of work outputs. For the heat source at 100°C, work outputs reach around 25 kW for high values of total HX area. For the heat sources at

150°C and 200°C, work outputs reach 50 kW and 100 kW, respectively. This illustrates the impact of heat source temperature on work output, and the potential of Rankine cycles in for instance aluminum industry to achieve higher work output by upgrading heat source temperature.

The general level of HX area is similar for the cases studied in the current work, but relatively high in the project work. This is because HRHE outer area, being ten times higher than inner area, was calculated in the project work. The calculated HRHE area was changed to inner area in the current work to compare the condenser and HRHE on a more similar basis.

The project work case with a heat source at 150°C shows poor potential for working fluid mixtures to increase work output. The mixtures do outperform the pure fluids for relatively high values of total HX area, but the potential is low and the high areas cause excessively low pinch points. For case 3 with a heat source at 200°C, the pure fluid outperformed the mixture for all values of total HX area. However, the pinch point analysis showed that other mixtures might have had potential to increase work output compared to the pure fluid.

Case 4 showed that the use of an IHX can improve work output between 1.5 % and 11.6 % without increases in total HX area, but also showed that high areas are required for significant improvements. The mixture achieves greater increases in work output with IHX, reaching levels comparable to the pure fluid. In fact, the mixture may be more feasible for implementation of IHX in this case, as its pinch points are higher for the same values of total HX area.

Case 1 and 2 show the greatest potential of working fluid mixtures. In case 1, ethane-propane (0.6/0.4) achieves on average 22.5 % improvement in work output compared to both ethane and butane. For high values of total HX area, the mixture outperforms butane by almost 34 %, which indicates that transcritical mixtures have a significant potential compared to pure subcritical fluids. However, pressure levels are ten times higher, which could be challenging for cycle implementation, both technically and economically. In case 2, optimization of heat sink outlet temperature allows a slight increases in work output due to the ability of the pure fluids to decrease expander outlet pressure for the same area. Improvement was higher for the pure fluids, but was probably overestimated more so than for the mixture. This is because the heat sink pumping power does not account for increases in heat sink pressure loss with increasing mass flow.

In general, the behavior of working fluid mixtures compared to pure fluids does not appear to follow any fixed patterns. Sometimes the mixture has lower work output than the pure fluid for the same area, and other times higher. In some cases, the mixture outperforms the pure fluid at high areas, but is outperformed by the pure fluid at low areas. The cases studied suggest that lower heat source temperatures increases the ability of mixtures to outperform pure fluids. It is also possible that the absence of a lower limit on heat source outlet temperature, as for case 1 and 2, further favors working fluid mixtures.

9.5 Model evaluation

Compared to the project work, the model has been adjusted by implementing new heat transfer correlations developed and tested for hydrocarbons, which is likely to more accurately predict HTCs of the fluids under study. Moreover, the evaporating heat flux is calculated more accurately, which is likely to improve prediction of evaporating HTCs. This change is less significant, as only one of the fluids evaporates in the HRHE. Furthermore, the model has been developed to include IHX, and the HTC is made to vary with pinch point as well as pressure loss, $U = f(\Delta p) \rightarrow U = f(\Delta p, T_{pinch})$. The effect of the latter change is studied in Table 9-2, where deviation between estimated and calculated area is listed both with the use of $U = f(\Delta p)$ and with the use of $U = f(\Delta p, T_{pinch})$.

Table 9-2 Estimated area versus calculated area at 200 m^2 for case 3 and 4.

Working fluid	HX	Deviation between estimated and calculated area for $U = f(\Delta p)$ [%]	Deviation between estimated and calculated area for $U = f(\Delta p, T_{pinch})$ [%]
Butane	Condenser	- 7.6	- 20.1
	HRHE	+ 3.2	- 0.7
Butane-propane (0.6/0.4)	Condenser	+ 1.9	- 10.4
	HRHE	+ 0.6	- 0.8
Butane with IHX	Condenser	- 4.6	- 14.6
	HRHE	+ 4.5	- 0.9
Butane-propane (0.6/0.4) with IHX	Condenser	+ 3.9	- 3.9
	HRHE	- 0.4	- 2.4

The table shows that some deviations between estimated and calculated area increase from the old method, $U = f(\Delta p)$, to the new, ($U = f(\Delta p, T_{pinch})$, whereas other decrease. Even though

some areas are calculated more accurately with the old method, absolute average deviation increases from 3.3 % to 12.7 %. In addition, there are more "extreme values" with the old method (absolute deviation for the butane condenser is as high as 20.1 %). Consequently, the old method causes greater "shifts" in the results between the different fluids. For purposes of working fluid comparison, calculating overall HTC as a function of both pressure loss and pinch point appears to give a more "fair" comparison between fluids. For improved accuracy of estimated area, it is probably better to calculate overall HTC as a function of pressure loss and *average LMTD*, where the latter is more representative for HX area and overall HTC; pinch point is generally less representative for temperature differences throughout the HXs. Calculating HTC as a function of pinch point is especially troublesome for case 1 and 2, where varying heat source and heat sink outlet temperatures significantly changes the shape of temperature profiles for given pinch points. Another improvement in estimated area would be to use LMTD in the HX models, and not AMTD.

The HX models are characterized by simple geometries and constant heat transfer coefficients for the heat source and heat sink. Heat sink pressure loss is assigned a constant value, and heat source pressure loss is not considered. The HX models are poor representations of physical heat exchangers, but at the same time simplifications that allow easy comparison between the working fluids. With the assumption that "full design" on heat sink and heat source side does not differ significantly for the fluids, working fluid comparisons made in the current work can still be relevant. This is less true for case 2, where full design on heat sink side would probably penalize the pure fluids at low heat sink outlet temperatures in terms of increased heat sink pumping power. Another simplification made in the models is equal distribution of HX pressure loss, which is not accurate, as illustrated in Figure 6-4 and Figure 6-5.

Despite simplified HX models, the cycle and optimization model is fairly detailed, and allows for comparison of work output on the basis of equal HX area. HX area could be used as a measure of HX costs, which allows a more fair comparison between the fluids than pinch point analysis. However, in reality several other HX parameters are significant for HX costs, such as geometry, volume and weight. Moreover, the expander, pump, piping system and other system components may contribute to significant costs. Different working fluids and operating conditions will also influence expander efficiency.

A challenge with the excel optimization tool (the problem solver) is reaching the optimum global solution. This does not appear to be an issue for the optimization involved in case 1, 2 and 3. However, for case 4 with IHX, the optimization at times reached different values of maximum work output for the same value of pre-defined area when using different starting values for the optimization variables. This was attempted remedied by optimizing work output for different values of IHX heat load. An alternative method for calculating IHX area is to let the optimization tool decide tube length as well, such that calculation of heat transfer coefficients would not be necessary. However, this would involve yet another optimization variable and is not recommended for further work in excel.

Working fluid screening would have been more definitive if all mixture compositions had been tested, but time was not sufficient to allow this. The "temperature-match" method used to single out a few compositions is the best available method to the author.

9.6 Correlation evaluation

In Appendix C, the implemented heat transfer correlations are compared to the correlations used in the project work. Section C.1.1 compares the pure fluid correlations for condensation and Section C.1.2 compares the mixture correlations for condensation. A set of fixed parameters that specify tube diameter, number of tubes, reduces pressure and mass flux are used as basis for comparison between the correlations.

9.6.1 Pure fluid condensation correlations

Recall that correlation 1 was used in the project work and correlation 6 has been implemented in the current work. Figure 12-1 plots HTC versus vapor quality for butane with both correlations, with HX design and operating parameters given in Table 12-5. The figure shows that the correlations give approximately the same HTCs, except for high values of vapor quality where correlation 6 stagnates and then decreases. This is actually the more "physical" development in HTC, as the fluid approaches one-phase liquid at a vapor quality of one, where the HTC is relatively low. The pure fluid HTC given by Equation 5-6 is only scaled with vapor quality through a factor on the form $(1 + x^{0.5})$, which does not enable stagnation and decrease in the HTC with vapor quality. Correlation 6 varies with vapor quality through a factor on the

form $\left(\frac{x}{1-x}\right)^{0.8}$, which enables this development in HTC. Despite the discrepancy between the two correlations at high vapor quality, the condenser area and length calculated for the specified HX and heat sink parameters is relatively equal (17.08 m^2 vs 17.91 m^2).

As shown in Figure 12-2 to Figure 12-5, the variation in HTC with mass flux and tube diameter is relatively similar for the two correlations. The exception is for high vapor qualities where correlation 6 has lower HTCs, which is related to the mentioned factor. Moreover, correlation 1 gives higher HTCs than correlation 6 at low reduces pressure and lower HTC at higher reduced pressure. As seen in Table 12-1 to Table 12-3, reduces pressures mostly optimize in the low or high range ($\sim$0.1 or $\sim$0.8).

9.6.2 Mixed fluid condensation correlations

As observed in Figure 12-8, mixture HTCs for butane-propane (0.6/0.4) calculated with correlation 6 exceed those calculated with correlation 1. The difference between the correlations is higher than the pure fluid correlations. Consequently, areas deviate more (25.28 m^2 vs. 26.97 m^2), and is higher for correlation 1, which has the lowest HTCs. Recall that correlation 6 is a "composite" calculation method for both pure fluids and mixtures, developed based on a dataset of pure fluids and mixtures. Thus, the correlation does not account for the mass transfer resistance of mixtures, and the consequent reduction in HTCs. Correlation 1, on the other hand, has a resistance factor that scales with temperature glide, giving a heat transfer penalty for mixtures. This could explain why correlation 6 gives higher mixture HTCs than correlation 1. If in fact correlation 6 overestimates mixture HTC, the calculated mixture areas are too low, and work outputs too high at the given values of pre-defined area.

Tends in variation of HTC with mass flux, tube diameter and reduced pressure remain the same as for the pure fluids, but HTCs calculated with correlation 6 are now generally higher for correlation 6, as opposed to the pure fluid correlations.

9.6.3 General remarks on correlations

The condensation correlation implemented in the project work applies the simplified method of Bell and Ghaly, and the correlation applied in the current work is a relatively non-comprehensive empirical correlation. Both these correlations are amongst the least comprehensive and representative for variations in fluid operating conditions. Other relevant, more comprehensive correlations were considered for implementation, but showed either non-physical results, were complex to implement or irrelevant in terms of working fluids.

Calculation of HX area could be improved through implementation of some of the more comprehensive correlations. However, results for work output versus HX area indicate that the effect of temperature differences dominate over overall HTC, at least in the high area regions. Consequently, accuracy of HTCs has less impact on the variation in work output with HX area. Moreover, accuracy in prediction does not appear to improve significantly with correlation complexity.

Evaporation correlations have been given less focus in the thesis, both in the literature survey and in terms of correlation evaluation. As only subcritical butane in case 1 evaporated, this has been judged as acceptable. Moreover, pressure loss correlations have been studied less than heat transfer correlations, as these are similar for pure fluids and mixtures. A newly developed method for propane which has been validated for experimental data of several fluids was discussed in the literature survey. However, the method proved tedious to implement, and was not used in the current work. Instead, the method used in the project work was applied, for which an extensive comparison with experimental data showed relatively high deviations between calculated and measured data. The method was more accurate for an experiment on isobutene, but this included a limited number of data. Thus, further study and implementation of new pressure loss correlations is advisable.

10 CONCLUSION

Case 1 represents a present application of Rankine cycles in cooling of offshore compressed gas. The heat source is cooled from 100°C with no lower limit on outlet temperature. The results for this case indicate that mixtures have significant potential to increase work output compared to pure fluids for the same value of total HX area. Average improvement in work output from both butane and ethane to ethane-propane (0.6/0.4) was 22.5 %, and improvement reached almost 34 % compared to butane for high values of total HX area. However, there are challenges related to the high operating pressures of the transcritical mixture. A further, relatively small improvement in work output could be achieved with optimization of heat sink outlet temperature, but the improvement potential is higher for the pure fluids. Simplifications in the HX model limits a thorough study of changes in parameters of the heat sink.

The heat source temperature of offshore compressed gas is generally somewhat higher than 100°C, and thus potential might be lower than what has been observed in the current work (due to the coupling between lower heat source temperature and mixture performance). The results for case 1 are still highly relevant for ground heat sources with temperatures of around 100°C.

Higher heat source temperatures give rise to higher work outputs, and therefore present applications of Rankine cycles in aluminum industry have potential to achieve increased work output in the future by upgrading heat source temperature. This scenario is represented by case 3 in the current work. As seen by comparison with the project work results, increasing heat source temperature from 150°C and 200°C could contribute to an increase in work output of up to 50 kW, or 50 %. There could be further potential for work output improvement between 1.5 % and 11.6 % by including an IHX, but a relatively large system is necessary in terms of total HX area. Significant increases in work output for heat sources temperatures between 150°C and 200°C by using mixtures instead of pure fluids has not been demonstrated. However, a working fluid screening suggests that there are mixtures that could contribute to increases in work output for a heat source at 200°C.

Calculation of HX area can be improved through implementation of correlations that are more representative of physical heat transfer. However, results indicate that the effect of temperature differences dominate over overall HTC, at least in the high area regions. Consequently, HTCs

are less important for the variation in work output with HX area for the different fluids. To obtain a more fair comparison between different working fluids, it could be more useful to implement a “full” HX model that allows design on both heat source and heat sink side. Moreover, instead of comparing fluids on the basis of the same HX area, fluids could be compared on the basis of similar HX weight or cost, which gives a more fair basis of comparison.

It was found that the working fluid affects HX designs significantly in terms of pinch points and distributions between condenser and HRHE area, which is determined by the temperature profile and overall HTC of the fluids. Moreover, HX pressure loss is governed by working fluid overall HTCs and operating pressure, and the number of tubes and tube diameter is mostly affected by the fluid pressure levels. In particular, higher values of total HX area, and lower overall HTCs, contribute to lower pressure loss, and pressure loss is greater in the HRHE where operating pressure is relatively high. Low operating pressures contribute to relatively high optimum tube diameters, and few number of tubes. In general, these results indicate that optimum HX design is different for different working fluids.

11 FURTHER WORK

Further work may include the study of CO_2 mixtures and heat transfer correlations for mixtures between CO_2 and hydrocarbons. Even though CO_2 mixtures may not provide as high work output as hydrocarbon mixtures, CO_2 decreases the flammability of hydrocarbons. A penalty in work output compared to hydrocarbon mixtures may be acceptable if the flammability decreases.

Further work could include the study of different cases, such as a case more representative for cooling of offshore compressed gas than case 1. Different working fluid mixtures should be tested for the IHX-case, and especially one that achieves higher work output than butane in the pinch point analysis. The pinch point analysis for working fluid screening could be replaced by studying more fluids in “step 3” for a given case.

An option for improved prediction of HX area is to implement heat transfer and pressure loss correlations that are more physically representative. As mentioned, overall HTCs appear to have a smaller impact on HX area and work output than temperature differences. If fast and easy comparison is desirable on the basis of approximately equal total HX area, comparison on the basis of similar UA-values could be an alternative that is fairly representative for the variation in work output with HX area.

If a substantial improvement in HX models and fair working fluid comparison is desirable, full HX models should be implemented and comparison should be made on the basis of similar HX weight, volume or cost. If an improvement in cycle model is desirable in terms of simulation time and optimization accuracy, another optimization program should be used. This would allow for “full optimization” of HX design simultaneously with work output.

Finally, heat transfer of working fluid mixtures through plate heat exchangers could be studied. This type of HX design could involve different behaviors of working fluid mixtures compared to pure fluids. Pressure loss correlations validated for relevant working fluids should also be implemented.

12 APPENDIX

Appendix A Condenser and HRHE operating conditions

Appendix A.1 Case 1

Table 12-1 HX operating conditions at a total HX area of 50 m^2.

Working fluid	HX	$\dot{m}$ [kg/s]	G [kg/m^{2}s]	T_{in} [°C]	p_{in} [bar]	p_{red}
Butane	Condenser	0.35	46.9	41.7	3.0	0.08
	HRHE	0.35	70.5	26.4	8.9	0.23
Ethane	Condenser	0.71	163.3	53.8	41.4	0.85
	HRHE	0.71	217.3	33.5	74.1	1.52
Ethane-propane (0.6/0.4)	Condenser	0.58	124.4	45.7	24.2	0.48
	HRHE	0.58	206.0	24.2	52.6	1.03

Table 12-2 HX operating conditions at a total HX area of 150 m^2.

Working fluid	HX	$\dot{m}$ [kg/s]	G [kg/m^{2}s]	T_{in} [°C]	p_{in} [bar]	p_{red}
Butane	Condenser	0.45	23.3	38.6	2.7	0.07
	HRHE	0.45	45.5	23.5	8.2	0.22
Ethane	Condenser	0.87	93.9	53.6	39.7	0.81
	HRHE	0.87	135.0	31.3	74.5	1.53
Ethane-propane (0.6/0.4)	Condenser	0.73	65.1	44.7	21.5	0.42
	HRHE	0.73	144.5	19.0	53.3	1.04

Appendix A.2 Case 3

Table 12-3 HX operating conditions at a total HX area of 200 m^2.

Working fluid	HX	$\dot{m}$ [kg/s]	G [kg/m^{2}s]	T_{in} [°C]	p_{in} [bar]	p_{red}
Butane	Condenser	1.11	29.1	75.4	2.7	0.07
	HRHE	1.11	314.5	28.1	49.0	1.29
Butane-propane (0.6/0.4)	Condenser	1.03	34.8	85.5	4.4	0.10
	HRHE	1.03	227.0	21.3	64.6	1.53
Butane with IHX	Condenser	1.26	36.2	47.2	2.9	0.08
	HRHE	1.26	302.0	46.6	44.9	1.18
Butane-propane (0.6/0.4) with IHX	Condenser	1.25	36.4	43.2	4.8	0.12
	HRHE	1.25	258.4	50.7	56.4	1.34

Appendix B Heat transfer correlations

In this section, heat transfer coefficients calculated with the new and old correlations are compared for different mass fluxes, tube diameters and reduced pressures. Pressure loss is not considered.

Appendix B.1 Condensation

Pure fluid correlations are compared for pure butane and mixture correlations are compared for butane-propane (0.6/0.4). Where nothing else is specified, HX design and operating conditions are set to the fixed values given in Table 12-5, which are the average values for condensation from Appendix A and HX design Section 0.

Table 12-4 Fixed HX design and operating conditions for condensation.

Fixed parameter	Value
Tube diameter	10 mm
Number of tubes	360
Reduced pressure	0.3
Mass flux	70 kg/m^{2}s

Appendix B.1.1 Pure fluid correlations

With the parameters set in Table 12-4, the variation in HTC with vapor quality for both correlations is plotted in Figure 12-1. For heat sink inlet and outlet temperatures as specified in case 1 and 3, the condenser area and length calculated with both correlations is given in Table 12-5.

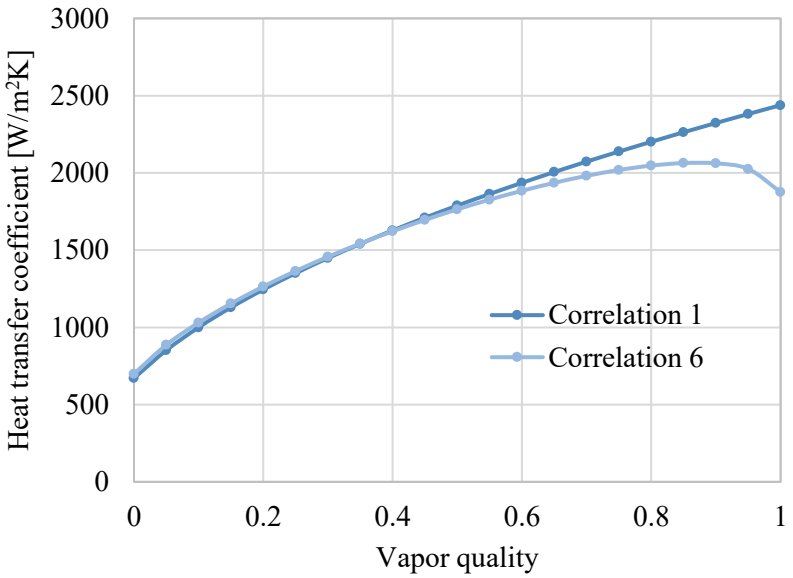

Figure 12-1 Heat transfer coefficient versus vapor quality for correlation 1 and 6.

Table 12-5 Condenser area and length calculated with correlation 1 and 6 for parameters given in Table 12-5.

Correlation	Condenser area [m^2]	Tube length [m]
1	17.08	1.51
6	17.19	1.52

In Figure 12-2 and Figure 12-3, HTC is plotted against mass flux for different vapor qualities. In Figure 12-4 and Figure 12-5, HTC is plotted against tube diameter for different vapor qualities, and in and Figure 12-6 and Figure 12-7, HTC is plotted against reduced pressure for different vapor qualities.

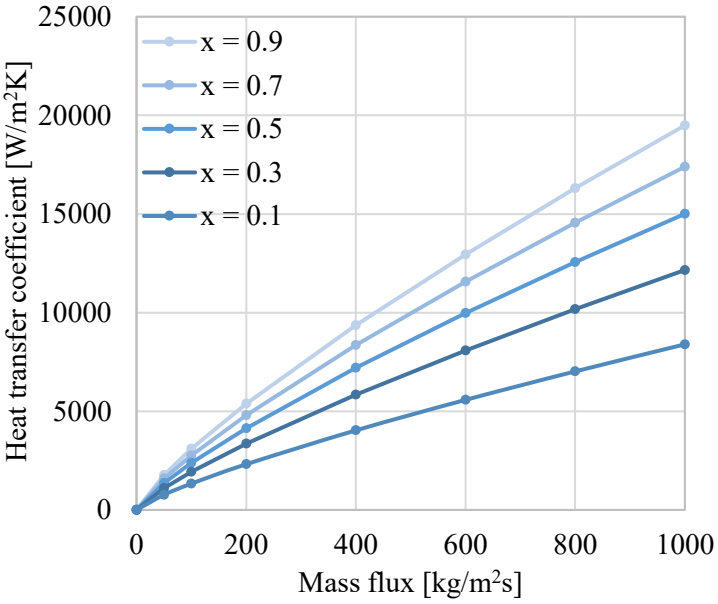

Figure 12-2 Correlation 1: Heat transfer coefficient versus vapor quality for different mass fluxes.

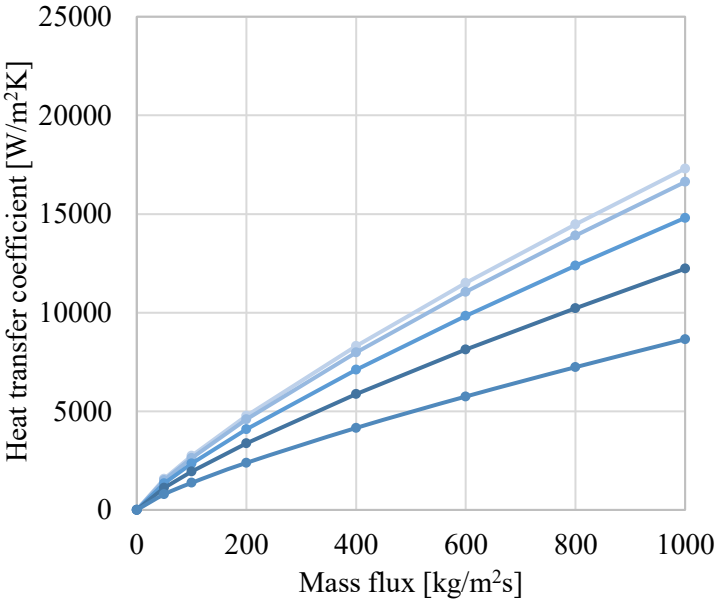

Figure 12-3 Correlation 6: Heat transfer coefficient versus vapor quality for different mass fluxes.

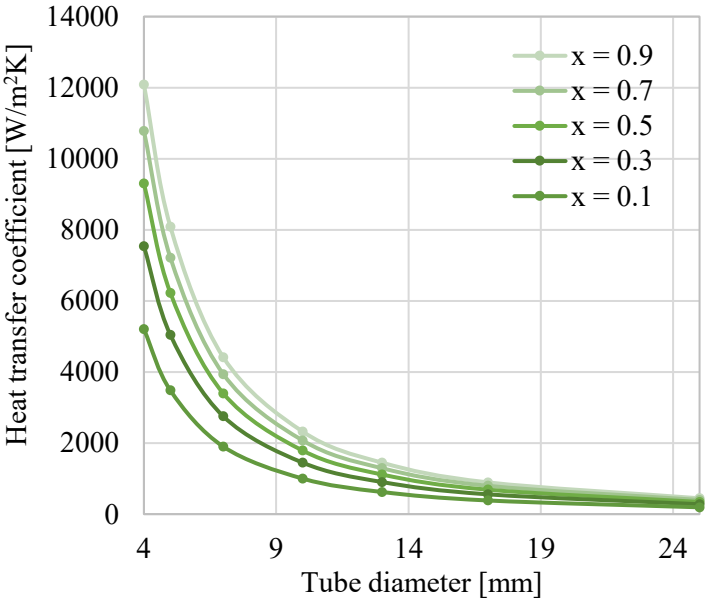

Figure 12-4 Correlation 1: Heat transfer coefficient versus tube diameter for different vapor qualities.

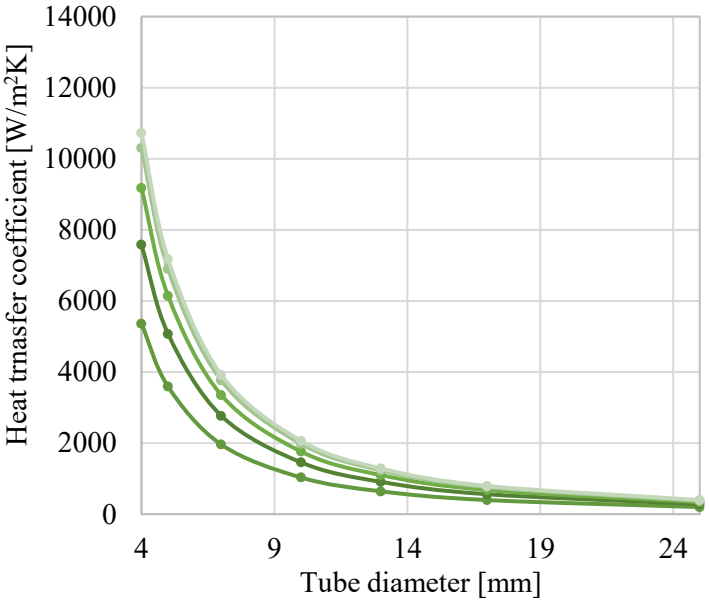

Figure 12-5 Correlation 6: Heat transfer coefficient versus tube diameter for different vapor qualities.

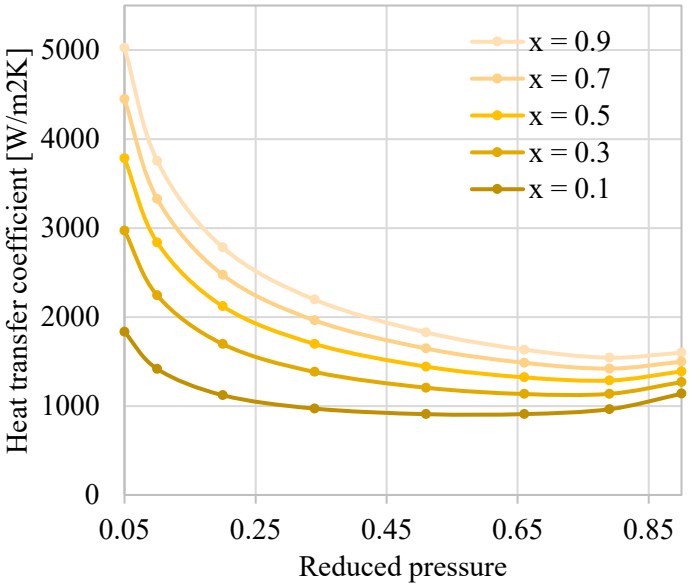

Figure 12-6 Correlation 1: Heat transfer coefficient versus reduced pressure for different vapor qualities.

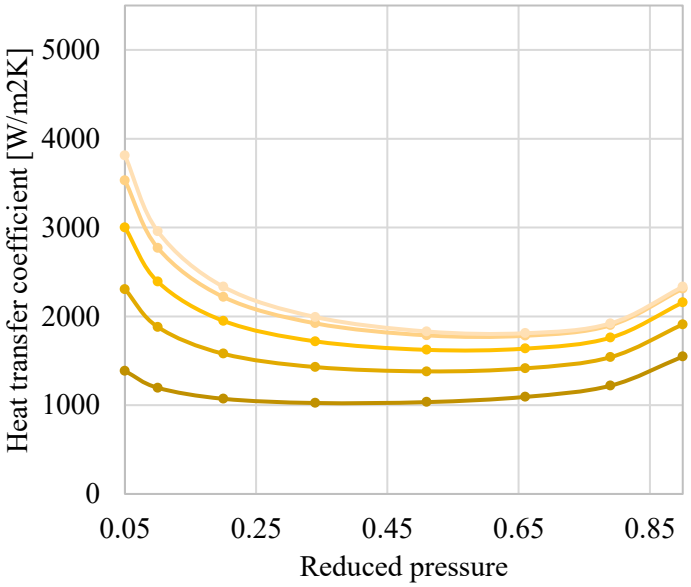

Figure 12-7 Correlation 6: Heat transfer coefficient versus reduced pressure for different vapor qualities.

Appendix B.1.2 Mixture correlations

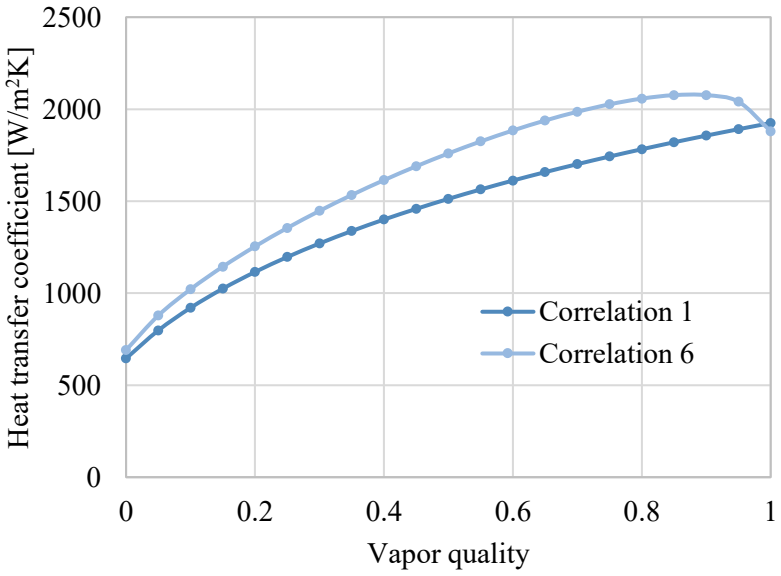

Figure 12-8 Heat transfer coefficient versus vapor quality for correlation 1 and 6.

Table 12-6 Condenser area and length calculated with correlation 1 and 6 for parameters given in Table 12-5.

Correlation	Condenser area [m^2]	Tube length [m]
1	26.94	2.38
6	25.28	2.24

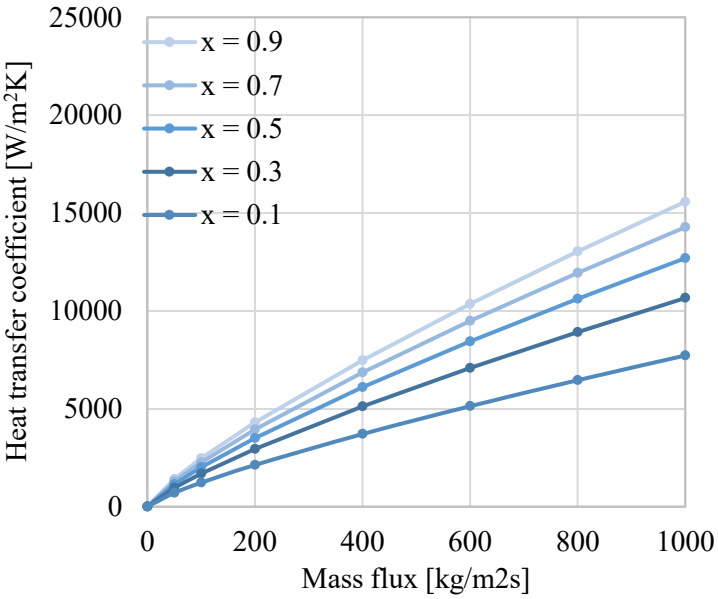

Figure 12-9 Correlation 1: Heat transfer coefficient versus vapor quality for different mass fluxes.

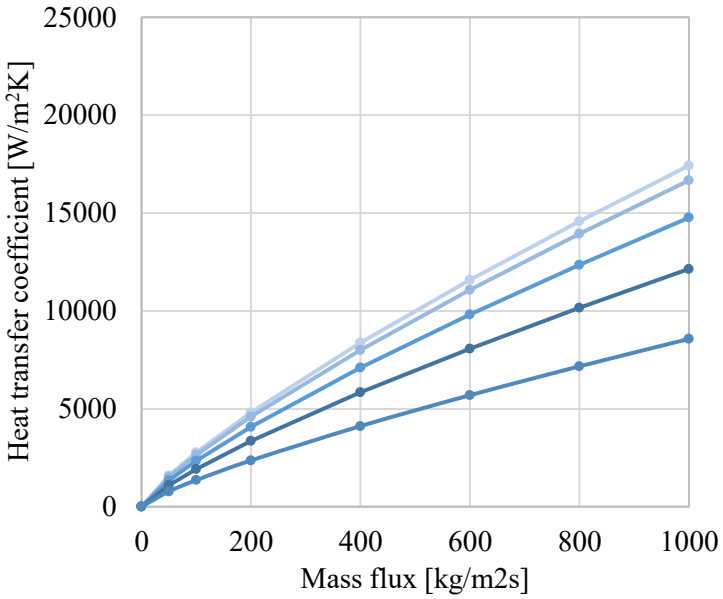

Figure 12-10 Correlation 6: Heat transfer coefficient versus vapor quality for different mass fluxes.

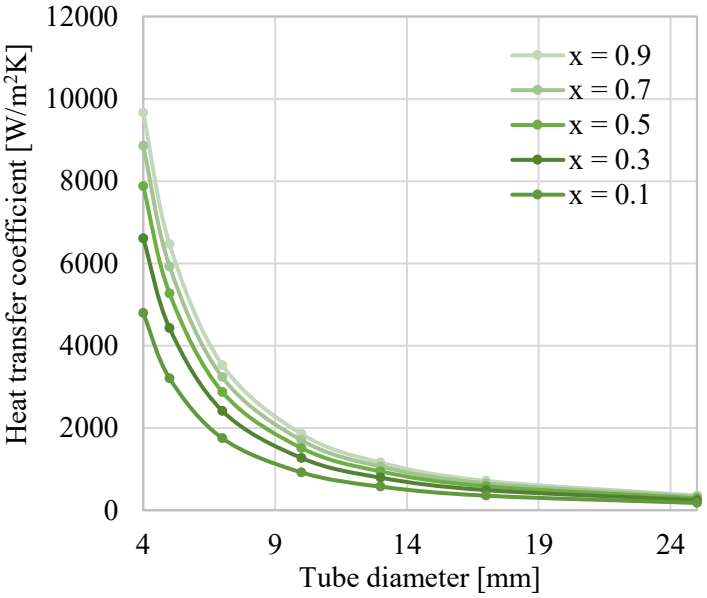

Figure 12-11 Correlation 1: Heat transfer coefficient versus tube diameter for different vapor qualities.

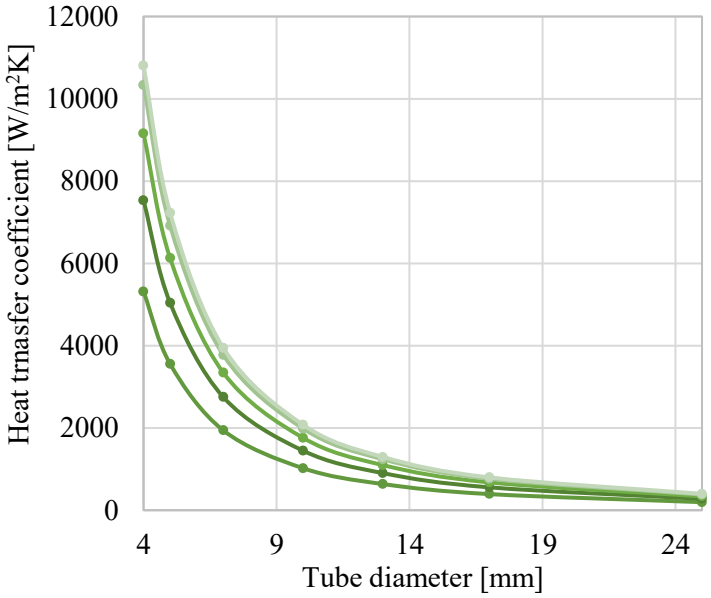

Figure 12-12 Correlation 6: Heat transfer coefficient versus tube diameter for different vapor qualities.

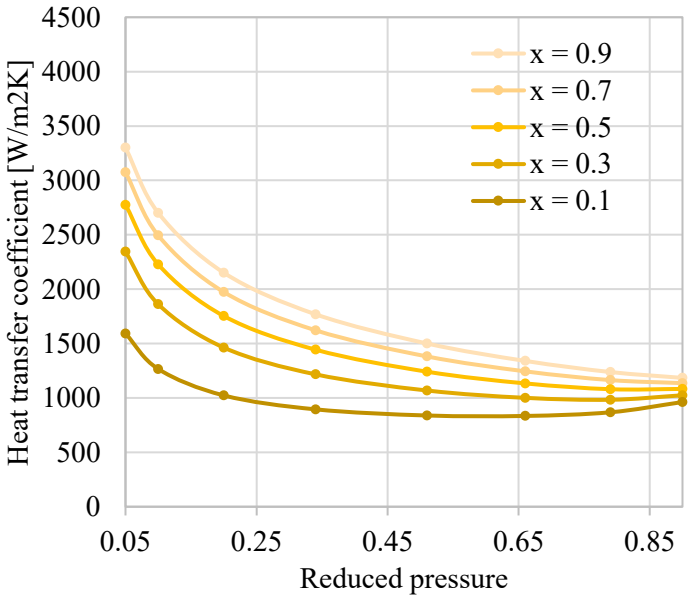

Figure 12-13 Correlation 1: Heat transfer coefficient versus reduced pressure for different vapor qualities.

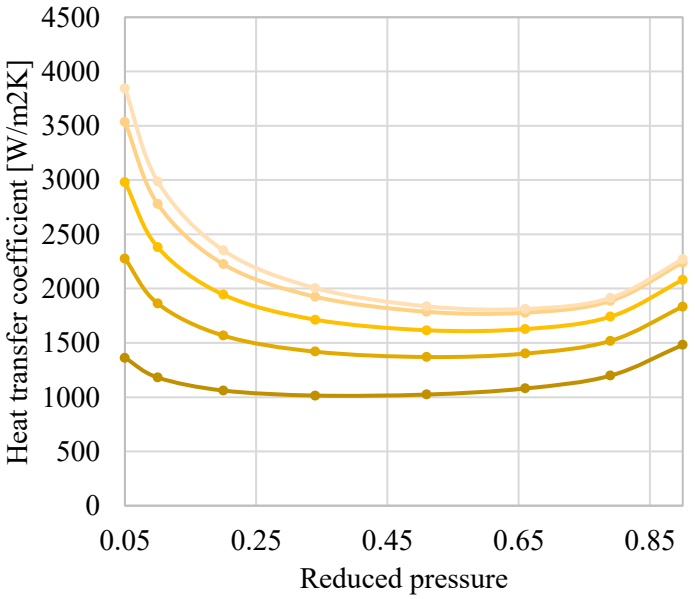

Figure 12-14 Correlation 6: Heat transfer coefficient versus reduced pressure for different vapor qualities.

REFERENCES

Aakenes, F. (2012), 'Frictional pressure-drop models for steady-state and transient two-phase flow of carbon dioxide', (NTNU).

Barraza, Rodrigo, et al. (2016), 'Measured and predicted heat transfer coefficients for boiling zeotropic mixed refrigerants in horizontal tubes', *International Journal of Heat and Mass Transfer,* 97, 683-95.

Bell, Kenneth J. and Ghaly, Mohamed A. (1973), 'An Approximate Generalized Design Method for Multicomponent/Partial Condenser', *AIChE Symp. Ser.,* 69, 72-79.

Boyko, L. D. and Kruzhilin, G. N. (1967), 'Heat transfer and hydraulic resistance during condensation of steam in a horizontal tube and in a bundle of tubes', *International Journal of Heat and Mass Transfer,* 10 (3), 361-73.

Cavallini, A., et al. (2002a), 'A tube-in-tube water/zeotropic mixture condenser: design procedure against experimental data', *Experimental Thermal and Fluid Science,* 25 (7), 495-501.

Cavallini, Alberto and Zecchin, Roberto (1974), 'A Dimensionless Correlation for Heat Transfer

in Forced Convection Condensation ', *Proceedings of 5th International Heat Transfer Conference* (3), 309-13.

Cavallini, Alberto, et al. (2002b), 'Condensation of Halogenated Refrigerants Inside Smooth Tubes', *HVAC&R Research,* 8 (4), 429-51.

Chang, Y. S., Kim, M. S., and Ro, S. T. (2000), 'Performance and heat transfer characteristics of hydrocarbon refrigerants in a heat pump system', *International Journal of Refrigeration,* 23 (3), 232-42.

Colburn, A.P. and Drew, T.B. (1937), 'The condensation of mixed vapors', *Trans. AIChE,* 33, 197–215.

Del Col, D., Cavallini, A., and Thome, J. R. (2005), 'Condensation of zeotropic mixtures in horizontal tubes: New simplified heat transfer model based on flow regimes', *Journal of Heat Transfer,* 127 (3), 221-30.

Deng, H. (2016), 'Boiling and condensation heat transfer of zeotropic mixtures in smooth tubes', PhD (Norwegian university of science and technology).

Filip, Alina, Băltăreţu, Florin, and Damian, Radu-Mircea (2014), 'Comparison of Two-Phase Pressure Drop Models for Condensing Flows in Horizontal Tubes', *Mathematical Modelling in Civil Engineering* (10), 19.

Friedel, L. (1979), 'Improved friction pressure drop correlation for horizontal and vertical two phase pipe flows', *European two phase flow group meeting*.

Granryd, E. (1991), 'Heat transfer in flow evaporation of non-azeotropic refrigerant mixtures - A theoretical approach', *Proc. 18th Int Congress of Refrigeration* (3), 1330-34.

Gungor, K. E. and Winterton, R. H. S. (1986), 'A general correlation for flow boiling in tubes and annuli', *International Journal of Heat and Mass Transfer,* 29 (3), 351-58.

--- (1987), 'Simplified general correlation for saturated flow boiling and comparisons of correlations with data ', *Chemical Engineering Research and Design,* 65 (2), 148-56.

Incropera, Frank P., et al. (2013), *Principles of Heat and Mass Transfer, International Student Version* (7 edn.; Singapore: John Wiley & Sons).

Jin, D. X., Kwon, J. T., and Kim, M. H. (2003), 'Prediction of in-tube condensation heat transfer characteristics of binary refrigerant mixtures', *International Journal of Refrigeration,* 26 (5), 593-600.

Jung, D. S. and Radermacher, R. (1989), 'Prediction of pressure drop during horizontal annular flow boiling of pure and mixed refrigerants', *International Journal of Heat and Mass Transfer,* 32 (12), 2435-46.

Kim, Byong Joo (1998), 'A model for the condensation heat transfer of binary refrigerant mixtures', *KSME International Journal,* 12 (2), 281-90.

Liu, Z. and Winterton, R. H. S. (1991), 'A general correlation for saturated and subcooled flow boiling in tubes and annuli, based on a nucleate pool boiling equation', *International Journal of Heat and Mass Transfer,* 34 (11), 2759-66.

Macdonald, Malcolm (2015), 'Condensation of pure and zeotropic mixtures of hydrocarbons in smooth horizontal tubes', (Georgia Institute of Technology).

Macdonald, Malcolm and Garimella, Srinivas (2016a), 'Hydrocarbon mixture condensation inside horizontal smooth tubes', *International Journal of Heat and Mass Transfer,* 100, 139-49.

--- (2016b), 'Hydrocarbon condensation in horizontal smooth tubes: Part I – Measurements', *International Journal of Heat and Mass Transfer,* 93, 75-85.

--- (2016c), 'Hydrocarbon condensation in horizontal smooth tubes: Part II – Heat transfer coefficient and pressure drop modeling', *International Journal of Heat and Mass Transfer,* 93, 1248-61.

Müller-Steinhagen, H. and Heck, K. (1986), 'A simple friction pressure drop correlation for two-phase flow in pipes', *Chemical Engineering and Processing: Process Intensification,* 20 (6), 297-308.

Radermacher, Reinhard and Hwang, Yunho (2005), 'Heat Transfer of Refrigerant Mixtures', *Vapor Compression Heat Pumps with Refrigerant Mixtures* (CRC Press), 237-78.

Sardesai, R. G., Shock, R. A. W., and Butterworth, D. (1982), 'Heat and Mass Transfer in Multicomponent Condensation and Boiling', *Heat Transfer Engineering,* 3 (3-4), 104-14.

Shah, M. M. (1979), 'A general correlation for heat transfer during film condensation inside pipes', *International Journal of Heat and Mass Transfer,* 22 (4), 547-56.

--- (1982), 'Chart correlation for saturated boiling heat transfer: Equations and further study', *ASHRAE Transactions* (pt 1 edn., 88), 185-96.

--- (2015), 'A method for predicting heat transfer during boiling of mixtures in plain tubes', *Applied Thermal Engineering,* 89, 812-21.

Thome, J. R. (1989), 'Prediction of the Mixture Effect On Boiling in Vertical Thermosyphon Reboilers', *Heat Transfer Engineering,* 10 (2), 29-38.

--- (1996), 'Boiling of new refrigerants: a state-of-the-art review', *International Journal of Refrigeration,* 19 (7), 435-57.

--- (1998), 'Boiling and Evaporation of Fluorocarbon and other refrigerants: A State-of-the-Art Review', (Arlington, Virginia: Air-Conditioning and Refrigeration Institute (ARI)).

--- (2006), *Engineering Databook III* (3: Wolverine Tube, Inc).

Thome, J. R., El Hajal, J., and Cavallini, A. (2003), 'Condensation in horizontal tubes, part 2: new heat transfer model based on flow regimes', *International Journal of Heat and Mass Transfer,* 46 (18), 3365-87.

Wattelet, J. P., et al. (1993), 'Evaporative Characteristics of R-134a, MP-39, and R-12 at Low Mass Fluxes', in Air Conditioning and Refrigeration Center (ed.), (University of Illinois).

Webb, D. R., Fahrner, M., and Schwaab, R. (1996), 'The relationship between the colburn and silver methods of condenser design', *International Journal of Heat and Mass Transfer,* 39 (15), 3147-56.

Wilson, M. J., et al. (2000), 'A Study of Refrigerant Pressure Drop and Void Fraction in Flattened Copper Tubes', *International Refrigeration and Air Conditioning Conference*.

Zou, X., et al. (2015), 'Heat Transfer Correlations for Flow Boiling of Hydrocarbon Mixtures inside Horizontal Tubes', *Physics Procedia,* 67, 655-60.

Zou, X., et al. (2010), 'Experimental study on saturated flow boiling heat transfer of R170/R290 mixtures in a horizontal tube', *International Journal of Refrigeration,* 33 (2), 371-80.

NTNU HMS	Kartlegging av risikofylt aktivitet	Utarbeidet av	Nummer	Dato
		HMS-avd.	HMSRV2601	22.03.2011
		Godkjent av		Erstatter
		Rektor		01.12.2006

Enhet: Institutt for Energi og Prosessteknikk **Dato:** 13.01.17

Linjeleder: Olav Bolland

Deltakere ved kartleggingen (m/ funksjon): Petter Nekså, Monika Nikolaisen
(Ansv. veileder, student, evt. medveiledere, evt. andre m. kompetanse)

Kort beskrivelse av hovedaktivitet/hovedprosess: Masteroppgave student Monika Nikolaisen. Evaluation of Rankine cycles with mixed component working fluids.

Er oppgaven rent teoretisk? (JA/NEI): JA *«JA» betyr at veileder innestår for at oppgaven ikke inneholder noen aktiviteter som krever risikovurdering. Dersom «JA»: Beskriv kort aktiviteteten i kartleggingskjemaet under. Risikovurdering trenger ikke å fylles ut.*

Signaturer: *Ansvarlig veileder:* Petter Nekså *Student:* Monika Nikolaisen

ID nr.	Aktivitet/prosess	Ansvarlig	Eksisterende dokumentasjon	Eksisterende sikringstiltak	Lov, forskrift o.l.	Kommentar
	Teoretisk arbeid på data	PN				